Rui Miguel Amaral Lopes

Mestre em Engenharia Electrotécnica e de Computadores

Extending nearly Zero-Energy Buildings Load Matching Improvement to Community-Level

Dissertação para obtenção do Grau de Doutor em
Engenharia Electrotécnica e de Computadores

Orientador: João Francisco Alves Martins,
Professor Auxiliar, Universidade Nova de Lisboa

Co-orientadores: Celson Pantoja Lima,
Professor Adjunto, Universidade Federal do Oeste do Pará

Daniel Aelenei, Professor Auxiliar,
Universidade Nova de Lisboa

Júri:

Presidente: Prof. Doutor Luis Manuel Camarinha-Matos
Arguentes: Prof. Doutor João Abel Peças Lopes
Prof. Doutor Sílvio José Pinto Simões Mariano

Vogais: Prof. Doutor António Carlos Sepúlveda Machado e Moura
Prof. Doutor Luís Filipe dos Santos Gomes
Prof. Doutor João Francisco Alves Martins

FACULDADE DE CIÊNCIAS E TECNOLOGIA
UNIVERSIDADE NOVA DE LISBOA

Dezembro 2017

Extending nearly Zero-Energy Buildings Load Matching Improvement to Community-Level

To Ana Sofia.

Acknowledgements

I would like to express my sincere gratitude to my supervisor and mentor Professor João Martins and my co-supervisors Professor Celson Lima and Professor Daniel Aelenei for the continuous support and motivation of my research work and for sharing with me their immense knowledge.

I also would like to thank the members of the Thesis Accompanying Committee, represented by Professor Luis Gomes and Professor João Peças Lopes, for the important comments and suggestions provided during the development of this work. I acknowledge the Faculdade de Ciências e Tecnologia da Universidade Nova de Lisboa for the institutional support and Fundação para a Ciência e a Tecnologia for the provided funding through Doctoral Grant SFRH/BD/87733/2012.

An acknowledgement is also due to my lab colleagues and good friends Bruno Mozzaquatro, João Guerreiro, Pedro Arsénio, Pedro Ferreira, and Pedro Magalhães for the companionship and help provided on countless situations. At the international level, I thank my colleagues from the International Energy Agency's Energy in Buildings and Communities Programme Annex 67 "Energy Flexible Buildings" for the knowledge and opportunities offered during the last three years and Graham Storer for his help during a critical time of my work.

I thank the unconditional friendship of a very special group of people that were always with me. The list is too long to include here but not referring Alexandre Costa, Cláudio Rosário, Pedro Rosa, and Samuel Reis would not be fair.

I would like to express my deepest gratitude to my parents for their love and friendship and for the huge efforts conducted in order to provide me with the best education. A special word to my little sister and brother – your love was essential during many periods. I also thank Mila and Agostinho for their contribution to my education and for their true friendship.

This work is dedicated to Ana Sofia, my fiancée, that unconditionally supported me during this journey. Thank you for everything – I will pay you back in the form of love during the many years we have ahead of us.

Resumo

O conceito de edifício com necessidades quase nulas de energia (nZEB) é visto como uma referência para o futuro do sector Europeu dos edifícios. Enquanto vários fatores contribuem para a introdução de instrumentos legais que promovem a adoção deste tipo de edifícios (e.g. eficiência energética), a relação destes com as redes de distribuição de energia elétrica em baixa tensão (LVGs) é muito mais complexa do que a dos edifícios comuns. Assim, de forma a melhorar a integração de nZEBs em particular, e de edifícios comuns equipados com sistemas de geração distribuída em geral, incentivos que promovem a melhoria do *Load Matching* (LM) têm sido introduzidos a nível mundial.

A literatura mostra que as medidas de melhoramento do LM, que utilizam a Flexibilidade Energética oferecida por dispositivos de consumo de eletricidade controláveis, são implementadas unicamente em edifícios individuais (i.e., ao nível do edifício) sem considerar os perfis de consumo e geração de eletricidade de outros edifícios. Deste modo, o primeiro objetivo deste trabalho consiste na avaliação de impactos originados por tais medidas em LVGs já existentes. De forma a amplificar os benefícios introduzidos para os proprietários dos edifícios e para os operadores das referidas redes, o segundo objetivo deste trabalho visa o desenvolvimento de uma nova abordagem para o melhoramento do LM. Para tal, o conceito de *Cooperative Net-Zero Energy Community* é introduzido, estendendo o melhoramento do LM para o nível de comunidade.

As experiências realizadas consideram um bairro composto por 33 edifícios e vários cenários de operação. Os resultados obtidos indicam que as medidas de melhoramento do LM implementadas ao nível do edifício podem prejudicar o operador da rede. As referidas experiências também mostram que o conceito proposto de *Cooperative Net-Zero Energy Community* aumenta os benefícios introduzidos para os proprietários dos edifícios e para o operador da rede.

Palavras-chave: Edifícios com necessidades quase nulas de energia, Geração Distribuída, Melhoramento do *Load Matching*, Flexibilidade Energética.

Abstract

The nearly Zero-Energy Building (nZEB) concept is foreseen as a reference for the future of the European building stock. While several factors contribute to the introduction of legal instruments that promote a fast adoption of these buildings (e.g. energy efficiency), their relationship with Low Voltage distribution Grids (LVGs) is far more complex than the one of the regular buildings. In order to improve the grid interaction of nZEBs in particular, and of regular buildings equipped with distributed generation systems in general, Load Matching (LM) improvement incentives are being promoted worldwide.

The literature shows that the existing LM improvement measures, that use the Energy Flexibility offered by controllable electricity demand devices, are only conducted at individual buildings (i.e. Building-Level) without taking into consideration the demand and on-site generation profiles of other buildings. Therefore, the first main objective of this research work refers to the assessment of impacts introduced by Building-Level LM improvement measures on existing LVGs. In order to improve the benefits offered to LVG operators and building owners (when compared to the existing Building-Level LM improvement measures), the second main objective concerns the development of a new LM improvement approach. For this purpose, the Cooperative Net-Zero Energy Community concept is introduced, extending the LM improvement to the Community-Level.

A neighborhood made up of 33 buildings is considered to conduct the necessary experiments, where the benefits offered to LVG operators are quantified by three important Performance Indictors and the benefits offered to building owners are quantified by the respective electricity bills. The obtained results show that Building-Level LM improvement measures can be harmful to LVG operators when large amounts of controllable electricity demand are shifted to coincident periods. The conducted experiments also show that the proposed Cooperative Net-Zero Energy Community concept improves the benefits offered to LVG operators and building owners.

Key-words: nearly Zero-Energy Buildings, Distributed Generation, Load Matching improvement, Energy Flexibility.

Table of Contents

List of Figures

List of Tables

Nomenclature

A	Area of each Photovoltaic module
a	Modified ideality factor
BD	Energy demand profile of a single building
BG	Energy generation profile of a single building
b	Identifier for a specific building
C_BD	Controllable energy demand profile of a single building
CD	Energy demand profile of the entire community
CG	Energy generation profile of the entire community
d	Energy demand profile of a single device or predicted original electricity demand profile of a single device
d^*	Predicted modified electricity demand profile of a single device
E	Energy losses by Joule effect
EA	Equivalent aging
F	Aggregated energy flexibility profile
F_{AA}	Aging acceleration factor
f	Energy flexibility profile of a single device
G	Global irradiance
g	Energy generation profile of a single device
I_L	Light current
IM	Demand instantly matched by the on-site generation
I_o	Diode reverse saturation current
idd	Energy demand profile of an individual device directly connected to the grid
idg	Energy generation profile of an individual device directly connected to the grid
K_{11}	Transformer thermal model constant
K_{21}	Transformer thermal model constant
K_{22}	Transformer thermal model constant
Lmax	Maximum peak load
LVG_D	Electricity demand profile at distribution transformer output or predicted original electricity demand profile at distribution transformer output
LVG_D*	Predicted modified electricity demand profile at distribution transformer output
LVG_G	Electricity generation profile at distribution transformer output or predicted electricity generation profile at distribution transformer output
$M_{EC,E}$	Export balance metric associated to a specific energy carrier
$M_{EC,I}$	Import balance metric associated to a specific energy carrier
N	Number of Photovoltaic modules
N_B	Number of buildings

N_b	Number of grid branches
N_C	Number of controllable devices
N_d_{EC}	Number of demand devices associated to a specific energy carrier
N_EC	Number of energy carriers
N_g_{EC}	Number of generation devices associated to a specific energy carrier
N_id	Number of individual devices directly connected to the grid
N_V	Number of control variables
NB	Energy net balance
NC_BD	Non-controllable energy demand profile of a single building
Net	Energy net profile
P	Period of analysis
R	Ratio of load losses at rated current to no-load losses
R_S	Series resistance
R_{SH}	Shunt resistance
Si	Power at grid node i
S_R	Transformer rated load
T	Balance period
WE	Weighted export
WI	Weighted import
X	Matrix containing the values of all control variables over the period of analysis
X_c	Matrix containing the values of all control variables associated to device c over the period of analysis
y_1	Exponential power of current versus winding temperature rise
y_2	Exponential power of total losses versus top-oil temperature rise

Greek symbols

$\Delta\theta_h$	Hot-spot to top-oil gradient at the load considered
$\Delta\theta_{hr}$	Hot-spot-to-top-oil gradient at rated current
$\Delta\theta_o$	Top-oil temperature rise at the load considered
$\Delta\theta_{or}$	Top-oil temperature rise in steady state at rated losses
β	Identifier for a specific grid branch
η_E	Efficiency of the power conditioning equipment
η_M	Time-varying modules' efficiency
θ_a	Ambient temperature
θ_c	Cell temperature
θ_h	Hot-spot temperature
θ_o	Top-oil temperature at the load considered
τ_o	Average oil thermal time constant

τ_w	Winding thermal time constant
μ	Efficiency temperature coefficient
ν	Identifier of a specific grid node

Abbreviations

AZEB	Autonomous Zero Energy Building
BL-LMI	Building-Level Load Matching Improvement
C-ADMIN	Community Administrator
C-EM	Community Energy Manager
CL-LMI	Community-Level Load Matching Improvement
CNet-ZEC	Cooperative Net-Zero Energy Community
DLC	Direct Load Control
EB	Event-Based device
EC	Energy Carrier
EPBD	Energy Performance in Buildings Directive
ES	Energy Storage device
EV	Electric Vehicle
EU	European Union
GA4S	Genetic Algorithm for Scheduling
GHG	Greenhouse Gases
H	Hypothesis
IDL	Indirect Load Control
IPCC	Intergovernmental Panel on Climate Change
LM	Load Matching
LV	Low Voltage
LVG	Low Voltage distribution Grid
M	Balance Metric
MV	Medium Voltage
Net-ZEB	Net-Zero Energy Building
nZEB	nearly Zero-Energy Building
NOCT	Nominal Operating Cell Temperature
PV	Photovoltaic
RQ	Research Question
SC	Self-Consumption
SS	Self-Sufficiency
STC	Standard Test Conditions
TC	Thermostatically-Controlled device
TOU	Time-of-Use

CHAPTER 1

Introduction

The importance of the nearly Zero-Energy Building (nZEB) concept for the European building stock is addressed in the first section of this introductory chapter. In Section 1.2, the research questions and respective hypotheses guiding this research are presented. The research method is explained in Section 1.3. To conclude this chapter, Section 1.4 depicts the structure of this dissertation.

1.1. Motivation

The heat storage effect occurring at Earth's atmosphere is of extreme importance to preserve the planet's average temperature within suitable levels for fauna and flora prosperity. Without this effect, the planet's surface temperature would not exceed -18 ºC and, therefore, life as we know it would not exist (Lang, 2006). Although oxygen and nitrogen represent Earth's atmosphere main constituents, with a contribution of 21 and 78 % respectively, it is the presence of other gases, known as Greenhouse Gases (GHG), that mainly contributes to store part of the incident solar energy (IPCC, 2014). Examples of such gases are water vapor (H2O), carbon dioxide (CO_2), methane (CH_4) or nitrous oxide (N2O) (EPA, 2017b).

GHG's atmospheric concentration is increasing and, consequently, Earth's energy balance is expected to reflect this variation. Figure 1.1 illustrates this scenario by depicting the anomaly registered in Earth's surface average temperature together with the atmospheric concentration of CO_2, CH4, and N2O (EPA, 2017a). Some effects related with Earth's surface average temperature

increase can already be observed: Artic Sea's ice is now declining at a rate of 13.4 % per decade, relative to the 1981-2010 average; Antarctica has been losing about 134 Gt of ice per year since 2002, while Greenland's ice sheet has been shortened out by an estimated 287 Gt per year; average sea level is increasing at a rate of 3.4 mm per year; and trees are flowering sooner (NASA, 2017b).

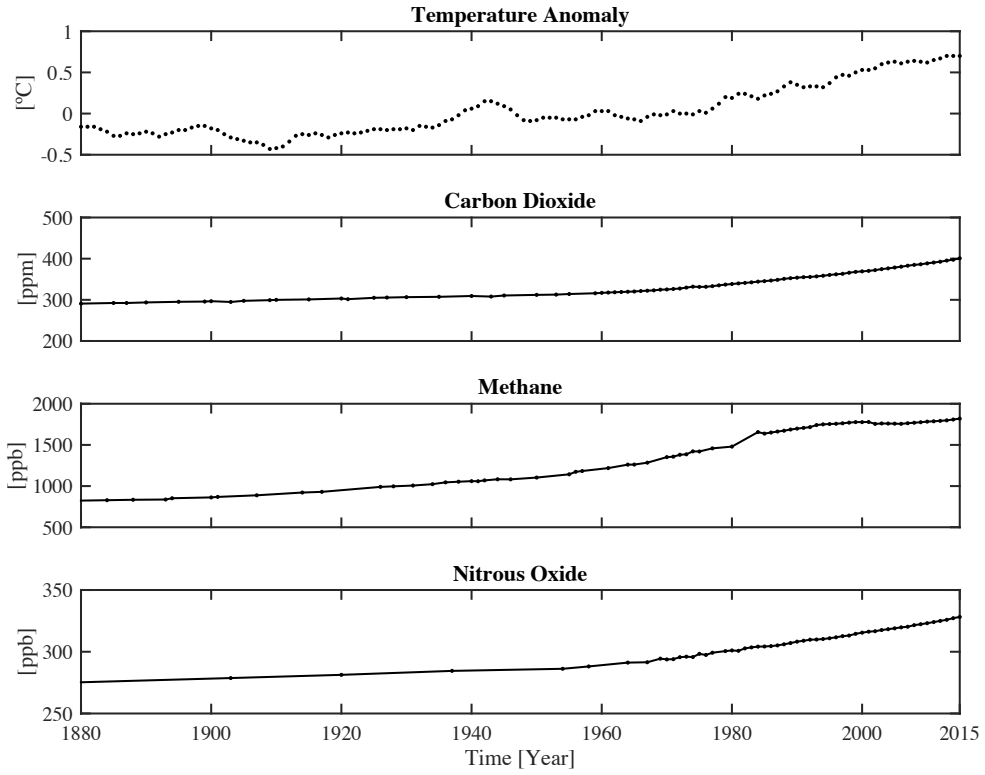

Figure 1.1 – Earth's average surface temperature and GHG concentration. Global surface temperature relative to 1951-1980 period. Data from (EPA, 2017a) and (NASA, 2017b).

The increase of GHG emissions is very likely human-induced, driven by economic and population growth (Hansen *et al.*, 2008). Anthropogenic CO_2-equivalent emissions are mostly due to fossil fuel combustion, cement production, flaring, and forestry and other land use (IPCC, 2014). Raising concerns about human-induced global warming led to the United Nations Framework Convention on Climate Change (UN, 1992), with the objective of stabilizing GHG concentration at a level that prevents a "*dangerous anthropogenic interference with the climate system*". For the Intergovernmental Panel on Climate Change (IPCC) (Solomon *et al.*, 2007) and others researchers, e.g. (Mastrandrea and Schneider, 2004), a global warming above 2-3 ºC relative to pre-industrial times may be considered as dangerous.

European Union (EU) has a framework to mitigate its CO_2-equivalent emissions. More specifically, the "*Roadmap for moving to a competitive low carbon economy in 2050*" (European Commission, 2011) aims to cut 80 % of CO_2-equivalent emissions by the year of 2050, relative

to 1990 values. Regarding the buildings sector, where a 90 % reduction is expected, the EU Energy Performance in Buildings Directive (EPBD) 2010 recast regulates that all new buildings, built from the beginning of 2021, should be at least nearly Zero-Energy Buildings[1] (nZEBs) (European Union, 2010). Additionally, the same directive recommends member states to set targets in order to stimulate the transformation of regular buildings into nZEB when these are renovated. It is expected that this recommendation will potentiate the nZEB adoption in countries like Portugal, where in 2011 more than 50 % of the buildings were at least 30 years old (INE, 2012).

1.2. Research Questions

Considering the distributed generation systems used by nZEBs to compensate their energy demand, the relationship between this type of buildings and the Low Voltage distribution Grids (LVGs) to which they are connected to is far more complex than the one of energy import-only buildings. The introduction of distributed generation into existing LVGs, that were originally designed to deal only with unidirectional power flows, has no negligible effects on LVGs' operation (Bollen and Hassan, 2011). These impacts strongly depend on the specific characteristics of the concerned LVGs, on the distributed electricity generation systems' properties, and on the type of interface used. Therefore, specific Performance Indicators should be considered for a fair assessment of the introduced impacts, which, in turn, is the basis for the development of measures to be taken.

A Performance Indicator describes the variation of a certain LVG's operation related parameter with the amount of introduced distributed generation. As an example, Figure 1.2 a) presents an illustrative Performance Indicator that increases with the amount of distributed generation. For small amounts of distributed generation, the considered Performance Indicator deteriorates but remains within the defined limits. However, for larger amounts of distributed generation, the Performance Indicator reaches unacceptable values and, as a consequence, the LVG's correct operation is compromised. This is the case, for instance, of the maximum voltage magnitude experienced at a specific LVG's section.

Other type of Performance Indicators follows a U-shape curves, as illustrated in Figure 1.2 b). For a reduced amount of distributed generation, the Performance Indicator is improved. Following this tendency, after reaching its minimum, the Performance Indicator increases until its original value, where no relative impacts are registered (denoted as point A in the figure). If the amount of distributed generation continues to increase, the Performance Indicator deteriorates, compared to its original value, and reaches unacceptable values (after the limit amount denoted

[1] See Section 2.1 for more information about the nearly Zero-Energy Building concept.

by point B in the figure). The losses by Joule Effect occurring at a distribution feeder or the risk of feeder overloading represent examples of Performance Indicators that follow U-shape curves.

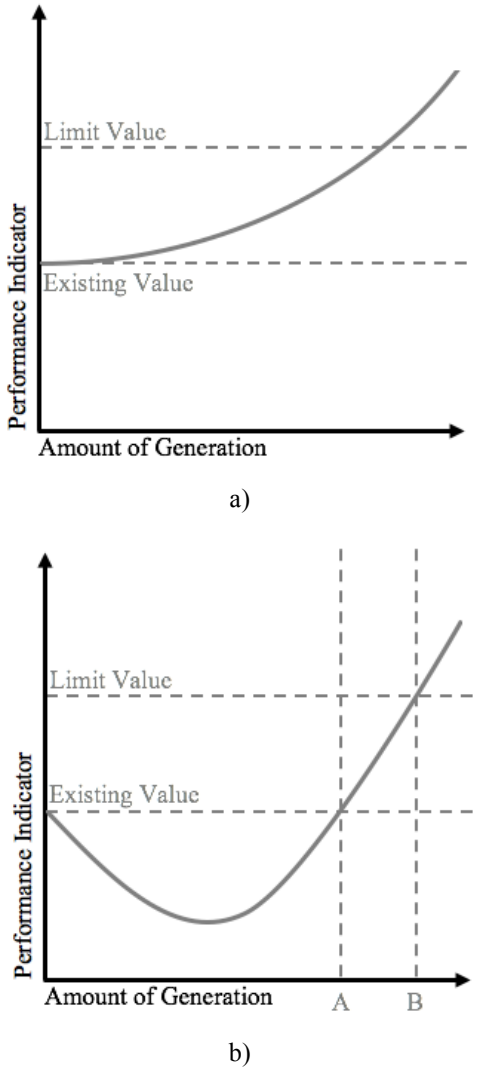

Figure 1.2 – Variation of two illustrative Performance Indicators as a function of the amount of distributed generation introduced into the respective LVG. Adapted from (Bollen and Hassan, 2011).

Different measures can be considered to mitigate the negative impacts introduced on LVGs, which are reflected on the considered Performance Indicators, due to the modification of existing power flows. The most common one is grid reinforcement to decrease feeders' impedance by e.g. adding new cables (EDP Distribuição, 2014). However, grid reinforcement measures are often associated with large investments. As a result, other options like reactive power provision (Collins and Ward, 2015; Liu, Cramer and Liao, 2015; Sampaio *et al.*, 2016), distributed generation systems' output curtailment (Tonkoski, Lopes and El-Fouly, 2011; Yap *et al.*, 2014; Bird *et al.*, 2016), transformers' tap-changer control strategies (Gao and Redfern, 2010; Kabiri *et al.*, 2015; Hu *et al.*, 2016) or Load Matching improvement, are being studied worldwide.

Among those techniques, Load Matching (LM) improvement is of special interest as incentives have been recently introduced in several countries to promote it (see Chapter 3). LM improvement refers to the process of increasing both Self-Consumption[2] (SC) and Self-Sufficiency[3] (SS) ratios of a specific building. It is normally implemented using the Energy Flexibility offered by some electrical devices that are associated to the respective building. The introduction of the referred incentives is motivated by the following assumptions (European Commission, 2015): i) building owners can reduce their electricity bill when faced with scenarios where the value received by the exported electricity is lower than the price paid by the imported electricity; and ii) the negative impacts caused on LVGs operation are mitigated due to a reduction of the building-LVG interaction (power and/or energy).

While aiming at contributing to the improvement of nZEBs-LVG interaction, the work presented in this dissertation intends to answer the following Research Questions (RQs):

RQ #1: In what circumstances, if any, is Load Matching improvement harmful to LVGs operation?

RQ #2: How Load Matching improvement measures can be implemented in order to increase the benefits offered to both LVG operators and building owners?

The following Hypotheses (H) are proposed to address these Research Questions (H #1 is related with RQ #1 and H #2 with RQ #2):

H #1: Load Matching improvement on individual buildings (i.e. at the Building-Level) can have a negative impact on some Performance Indicators if large amounts of uncorrelated buildings' electricity demand are shifted to coincident periods.

H #2: The benefits offered to building owners and LVG operators are enhanced if Load Matching improvement measures are implemented at an aggregated and cooperative level (i.e. Community-Level) rather than at Building-Level.

In this work, the referred benefits offered to building owners were quantified as Electricity Costs reductions resulting from applied LM improvement measures. To assess the benefits offered to

[2] Self-consumption ratio measures the amount of building's on-site generation that is instantaneously matched by building's electricity demand over a certain period of time.

[3] Self-sufficiency ratio measures the amount of building's electricity demand that is instantaneously matched by building's on-site generation over a certain period of time.

LVG operators, the following Performance Indicators were considered on account of their importance to LVGs operation:

- Peak Load – It is a critical input for the LVG components' sizing (e.g. feeder sections or protective devices). Peak load underestimation can lead to component overload and result on a quality of service decrease (e.g. number and duration of supply interruptions) (Lakervi and Holmes, 2003).
- Energy Losses – Energy losses resulting from electricity distribution are normally quantified and reflected on electricity bills. In some countries (e.g. Portugal), the regulatory authority establishes a mechanism to encourage LVGs' global losses reduction, which is intended to influence LVG operator's investment decisions. This mechanism allows the operators to receive an additional remuneration if they are able to reduce losses below a reference value, being penalized otherwise (EDP Distribuição, 2014).
- Transformer Aging – Being amongst the most expensive devices integrating electrical power grids, transformers play a key role by interconnecting parts of the power system operating at different voltage levels. LVG operators are thus engaged in maximizing the lifespan of these transformers in order to achieve an effective and profitable grid operation. In Portugal alone, by December 2016, 68,255 MV/LV transformers were an active asset on the distribution side of the power system (EDP Distribuição, 2016).

1.3. Research Method

The research method guiding the development of the work presented in this dissertation is made up of the flowing six phases:

1. Research Questions Formulation – Taking into consideration the near future role attributed to nZEBs, two Research Questions were formulated in this phase. The first one aims to evaluate the assumption that LM improvement is always benefic to LVGs operation. If evidences on the contrary are found, RQ #1 also intend to clarify the respective circumstances. The second aims to find a novel LM improvement approach that enhances the benefits offered to LVG operators and building owners.
2. Literature Review – Literature on LM improvement was reviewed in order to collect the main findings published in the area so far and to identify the existing knowledge gaps.
3. Hypotheses Formulation – Considering the proposed Research Questions, findings reported in the literature and the existing knowledge gaps, H #1 and H #2 were formulated.
4. Hypotheses Test Preparation – The proposed hypotheses were tested through detailed experiments carried out in this work. These experiments were planed considering

different scenarios. The Community-Level LM Improvement (CL-LMI) measure, proposed to address RQ #2, was also developed here.

5. Collect Data and Hypotheses Test – Using the planned experiments, data were collected and the proposed hypotheses were tested.
6. Findings Publication – A continuous publication of findings produced during this research work was adopted, which comprises the present dissertation.

1.4. Structure

This dissertation comprises seven chapters (introduction, five core chapters and conclusion), which in turn are organized in several sections. Figures, tables, and equations, presented throughout these chapters are numbered as (x.y), where x refers to the chapter and y to the respective order number. Vectors' names associated with these equations are presented in bold. The bibliographic references are cited as (Author, …, Author, Year), where "Author" concerns the surname of each author and "Year" is the publication year. A lowercase letter is added to distinguish references associated to the same author or set of authors and concerning the same year.

The remaining of this dissertation is structured as follows:

- Chapter 2 – Offers background information related with the nZEB concept, giving a special focus on Net-Zero Zero Energy Buildings (Net-ZEBs) and the respective Net-Balance computation (Net-ZEBs are a specific type of nZEB). Additionally, this chapter addresses the on-site electricity generation system most used in Net-ZEBs (i.e. Photovoltaic system) and describes the solar resource used as input during the respective conversion process.
- Chapter 3 – Provides a literature review on LM improvement. It is, in fact, the output of the previously referred research method's second step. Apart from existing LM improvement measures, this chapter provides information related with LM improvement incentives and metrics typically used.
- Chapter 4 – Presents the Cooperative Net-Zero Energy Community (CNet-ZEC) concept, which refers to the proposed CL-LMI measure used to test hypothesis H #2. The different components of the CNet-ZEC concept are detailed in this chapter.
- Chapter 5 – Describes the experiments carried out to test the proposed hypotheses. This description comprises the considered neighborhood and the different scenarios used to collect the required data. The Performance Indicators associated to the studied LVG and the Electricity Costs structure used in this work are also addressed.

- Chapter 6 – Presents and analyses the obtained results and assesses the proposed hypotheses. Apart from the Performance Indicators and Electricity Costs associated with each scenario, presented results also focus the observed LVG's load profiles and LM values computed at different time-scales.
- Chapter 7 – Concludes about the research work carried out. More specifically, it provides an overview of the research activities presented in this dissertation in addition to a description of the main findings and a list of future works left opened by this research.

CHAPTER 2

Background Information

The information provided in this chapter focus the nZEB concept adoption under the existing European legal framework. Nevertheless, similar policies were also adopted in other developed countries like the USA or Canada (Voss and Musall, 2013). In fact, nowadays, more than 300 nZEBs can already be found around the world (see Figure 2.1), mostly using Photovoltaic (PV) systems to generate energy on-site. Aiming to provide the required background information for the remaining of this dissertation, Section 2.1 addresses the nZEB concept while Sections 2.2 and 2.3 are focused on the solar resource availability and its conversion to electricity using PV systems, respectively.

2.1. Nearly Zero-Energy Buildings

The EU Energy Performance in Buildings Directive (EPBD) 2010 recast refers to a nearly Zero-Energy Building as "*a building that has a very high energy performance and that the nearly zero or very low amount of energy required is covered to a significant extent by energy from renewable sources, including energy from renewable sources produced on-site or nearby*". Additionally, specific timeframes were set, namely: "*Member States shall ensure that: a) by 31 December 2020, all new buildings are nearly zero-energy buildings; and b) after 31 December 2018, new buildings occupied and owned by public authorities are nearly zero-energy building*" (European Union, 2010).

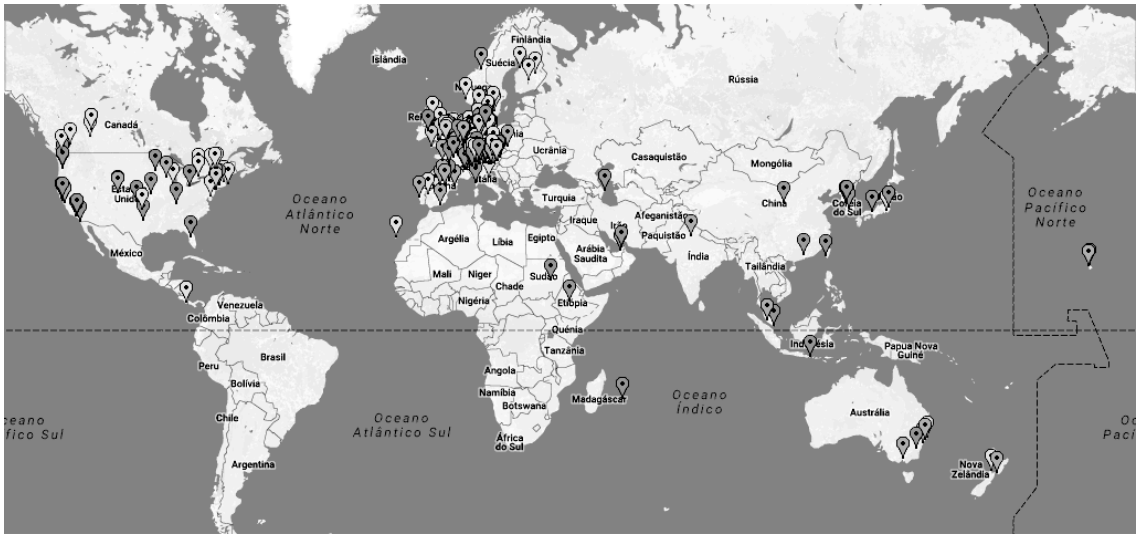

Figure 2.1 – Map with the location of approximately 300 nZEBs worldwide (EnOB, 2013).

EPBD 2010 recast configures a step forward towards a larger set of efficient buildings and to a broader adoption of distributed generation systems (Voss and Musall, 2013). However, despite the defined timeframe and the member states accountability for developing the respective standards according to their building stock specificities, not all countries have set specific energy performance targets. Nevertheless, the Passive House requirements are often used as benchmark to nZEBs' energy performance, which comprises, among others, the following (PHPT, 2017):

- Space heating energy demand lower than 15 kWh per square meter or maximum heating load lower than 10 W per square meter;
- Space cooling energy demand lower than 15 kWh per square meter or maximum heating load lower than 10 W per square meter;
- Primary energy demand lower than 120kWh per square meter;
- Minimum and maximum internal temperatures of 20 ºC and 26 ºC, respectively; and
- Internal temperatures higher than 26 ºC allowed only during 10 % of the time.

nZEBs equipped with on-site energy generation systems large enough to satisfy their entire energy requirements can be further defined as Autonomous Zero Energy Buildings (AZEBs) or Net-Zero Energy Buildings (Net-ZEBs) (Sartori, Napolitano and Voss, 2012). Both types refer to efficient buildings able to generate energy on-site, typically from renewable sources, to compensate for their energy demand. The main difference is related with the time-scale in which this compensation is achieved. On one hand, AZEBs are autonomous buildings, disconnected from existing energy grids[4], that use large on-site energy generation and storage devices to compensate their energy demand instantaneously. On the other hand, Net-ZEBs do not exist in

[4] Energy grids refer to supply systems for energy carriers such as electricity, natural gas, thermal heating/cooling, biomass, and other fuels.

isolation and are equipped with smaller on-site generation devices to compensate their energy consumption over a specific balance period. The wording 'Net' underlines the fact that there is a Net Balance (*NB*) between energy taken from and supplied back to the energy grids. Therefore, a nZEB is considered Net-ZEB when it presents a zero *NB*.

Since this work is focused on nZEBs integration into existing LVGs, Net-ZEBs are considered throughout this dissertation. Sections 2.1.1 – 2.1.3 address the main concepts involved in the NB computation. The information reported here is essentially based on the work developed in the International Energy Agency joint Solar Heating and Cooling Task 40 and Energy Conservation in Buildings and Community Systems Annex 52 titled "*Towards Net Zero Energy Solar Buildings*" (IEA-SHC, 2017).

2.1.1. Balance Boundary

The Balance Boundary sets the generation and consumption devices, associated to a specific building, that are taken into consideration during the NB computation. The total building's demand ($\boldsymbol{BD}_{EC}$) and generation ($\boldsymbol{BG}_{EC}$) profiles for each Energy Carrier (EC) are given by Equations 2.1 and 2.2, respectively, where N_d_{EC} and N_g_{EC} are the number of considered demand ($\boldsymbol{d}_{EC}$) and generation ($\boldsymbol{g}_{EC}$) devices associated to that EC[5], respectively. Therefore, assuming the possibility of self-consumption in each energy carrier, the net profile ($\boldsymbol{Net}_{EC}$) is given by the difference between the associated total demand and total generation, as denoted by Equation 2.3. By convention, a negative value of $\boldsymbol{Net}_{EC}$ indicates an exporting behavior whereas a positive value is associated to an importing performance. For some energy carriers (e.g. natural gas), the local distribution grids do not allow energy surplus exports. In these cases, the energy imported through the one-way distribution grids can be compensated by the energy exported through the remaining two-way energy distribution grids. A typical example of this scenario is observed in some Portuguese cities (e.g. Lisbon), where it is possible to import natural gas but energy exports are only allowed through the electricity distribution grid.

$$\mathbf{BD}_{\mathrm{EC}}(\mathrm{n}) = \sum_{\mathrm{i}=1}^{\mathrm{N}\_d_{EC}} \mathbf{d}_{\mathrm{EC,i}}(\mathrm{n}) \tag{2.1}$$

$$\mathbf{BG}_{\mathrm{EC}}(\mathrm{n}) = \sum_{\mathrm{i}=1}^{\mathrm{N}\_g_{EC}} \mathbf{g}_{\mathrm{EC,i}}(\mathrm{n}) \tag{2.2}$$

[5] In the remaining of this document the subscript EC is omitted when electricity is the only Energy Carrier considered.

$$\mathbf{Net}_{\mathrm{EC}}(\mathrm{n}) = \mathbf{BD}_{\mathrm{EC}}(\mathrm{n}) - \mathbf{BG}_{\mathrm{EC}}(\mathrm{n}) \quad (2.3)$$

2.1.2. Balance Period

The Balance Period (T) refers to the time-scale associated to the NB computation. A Balance Period of one year is normally assumed by the entities using the Net-ZEB concept since it is suitable to cover all the operation settings with respect to the meteorological conditions (Garde *et al.*, 2017). PV based Net-ZEBs normally present importing profiles during the winter and exporting profiles during the summer, following the solar resource availability and, in some cases, building's heating demand (Athienitis and O'Brien, 2015). However, on an annual basis, these buildings present a zero NB.

A much wider time span, in the order of decades, can also be selected if the entire building's life cycle should be taken into account. In this case, the embodied energy in materials and devices, as well as the energy spent during the construction and demolition phases, can be dissolved along the entire Balance Period and be represented by a virtual consumption device in Equation 2.1. Figure 2.2 shows the ZEB Living Lab, which is a Net-ZEB located at the Norwegian University of Science and Technology (ZEB, 2017) characterized by having a Balance Period large enough to take into consideration its life cycle NB. In this case, on a yearly basis, the generation device (PV system) produces more energy than it is locally consumed.

Figure 2.2 – ZEB Living Lab (Norwegian University of Science and Technology). Picture credits: (ZEB, 2017).

2.1.3. Balance Metric

The Balance Metric ($\boldsymbol{M}$) allows to take into consideration the so-called fuel switching effect when, for instance, a building exports PV generated electricity during the summer to compensate the import of biomass or fossil fuels during the winter for heating proposes. Four different types of Balance Metrics are normally considered: site energy, primary energy, equivalent CO_2 emissions and energy costs (Voss and Musall, 2013). There is not an absolute correct Balance Metric because choosing it depends on the scenario under consideration. Furthermore, the Balance Metric may include considerations not directly related with the physical processes in order to promote or discourage the adoption of certain technologies or energy carriers. For example, if equivalent CO_2 emissions are considered as a Balance Metric, then biomass will have a relative low value associated, making it an attractive solution. However, the availability of biomass is not infinite and it needs to be used furthermore for non-energy purposes such as food production. Therefore, it may be desirable to 'politically' increase the value of the Balance Metric to reduce the attractiveness of this energy carrier and promote other solutions instead.

Another important issue is the symmetry of the chosen Balance Metric. Each two-way energy carrier can be weighted symmetrically, where the same metric value is used for the import and export of energy, or asymmetrically, using different metric values. $\boldsymbol{M}_I$ and $\boldsymbol{M}_E$ are used in this work to denote import and export Balance Metric values, respectively. On one hand, a symmetric Balance Metric is used in scenarios where the exported energy will avoid an equivalent generation somewhere else in the energy system. On the other hand, an asymmetric Balance Metric is considered when the exported energy should be valued or penalized. Asymmetric Balance Metrics can be used, for instance, to promote some technology diffusion or to take into consideration costs and losses in the grid side associated with the distribution of the respective energy carrier. The difference between the monetary value received by building owners for the exported electricity and the price paid by the electricity imports in Portugal constitutes a typical example of an asymmetric Balance Metric. Additionally, the chosen Balance Metric can have a time and seasonal dependency as it is the case of imported electricity in Portugal. Table 2.1 presents some conversion factors, according to EN 15603 (EN 15603, 2008), that can be used as Balance Metrics.

Table 2.1 – Conversion factors according to (EN 15603, 2008).

Energy carrier	Metric	Value
Electricity	PEI, n. r.	3.14
	PEI, total	3.31
	CO_2-equivalent	617.00
Natural gas	PEI, n. r.	1.36
	PEI, total	1.36
	CO_2-equivalent	277.00
Oil	PEI, n. r.	1.35
	PEI, total	1.35
	CO_2-equivalent	330.00
Wood	PEI, n. r.	0.09
	PEI, total	1.09
	CO_2-equivalent	14.00
Key: PEI – primary energy indicator ($kWh_{primary}/kWh_{delivered}$); n. r. – non renewable part; CO_2-equivalent – equivalent CO_2 emissions ($g/kWh_{delivered}$).		

2.1.4. Energy Balance Computation

To compute the NB of a specific Net-ZEB, metrics relating building's energy imports and exports are needed. These metrics are obtained using the concepts of Balance Boundary, Balance Period, and Balance Metric addressed in Sections 2.1.1 – 2.1.3 and can be expressed as Weighted Import (WI) and Weighted Export (WE), as described by Equations 2.4 and 2.5, respectively. These equations consider the energy demand ($\boldsymbol{BD}_{EC}$) and on-site generation ($\boldsymbol{BG}_{EC}$) profiles, associated to each one of the N_EC energy carriers, the time dependent import ($\boldsymbol{M}_{EC,I}$) and export ($\boldsymbol{M}_{EC,E}$) Balance Metrics and the Balance Period T. NB is then given by Equation 2.6.

$$\mathrm{WI} = \sum_{\mathrm{EC}=1}^{\mathrm{N\_EC}} \sum_{\mathrm{n}=1}^{\mathrm{T}} \left(\mathbf{M}_{\mathrm{EC,I}}(\mathrm{n}) \times \mathbf{BD}_{\mathrm{EC}}(\mathrm{n}) \right) \tag{2.4}$$

$$\mathrm{WE} = \sum_{\mathrm{EC}=1}^{\mathrm{N\_EC}} \sum_{\mathrm{n}=1}^{\mathrm{T}} \left(\mathbf{M}_{\mathrm{EC,E}}(\mathrm{n}) \times \mathbf{BG}_{\mathrm{EC}}(\mathrm{n}) \right) \tag{2.5}$$

$$\mathrm{NB} = \mathrm{WE} - \mathrm{WI} \tag{2.6}$$

A common approach to represent Net-ZEBs' NB is through the graphical representation sketched in Figure 2.3. This figure also presents the effects introduced on an existing building's energy

performance when it is renovated and converted to Net-ZEB. The conversion process starts by improving the existing building's energy efficiency, reducing, as a result, the Weighted Import. In this case, the Reference Building in Figure 2.3 refers to the WI of an existing building before the renovations works to improve its energy efficiency take place. Then, the resulting WI is compensated by introducing on-site energy generation systems able to produce a Weighted Export equal to WI. It is important to note that the conversion of an existing regular building to Net-ZEB can not be achieved by simply introducing oversized on-site energy generation systems without reducing its WI.

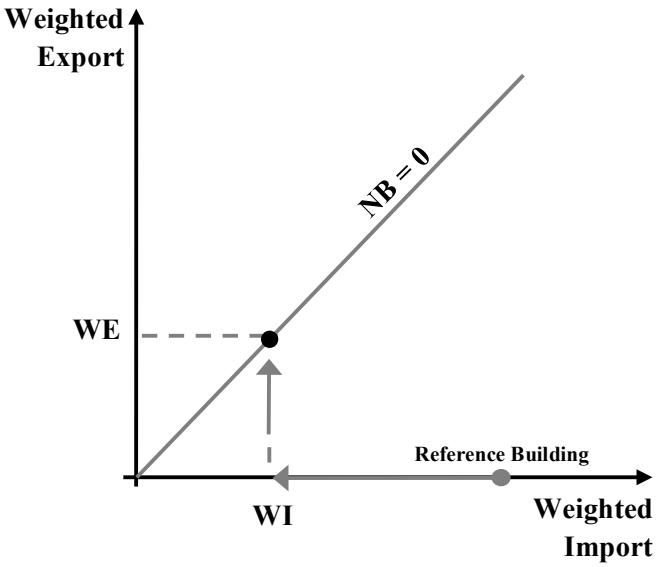

Figure 2.3 – Graphical representation of the Net Balance.

2.2. Solar Resource

The Sun is a completely gaseous body, mainly composed of hydrogen and helium, whose internal temperatures reach over 20 million K due to nuclear fusion reactions occurring at its core (Iqbal, 1983). At the Sun's surface, known as the photosphere, an effective temperature of 5772 K is registered (NASA, 2017c). Following Stefan-Boltzmann Law of Radiation, which states that the power density at a blackbody surface is proportional to the fourth power of the respective temperature, as described by Equation 2.7, one can find that the power density at the Sun's surface is approximately 6.3x107 W/m^2 (Planck and Masius, 1914). From the total power emitted by the Sun, which is obtained by multiplying the power density at Sun's surface by its surface area, only a fraction reaches Earth's surface. At the top of Earth's atmosphere, an average power of 1353 W passes through every square meter of the plane perpendicular to the direction of the sun (Freris and Infield, 2008). Due to the energy absorbed by Earth's atmosphere, the solar radiation reaching the planet's surface is only 77 % of this value (NASA, 2017a). This effect can be observed by

comparing the spectral distribution of extraterrestrial and terrestrial radiation, as depicted in Figure 2.4 and according to ISO 9845-1:1992. Gases like ozone, carbon dioxide or water vapor are responsible for the attenuations observed in the terrestrial spectral radiation curve. Nevertheless, on a yearly basis, an energy amount of 885 million terawatt hour reachs Earth' surface (IEA, 2014a), which is 5.6 thousand times higher than 2014 world's total primary energy supply (IEA, 2016).

$$P = \sigma T^4, \qquad (2.7)$$
$$\sigma = 5.67\times10^{-8} \mathrm{Js^{-1}m^{-2}K^{-4}}$$

The instantaneous value of the solar resource at Earth's surface, i.e. the incident solar radiation, is impacted by the 24 h rotation of the planet on its axis and by the revolution of the planet around the Sun. The latter (i.e. the revolution of the planet around the Sun) can be further decomposed in two effects. The first is related with Earth' eccentric orbit, which results on a $\pm$ 3.3 % variation along the year. The second concerns the angle registered between Earth's rotational axis and the plane in which the referred revolution is performed (i.e. the declination angle). On June 21st and December 22nd, this angle is 23.45 º and -23.45º, respectively, while on March 22nd and September 23rd it is null. Apart from these three effects, other ones related with local variations in the atmosphere, such as water vapor, clouds, or pollution, also impact the solar resource availability. The interested reader is referred to (Meeus, 1998) for detailed solar resource availability prediction models.

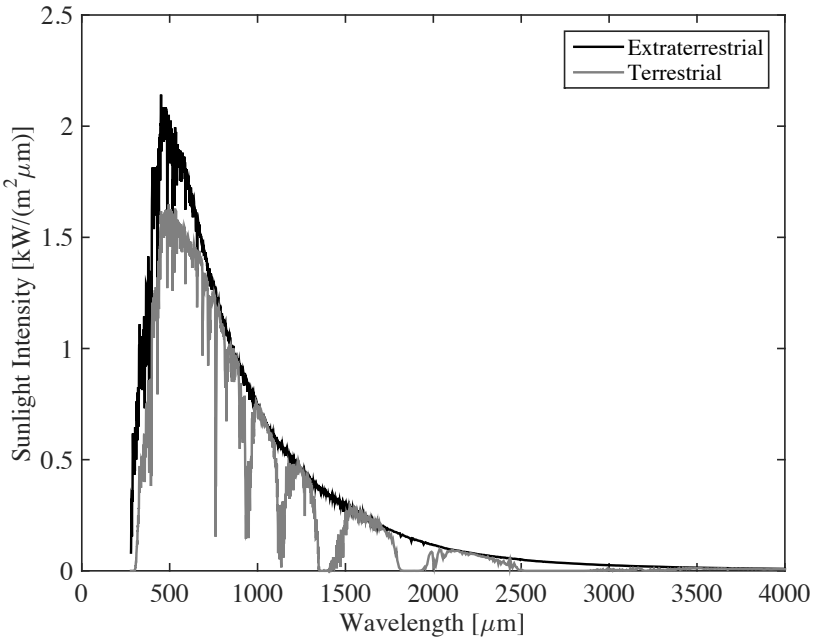

Figure 2.4 – Average Standard Solar Spectra for space and terrestrial use according to ISO 9845-1:1992. The presented terrestrial spectral radiation curve refers to Air Mass 1.5.

2.3. Photovoltaic Systems

Solar photovoltaic systems convert part of the incident solar radiation directly into electrical energy. Early in the 1950s, D. M. Chapin and his research team at Bell Labs accidentally discovered that pn junction diodes generated a voltage whose magnitude was affected by room light. In 1954 they published the preliminary findings reporting that a silicon based photocell was capable of delivering power from the sun into a resistive load at 60 W per square meter of photocell surface (Chapin, Fuller and Pearson, 1954). Since then, considerable progress has been made regarding solar photovoltaic technology efficiency (NREL, 2017) and installed capacity (IEA-PVPS, 2016b). The required effort for such evolution is mainly motivated by the following characteristics (Luque and Hegedus, 2011):

- Vast Primary energy source, widely accessible and free;
- Fairly predictable annual energy conversion output;
- No production of CO_2 equivalent emissions by the conversion process;
- The conversion process' main component (i.e. the PV module) normally lasts over 30 years;
- Allows small or large installed capacity expansions due to its modular architecture;
- Does not have any moving parts;
- Can be integrated into new or existing buildings; and
- Can be installed close to point-of-use, reducing losses and electrical grids' loads.

PV cells are mounted in modules, and multiple modules are arranged in arrays. Individual modules may have cells connected in series or parallel depending on the desired current and voltage levels (arrays of modules may likewise be connected in series or parallel). Figure 2.5 shows an equivalent circuit that can be used to represent the electrical behavior of cells, modules or arrays (Duffie and Beckman, 2013). At a fixed temperature and irradiance, the output current (I) and voltage (V) are related by:

$$\mathrm{I} = \mathrm{I_L} - \mathrm{I_D} - \mathrm{I_{SH}} = \mathrm{I_L} - \mathrm{I_O} \cdot \left[\exp\left(\frac{\mathrm{V} + \mathrm{I} \cdot \mathrm{R_S}}{\mathrm{a}} - 1\right)\right] - \frac{\mathrm{V} + \mathrm{I} \cdot \mathrm{R_S}}{\mathrm{R_{SH}}} \tag{2.8}$$

The remaining five parameters (i.e. light current (I_L), the diode reverse saturation current (I_o), the series resistance (R_s), the shunt resistance (R_{sh}) and the modified ideality factor (a)) are obtained using measurements of the current-voltage (I-V) characteristic at Standard Test Conditions[6] (STC), which are typically provided by the manufacturer. Due to its semiconductor nature, the current-voltage characteristic of a PV component is very sensitive to temperature and irradiance

[6] STC are characterized by a cell temperature ($T_{C,STC}$) of 25 ºC and a global irradiance (G_{STC}) of 1000 W/m^2.

variations. Figure 2.6 depicts this effect for the SunPower™ 300 Solar Panel, according to the model developed in (González-Longatt, 2005).

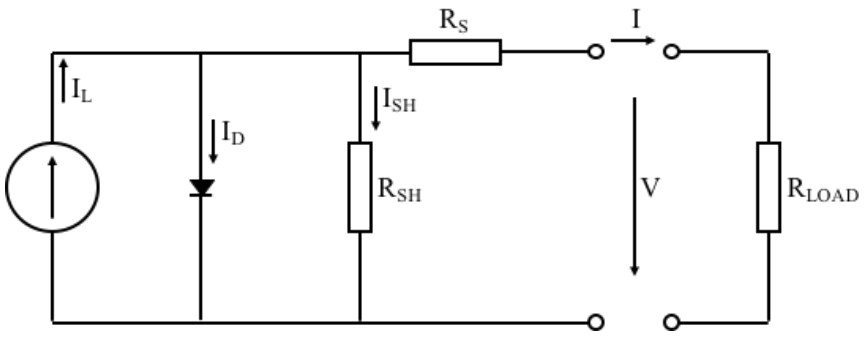

Figure 2.5 – Equivalent circuit for a PV generator.

The operating voltage *V* is adjusted in order to select the I-V pair that maximizes the module's power output, which corresponds to the rectangle of maximized area under the I-V curve. Power electronics equipment is used to implement Maximum Power Point Tracking (MPPT) algorithms. While there are many MPPT algorithms, normally the following three techniques are used (Bollen and Hassan, 2011):

- Perturb and Observe: The output voltage is perturbed in a certain direction and the resulting *dP/dV* is sampled. A positive acquired value indicates the right direction towards the maximum power point and vice versa.
- Incremental conductance: The incremental conductance *dI/dV* is used to calculate the sign of *dP/dV* as follows: $dP/dV = I + VdI/dV$. Then the voltage is adjusted accordingly as in the Perturb and Observe algorithm. Following this approach, the maximum power point is achieved faster but oscillations in power output can be registered if the atmospheric conditions change rapidly.
- Constant voltage method: The voltage that results in the maximum power is obtained assuming that the ratio between the cell voltage at maximum power and the respective open-circuit voltage is relatively constant throughout the operation range. The open-circuit voltage is acquired using an unloaded pilot cell near the module under control. This algorithm is fast and simple but its accuracy is dependent on the differences between the atmospheric conditions to which the pilot cell and the PV module under control are subjected.

A DC/DC converter is normally responsible for the implementation of the chosen MPPT algorithm. The output of this DC/DC converter feeds the DC/AC converter (inverter) that is connected to the building's AC bus (assuming that self-consumption is allowed and that energy surplus can be exported to the LVG). At the maximum power point, the building generation

profile, $\boldsymbol{BG}$, can be modeled by Equation 2.9, where N is the number of PV modules, A is the area of each module, $\boldsymbol{G}$ is the global irradiance, $\boldsymbol{\eta_M}$ is the time-varying modules' efficiency and η_E is the efficiency of the power conditioning equipment. Modules' efficiency depends on the temperature and global irradiance, being given by Equation 2.10, where $\eta_{STC}=\frac{BG_{STC}}{NAG_{STC}}$, μ is the temperature coefficient, $\boldsymbol{\theta_a}$ is the ambient temperature and $\theta_{c,NOCT} = 47\ ^{o}C$, $\theta_{a,NOCT} = 20\ ^{o}C$ and $G_{NOCT} = 800\ W/m^2$ are cell temperature, ambient temperature and irradiance at the so-called nominal operating cell temperature (NOCT), respectively (Evans and Florschuetz, 1977; Evans, 1981; Duffie and Beckman, 2013).

$$\mathbf{BG}(\mathrm{n}) = \mathrm{N} \cdot \mathrm{A} \cdot \mathbf{G}(\mathrm{n}) \cdot \boldsymbol{\eta}_{\mathbf{M}}(\mathrm{n}) \cdot \eta_{\mathrm{E}} \tag{2.9}$$

$$\boldsymbol{\eta}_{\mathbf{M}}(\mathrm{n}) = \eta_{\mathrm{STC}}\left[1 + \mu\left(\boldsymbol{\theta}_{\mathbf{a}}(\mathrm{n}) - \theta_{\mathrm{C,STC}} + \mathbf{G}(\mathrm{n})\frac{\theta_{\mathrm{C,NOCT}} - \theta_{\mathrm{a,NOCT}}}{\mathrm{G_{NOCT}}}(1 - \eta_{\mathrm{STC}})\right)\right] \tag{2.10}$$

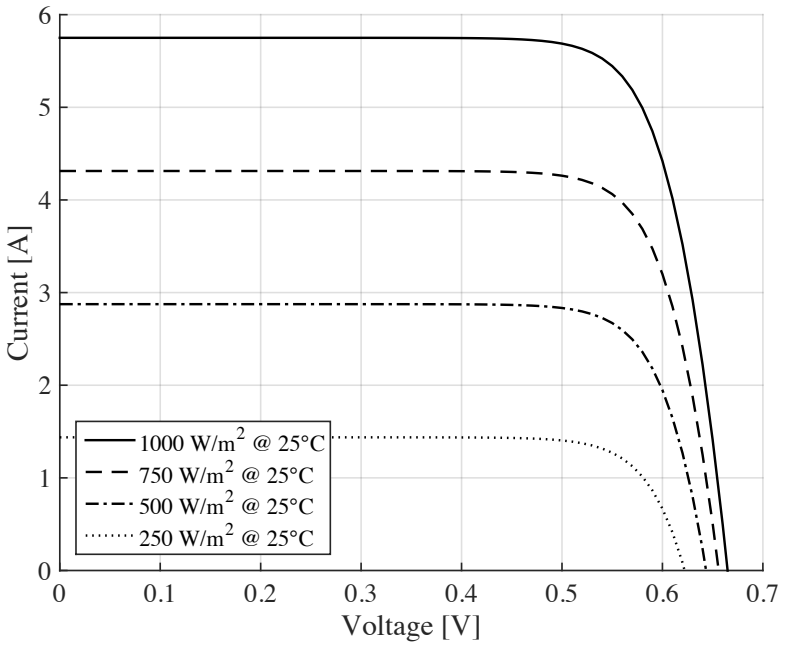

a)

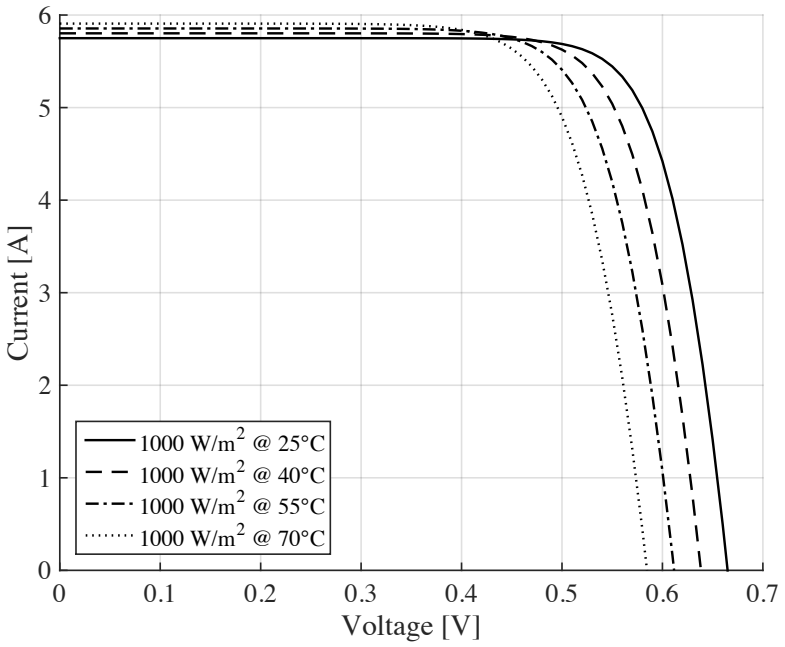

b)

Figure 2.6 – I-V characteristics for the SunPower™ 300 Solar Panel according to the model developed in (González-Longatt, 2005). a) operation at different radiation levels. b) operation at different temperatures.

CHAPTER 3

Load Matching Improvement in Buildings Equipped with Photovoltaic Systems

This chapter provides a literature review on Load Matching improvement in buildings that use PV systems to generate electricity on-site. More specifically, Section 3.1 addresses existing PV Load Matching improvement incentives, Section 3.2 provides the required Load Matching indicators, and Section 3.3 addresses existing improvement measures.

3.1. Load Matching Improvement Incentives

The traditional organization of electrical power system, adopted since the 1950s, was composed by three different levels: generation, transmission, and distribution. The generation level was typically characterized by large central power stations located far from major consumption locations. The reason for this detachment was related to technical and economic motivations (e.g. availability of the primary energy resource). The energy generated in these large electrical power stations was delivered through transmission grids, composed by high and very high voltage power lines, which could cover large distances. The electrical energy was then delivered to distribution grids, comprised by high, medium and low voltage feeders and distribution transformers, which delivered the electrical energy to final consumption entities. Due to this organization, the traditional electrical power system was characterized by unidirectional power flows from the

generation to the distribution level, leading to a straightforward system planning and operation (Lopes, Madureira and Moreira, 2013).

Due to the investments and technological evolution registered on the renewables sector in recent times, the penetration of distributed generation in the distribution level of the electrical power system has been increasing. For instance, world's installed PV capacity increased from 46 MW in 1992 to 228 GW in 2015 (IEA-PVPS, 2016b), as depicted in Figure 3.1. Additionally, under 2015 IEA WEO's New Policies Scenario, it is expected that the world's solar PV installed capacity achieves 1066 GW by 2040, corresponding to 10 % of world's installed capacity (IEA, 2015b). As a result, unidirectional power flows no longer fully characterize the planning and operation phases previously referred. This modification is undoubtedly bringing new challenges to be addressed by a new organization of the electrical power system where grids are no longer seen as passive elements (Lopes, Madureira and Moreira, 2013).

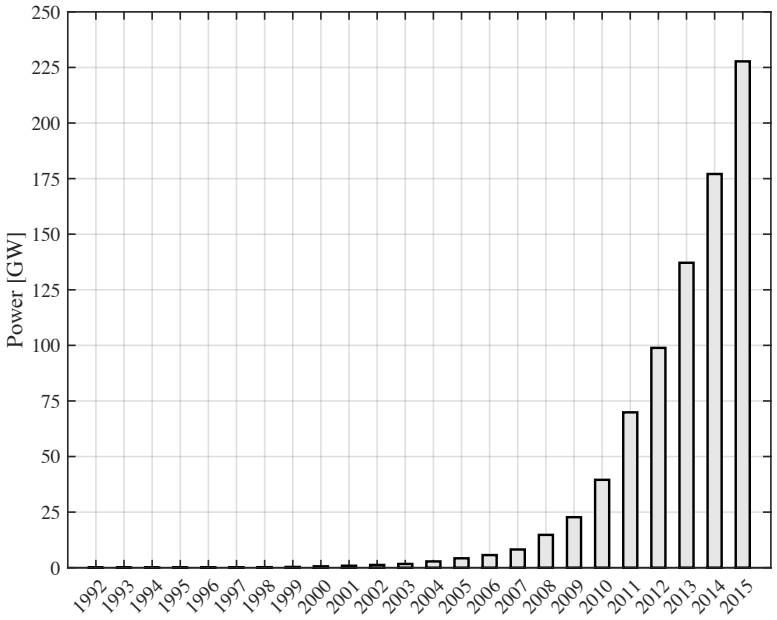

Figure 3.1 – Cumulative installed PV capacity from 1992 to 2015.

With societies so dependent on electricity, the balance between electricity supply and demand, under the new or the traditional electrical power system organization context, is ensured by both supply-focused and demand-focused strategies. Supply-focused strategies, such as building new power plants or grid reinforcement, are the most commonly used. However, demand-focused strategies have received special attention by the scientific community (Livengood, 2011). In particular, Load Management, which refers to a particular type of demand-focused strategies, have moved from pure research to implementation (Stifter *et al.*, 2016).

Load Management refers to the "*deliberate control or influencing of customer load in order to shift the time and amount of use of electric power and energy. The principal objectives of Load Management are to reduce the average cost of electricity, generally improve load factor, reduce the need for generation capacity by shifting electricity use from peak to off-peak periods, and improve system efficiency by reducing the share of electric energy provided by relatively inefficient units*" (IEEE, 1981). Two main classes of Load Management measures exist nowadays:

- Direct Load Control (DLC) – Refers to the control of specific costumers' electrical devices, performed by electric utilities, in order to conduct an efficient use of electrical power systems' resources. The controlled electrical devices are switched-off during peak periods or emergencies, which may result in some inconvenience or discomfort to customers. Therefore, economic incentives are normally offered to customers in order to encourage their participation and compensate for the referred discomfort. Space and water heating systems, as well as swimming pool pumps, are normally used as controllable devices in DLC.
- Indirect Load Control (ILC) – Consists on the use of economic incentives and disincentives to encourage voluntary changes in customers' electricity demand profiles. Such economic influences are achieved by applying specific electricity rate structures[7]. Unlike the previous referred Load Management class, under ILC electric power is always available to feed any electrical device. However, the applied electricity rate may vary with time of the day, and season of the year, in order to reduce costumers' electricity consumption during peak periods.

Taking into consideration the Load Matching improvement incentives being promoted worldwide (IEA-PVPS, 2016a), it can be concluded that these in fact represent ILC measures. The common approach is to allow local consumption of PV generation and provide a monetary compensation for the exported electricity. These ILC measures are designed in order to always benefit an electricity import and export reduction. In Portugal, for instance, according to 2014 legislation (MAOTE, 2014), self-consumption is allowed and the exported energy is paid at a value 10 % below the monthly average wholesale price. Thus, a direct benefit is offered to building owners when Load Matching values are improved. In a more general way, LM improvement is always promoted in electricity markets that lack net-metering or profitable feed-in support and where retail prices are higher than wholesale prices. This is the case for the German market, where a special rate for self-consumed electricity was introduced in 2009 aiming to promote the local consumption of on-site generated energy. This special rate was abandoned in 2012 when the feed-in tariffs became so low that a natural incentive for LM improvement was introduced (IEA-PVPS,

[7] Electricity rate design is a complex research filed with an already long history with its inception during the 1890s as reported by (Neufeld, 1987). The interested reader is referred to (Crew, Fernando and Kleindorfer, 1995) and (Sioshansi, 2013) for more details on this topic.

2013). Other countries like China, Italy or Spain have adopted similar measures (IEA-PVPS, 2016a).

3.2. Load Matching Indicators

At any given time-step n, the absolute electricity demand instantly matched by the on-site generation, denoted by $\boldsymbol{IM}(n)$, is delimited by the load itself or by the available on-site generation, as described by Equation 3.1, where $\boldsymbol{BD}(n)$ refers to building's electricity demand and $\boldsymbol{BG}(n)$ to building's on-site generation. Figure 3.2 shows the electricity demand and on-site PV generation profiles for an illustrative building[8], where the black area refers to the load instantly matched by the on-site generation, and the light grey and dark grey shaded areas are associated to the mismatch between $\boldsymbol{BD}(n)$ and $\boldsymbol{BG}(n)$ and are defined as generation surplus and demand surplus, respectively.

$$\mathbf{IM}(\mathrm{n}) = \min\{\mathbf{BD}(\mathrm{n}), \mathbf{BG}(\mathrm{n})\} \tag{3.1}$$

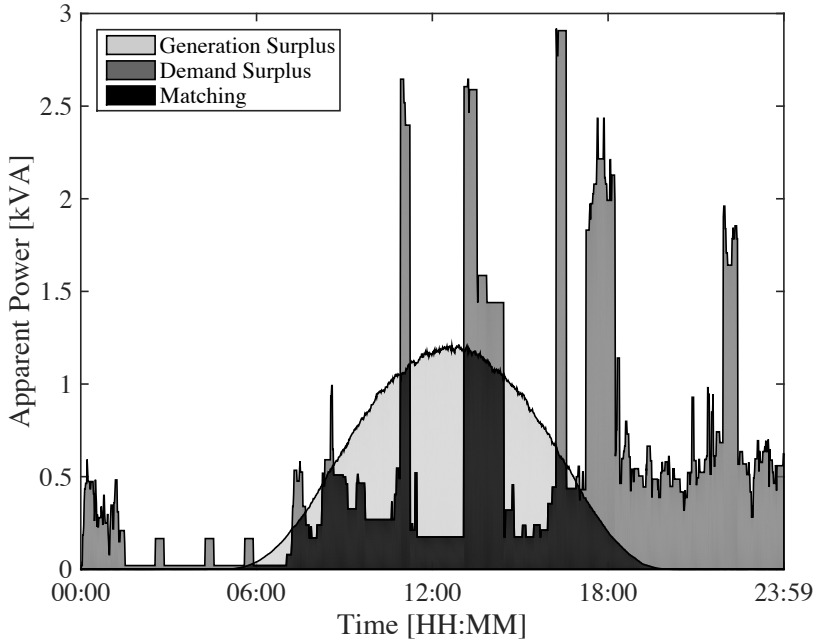

Figure 3.2 – Demand and on-site PV generation profiles for an illustrative building.

The Self-Consumption (SC) and Self-Sufficiency (SS) ratios are given by Equations 3.2 and 3.3, respectively, where n_1 and n_2 delimit the period of analysis. Equation 3.2 measures the amount of building's on-site generation that is instantaneously matched by building's electricity demand,

[8] The demand and on-site PV generation profiles used in Figures 3.2 – 3.6 were obtained using models described in Sections 5.3.1 and 5.3.2.

while Equation 3.3 measures the amount of building's electricity demand that is instantaneously matched by building's on-site generation, both over the time period defined by n_1 and n_2. Detailed reviews and assessments of LM indicators can be found in (Salom *et al.*, 2011, 2013, 2014; Berggren, Widen and Wall, 2012; Cao, 2014). Additionally, in (Cao, Hasan and Sirén, 2013a, 2013b, 2014; Cao *et al.*, 2014), a series of studies conducted by Cao et al. can be found on detailed LM assessments in buildings connected to heating, cooling and electrical grids and integrating on-site generation devices of these three energy forms.

$$\mathrm{SC} = \frac{\sum_{n=n_1}^{n_2} \mathbf{IM}(n)}{\sum_{n=n_1}^{n_2} \mathbf{BG}(n)} \cdot 100, \sum_{n=n_1}^{n_2} \mathbf{BG}(n) > 0 \tag{3.2}$$

$$\mathrm{SS} = \frac{\sum_{n=n_1}^{n_2} \mathbf{IM}(n)}{\sum_{n=n_1}^{n_2} \mathbf{BD}(n)} \cdot 100, \sum_{n=n_1}^{n_2} \mathbf{BD}(n) > 0 \tag{3.3}$$

Two relevant factors affect the computation of Equations 3.2 and 3.3, namely, the relative size of the installed PV generation system and the time resolution of the demand and on-site generation profiles. While the former is related to the physical process itself, the latter only impacts the output of the referred metrics.

3.2.1. Relative size of the PV generation

When the relative size of the PV generation increases, the electricity demand instantly matched by the on-site generation also increases or at least remains unchanged. This is illustrated in Figure 3.3 a), where the absolute electricity demand instantly matched (***IM***) increased from 4.9 kWh to 6.1 kWh, when compared with the scenario expressed in Figure 3.2. The SS ratio, calculated over the presented 24 h period (1-min resolution data), follows this trend and grows from 35.9 % to 44.6 %. Regarding the SC ratio, it goes on the opposite direction and decreases from 53.9 % to 44.7 %, reflecting the higher generation surplus. When the relative size of the PV generation decreases, as illustrated in Figure 3.3 b), the same reasoning holds and the SC ratio increases to 78.6 % while the SS decreases to 19.59 %.

On a yearly basis, in the case of Net-ZEBs, SC and SS ratios exhibit the same value if computed over the Balance Period. Figure 3.4 presents these two metrics, computed over a 1-year period, as function of the ratio between annual on-site generation and demand, where the interception between the curves refers to the Net-ZEB status (assuming the following: electricity as the only energy carrier involved in the operation of this building, site energy consumption as Balance Metric, and a 1-year Balance Period). SC and SS ratios are monotonically decreasing and increasing functions of the annual relative on-site generation, respectively. The electricity demand

instantly matched by the on-site generation (***IM***), found on the numerators of Equations 3.2 and 3.3, increases until all daytime electricity demand is covered by the on-site generation. After this point, the SC ratio continues to decrease as the annual on-site generation increases (which impacts Equation 3.2 denominator), while the SS ratio remains unmodified.

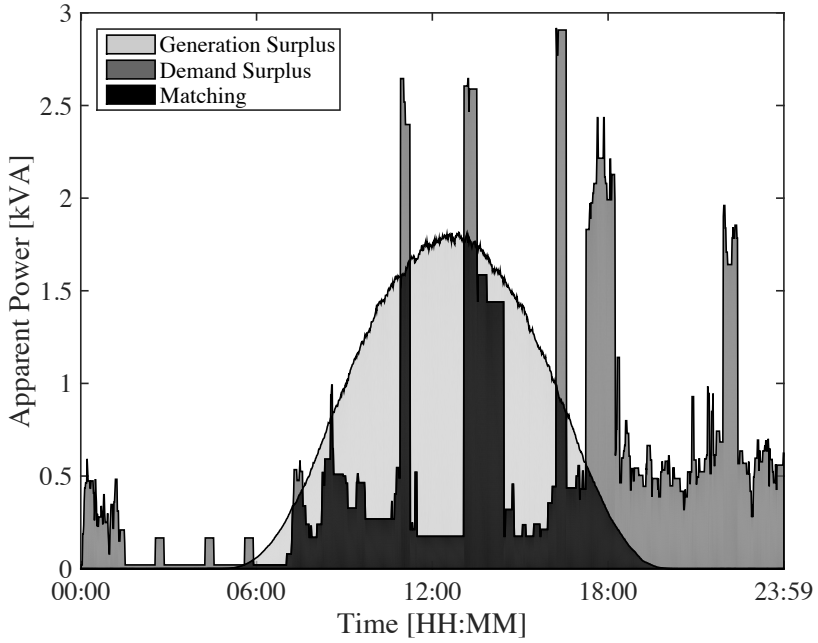

a)

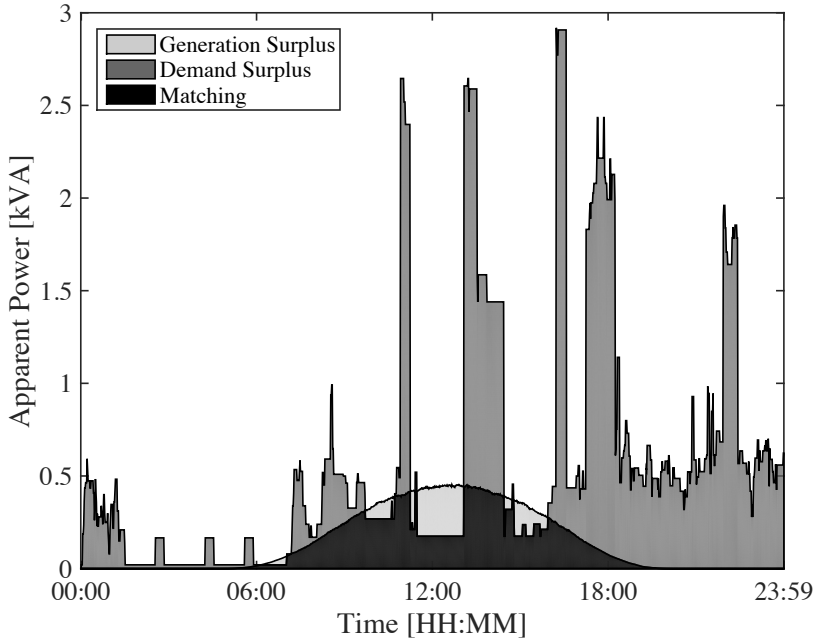

b)

Figure 3.3 – Impact of different relative PV generation sizes. a) Higher PV generation. b) Lower PV generation.

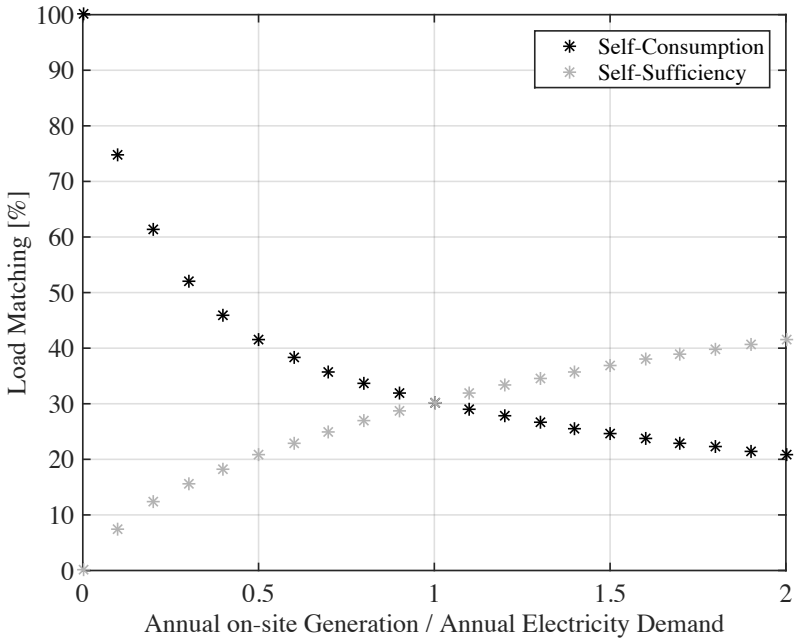

Figure 3.4 – SC and SS ratios as a function of the ratio between the annual on-site electricity generation and the annual electricity demand.

3.2.2. Time-resolution

SC and SS ratios are computed using discrete data series. Due to technical constrains (e.g. lack of large data storage resources), data series with 1-hour resolution are commonly used (Hoevenaars, 2012). However, such resolution may not be suitable to capture demand and generation fast variations that occur along the day. One example is the power generation of a PV system during a scattered cloudy day, where power output changes are distinctly observed depending on the time-resolution used, as depicted in Figure 3.5. Another example refers to electricity demand profiles, as fast electricity demand variations are covered up by lower time-resolution data series, as presented in Figure 3.6. In fact, the electricity demand peak is attenuated by almost 50 %, when comparing 1-min and 60-min resolution data series.

In recent years, several authors have studied the impact of selecting different time resolution data series in on-site generation analyses (Hawkes and Leach, 2005; Wright and Firth, 2007; Paatero and Lund, 2010; Hoevenaars and Crawford, 2012). The common conclusion is that lower time-resolutions result in higher errors. Regarding LM analysis, Cao and Sirén (2014) concluded that low resolution data series (1-hour) could introduce errors higher than 60 % on the obtained metrics.

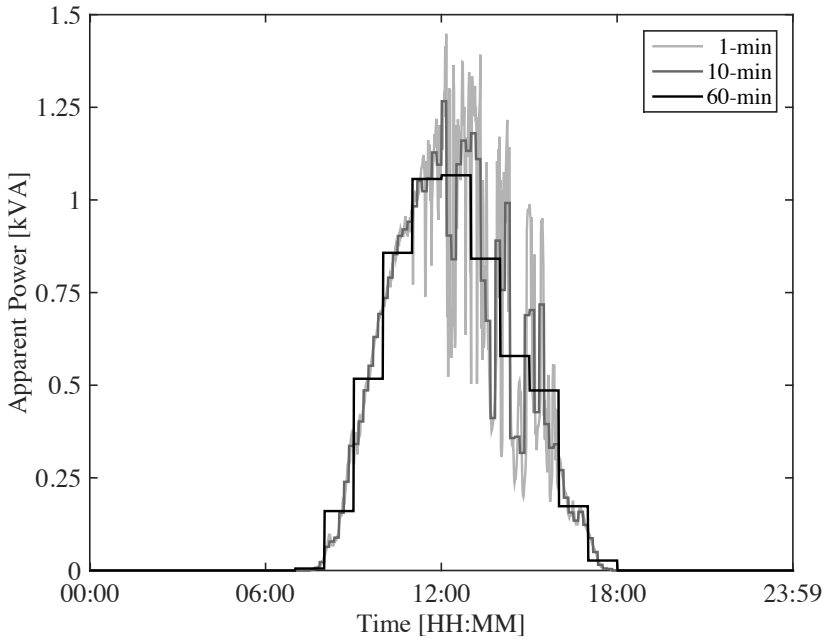

Figure 3.5 – PV generation profile during a scattered cloudy day considering different time-resolutions.

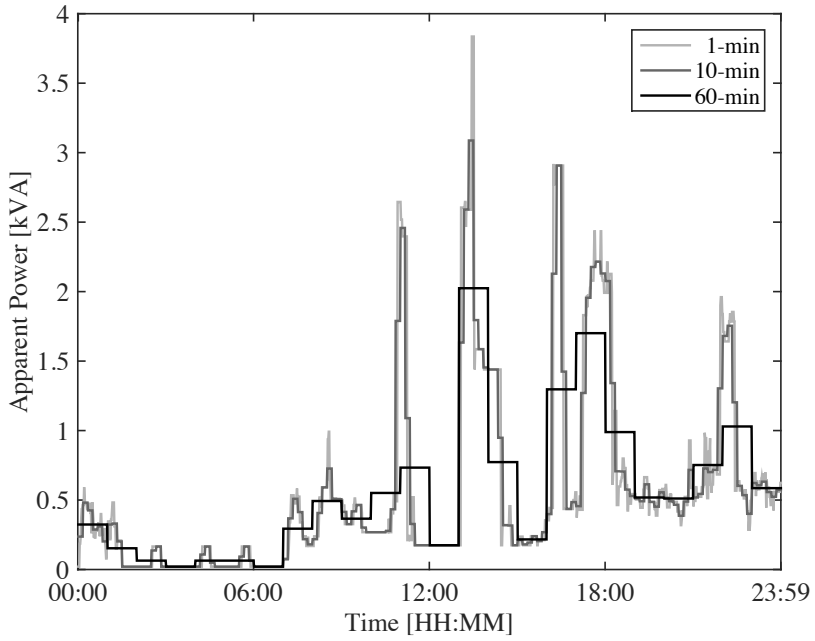

Figure 3.6 – Electricity demand profile of an illustrative building considering different time-resolutions.

3.3. Load Matching Improvement Measures

According to the ongoing International Energy Agency's Energy in Buildings and Communities Programme Annex 67 project "*Energy Flexible Buildings*" (IEA-EBC, 2017), the term "Energy Flexibility" refers to a building's ability to change its demand and/or generation according to local climate conditions, user needs and grid requirements. Regarding LM improvement, climate conditions are related with the on-site generation; user needs refer to the required comfort levels and electricity related costs; and the grid requirements concern the impacts introduced by buildings' operation. Taking this into consideration, Figure 3.7 illustrates the three possible strategies that can be followed to improve LM values using the existing Energy Flexibility. Strategies A and B refer to demand surplus shifting, as they consist in delaying and anticipating the operation of some electricity demand controllable devices, respectively. Strategy C concerns generation surplus shifting using energy storage devices.

The following sections review the existing LM improvement measures, clustering the respective studies by the type of electrical device used to shift demand or generation surplus. This literature review is focused on residential buildings that use PV systems to generate electricity on-site. This type of buildings is of special importance to the LM improvement field due to the intrinsic mismatch between the on-site generation and buildings' occupancy and, consequently, buildings' electricity demand (Luthander *et al.*, 2015). Instantaneous SC ratio values around 30 % are typically registered in the residential sector when no LM improvement measures are applied (European Commission, 2015).

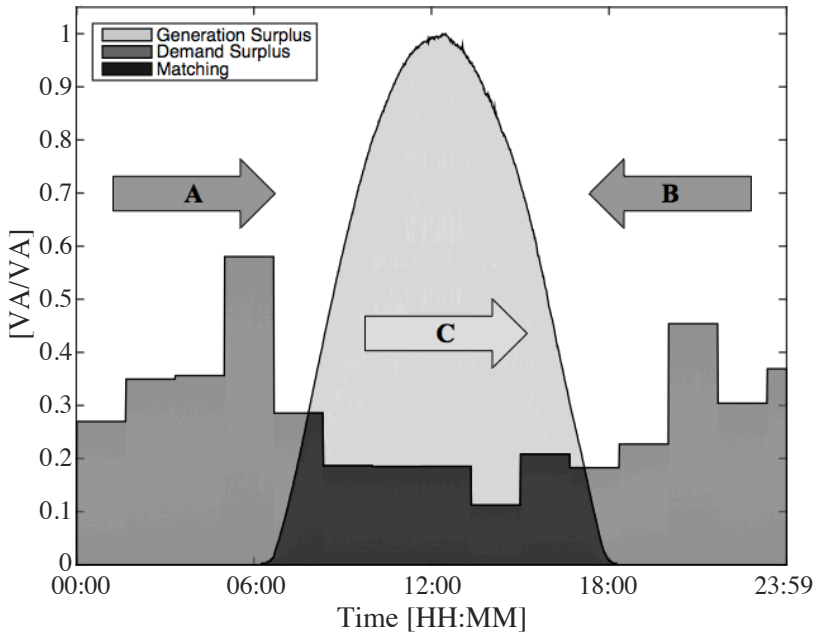

Figure 3.7 – Demand and on-site PV generation profiles for an illustrative building highlighting the options to improve LM.

3.3.1. Event-Based Devices

An Event-Based (EB) device is characterized by having a fixed electricity demand profile with working cycles that can range from minutes to hours. Among others, examples of electrical devices falling into this category are:

- Washing Machine;
- Clothes Dryer; or
- Dishwasher.

Although time invariant, the electricity demand profile of an EB device generally depends on its technological characteristics and selected working program. Generic patterns have been identified in (Stamminger, 2008) for the referred EB devices, as shown in Figure 3.8.

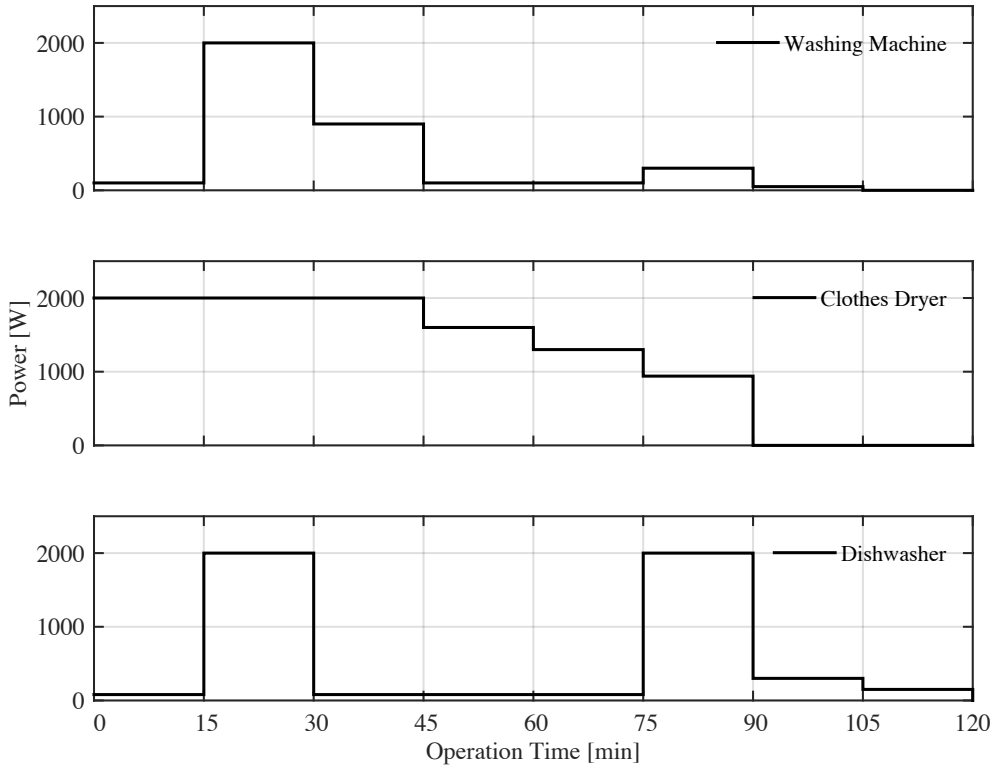

Figure 3.8 – Generic EB devices' load diagrams according to (Stamminger, 2008).

Based on the information provided in (Staats, de Boer-Meulman and van Sark, 2017), Table 3.1 describes the operation of the EB devices addressed in Figure 3.8 considering 15-min time-steps. Figure 3.9 presents the estimated normalized average load diagram of these devices in Portugal accordingly to (DGGE/IP-3E, 2004). While overlap between the estimated electricity demand and the solar resource availability may exist, there is still a large potential to improve LM values.

The user's need for the service provided by EB devices is normally decoupled from the respective energy consumption (D'hulst *et al.*, 2015). As a result, the operation starting time of these devices can be delayed over a shifting window (strategy A in Figure 3.7). Several studies focusing LM improvement implemented through the control of EB devices can be found in the literature (Widén, Wäckelgård and Lund, 2009; Castillo-Cagigal *et al.*, 2010, 2011; Nicola, Toledo and Zamb, 2013; Widén and Munkhammar, 2013; Widén, 2014). These studies refer to off-line scenarios, using measured and/or simulated data, and assuming 24 h shifting windows. Three factors affecting the LM improvement values can be identified, namely: i) some of the controllable demand is already matched by the energy generated on-site; ii) lack of PV surplus due to little or no primary energy resource (mainly in the winter); and iii) lack of PV surplus due to matching between not controllable demand and the energy generated on-site.

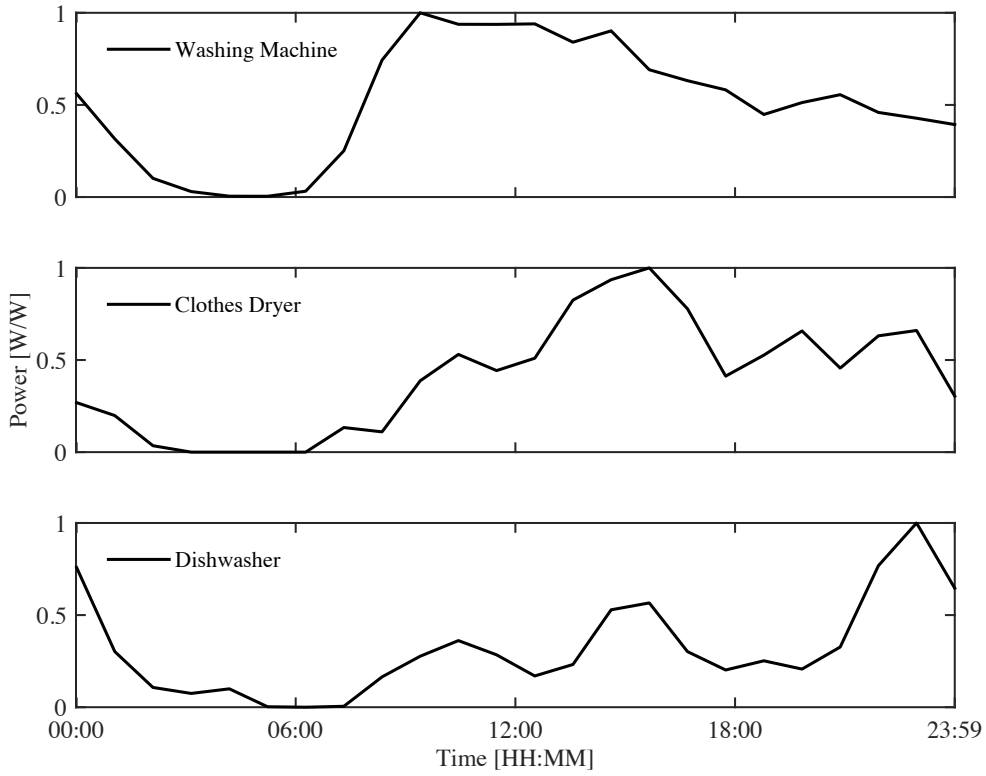

Figure 3.9 – Estimated normalized average power consumption profile of some Event-Based devices in Portugal according to (DGGE/IP-3E, 2004).

Table 3.1 – Generic electricity demand profiles for three EB devices.

Step	Washing Machine	Clothes Dryer	Dishwasher
1	Water pumping through detergent container Power: 100 W	Air heating and forced flow Power: 2000 W	Water pumping + spraying arm rotation Power: 80 W
2	Water heating + drum rotation Power: 2000 W	Air heating and forced flow Power: 2000 W	Water heating + spraying arm rotation Power: 2000 W
3	Water heating + drum rotation Power: 900 W	Air heating and forced flow Power: 2000 W	Spraying arm rotation Power: 80 W
4	Low speed drum rotation Power: 100	Air heating and forced flow Power: 1600 W	Spraying arm rotation Power: 80 W
5	Low speed drum rotation + water pumping Power: 100	Air heating and forced flow Power: 1300	Spraying arm rotation Power: 80 W
6	High speed drum rotation Power: 300	Air heating and forced flow Power: 940	Water heating + spraying arm rotation Power: 2000 W
7	Water pumping + residual power consumption of e.g. appliance console Power: 50	-	Water pumping Power: 300 W
8	-	-	Residual power consumption of e.g. appliance console Power: 150 W

3.3.2. Thermostatically-Controlled Devices

A Thermostatically-Controlled (TC) device is characterized by having its energy consumption related with the temperature registered on a certain system (e.g. the inner temperature of a specific building). Using the respective thermal storage properties, the energy consumption of these devices can be delayed (strategy A in Figure 3.7) or anticipated (strategy B in Figure 3.7). The following are examples of TC devices:

- Refrigerator;
- Heat pump;
- Floor heat radiator; or
- Electric water heater.

As an example, Figure 3.10 shows the electricity demand profile of a typical domestic refrigerator[9] and the respective inner temperature. The electricity consumption of this device is controlled by a thermostat that preserves the inside temperature within a certain range. The working cycles start when the inner temperature reaches the upper limit and stop when it reaches the bottom limit (energy losses are responsible for the temperature rising effect). Due to its thermal energy storage properties, refrigerator's electricity consumption can be shifted in time with no significant effects on the inner temperature. To illustrate the considered refrigerator's Energy Flexibility, its compressor was turned-off for 5 minutes when the respective working cycle was running. As it can be seen by Figure 3.10, this delay introduced on the refrigerator's electricity consumption had negligible effects on the service provided by the electrical device. Annex A describes the data acquisition and control system used to perform this experiment.

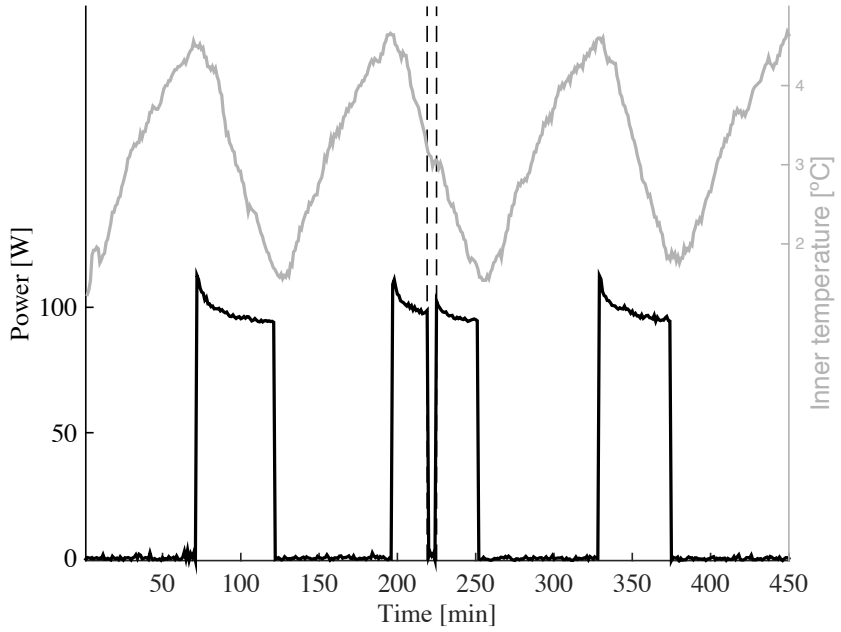

Figure 3.10 – Refrigerator's inner temperature and power consumption during the experiment where the compressor is turned-off for 5 minutes at time-step 219.

The experiment reported in Figure 3.10 illustrates how TC devices can be used to add some flexibility to buildings' electricity demand. In (Williams, Binder and Kelm, 2012; Reynders, Nuytten and Saelens, 2013; Sossan *et al.*, 2013; Dar *et al.*, 2014; Thygesen and Karlsson, 2014; Vanhoudt *et al.*, 2014; Lorenzi and Silva, 2016; Thygesen, 2016) different TC devices were used to improve PV LM (heat pumps, electric water heater, floor heat radiator). These studies are based on off-line assessments using measured and/or simulated data. Detailed building or device (e.g.

[9] Indesit BAN 12 equipped with a ZBT1112CY compressor.

electrical water heater) models are normally required. A considerable limitation of these methods is related with the seasonal mismatch between thermal demand and PV generation in cooler regions (e.g. users' comfort needs set restrictive limits to use a floor heat radiator during summer time to absorb PV surplus (Reynders, Nuytten and Saelens, 2013)). In warmer regions, where the electricity demand of air-conditioning devices correlates with daily and yearly solar energy availability, the LM improvement potential is higher.

3.3.3. Storage Devices

Energy Storage (ES) devices absorb energy and store it for a period of time before releasing it again. Through this process, ES devices are suitable to shift generation surplus to periods with demand surplus (strategy C in Figure 3.7). For LM improvement in residential buildings, the most used ES technologies are Electrochemical storage and Chemical (Hydrogen) storage (Luthander *et al.*, 2015).

Electrochemical storage is achieved by using batteries composed by two or more electrochemical cells that enable the flow of electrons resulting from the induced chemical reactions (IEA, 2014b). Different types of batteries can already be found as market-ready products, with lead acid and lithium-ion batteries being the most common solutions (Letcher, 2016). Lithium-ion batteries exhibit, in general, higher performance factors but are more expensive (Bocklisch, 2015). However, it is expected that this disadvantage will be attenuated in the near future with the effort of new and existing suppliers (e.g. Tesla, Panasonic or SMA).

Chemical (Hydrogen) storage solutions use on-site generated energy to split water into hydrogen and oxygen through electrolysis (this process takes place in a device called electrolyzer). The resulting hydrogen is normally stored in high pressure tanks and can be latter used to generate electricity using a fuel cell (IEA, 2014b). While self-discharge is close to zero, the round-trip efficiency of the process is around 36 % (this value can be increased if the heat resulting from the fuel cell operation is used to satisfy users' thermal needs) (IEA, 2015a). Additional storage tanks can be integrated along the life cycle of the respective storage systems to increase the storage capacity.

The relative high self-discharge rates of lead acid (2 to 20 % per month) and lithium-ion (1 to 5 % per month) batteries and their high round-trip efficiency (70 to 90 % for lead acid and 85 to 95 % for lithium-ion) make these solutions more suitable for short-term LM improvement (e.g. storage of generation surplus during midday to use during the evening when demand surplus is registered) (Letcher, 2016). On the other hand, due to its low self-discharge rates and capacity to integrate additional storage tanks along the time, chemical (Hydrogen) storage is best suitable for long-term LM improvement (e.g. storage of generation surplus during the summer to use during winter cloudy days).

A vast collection of studies addressing LM improvement using Electrochemical and Chemical (Hydrogen) storage can already be found in the literature (e.g. (M. Braun, K. Büdenbender, D. Magnor, 2009; Vrettos *et al.*, 2013; Bruch and Müller, 2014; Waffenschmidt, 2014; Weniger, Tjaden and Quaschning, 2014; Merei *et al.*, 2016; Vieira, Moura and de Almeida, 2017)). From these studies, it can be concluded that Electrochemical and Chemical (Hydrogen) storage are an effective mean to improve residential LM. In fact, if large enough capacities are considered, LM values close to 100 % can be obtained. In the referred studies, LM improvement is normally implemented at Building-Level, but real world application at a district-level have already been implemented. As an example, one can mention the recent case of island of Ta'u in American Samoa, where a 1.4 MW PV system, assisted by a lithium-ion based storage capacity of 6 MWh, was added to the existing microgrid (SolarCity, 2017). Before recurring to this solution, this island relied only on generators that consumed around 415,000 liters of diesel per year plus shipping. Although no specific LM values are provided, it is stated that the energy stored in the lithium-ion based Tesla Powerpacks (see Figure 3.11) is enough to supply the entire island (600 residents) for 3 days if no solar energy is provided and that it can be recharged in 7 hours if the primary energy resource is available. This PV system, supported by lithium-ion based batteries, allowed a mitigation of power intermittency and outages due to diesel supplying difficulties. A reduction on diesel generators CO_2-equivalent emissions was also pointed out as a motivation. However, the biggest advantage is referred to be the cost, since almost no diesel is needed nowadays and expenses related with shipping were minimized. Additionally, higher energy security was achieved by not relying only on fluctuating fossil fuel prices.

While improving the LM values, ES devices can also be controlled in order to reduce the respective building's feed-in power values. These control strategies are of special importance when feed-in restrictions exist, as it is observed in Germany (SMA, 2016). SMA company, through its product "Sunny Home Manager 2.0" (SMA, 2017), is already offering such solutions in the market. The followed strategy consists in saving storage capacity during the morning in order to absorb the higher feed-in power values registered around noon.

Figure 3.11 – Lithium-ion based Tesla Powerpacks (6 MWh) (SolarCity, 2017).

3.3.4. Electric Vehicles

In 2014, transport in general accounted for 30.5 % of EU CO_2 emissions, where 72.8 % of these were related with road transportation (European Commission, 2016). Electric Vehicles (EVs) are seen as part of the solution to mitigate such CO_2 emissions. As the prices of batteries in particular and EVs in general decrease, it is expected that a higher number of these vehicles are integrated in the transport system (Nykvist and Nilsson, 2015).

EVs' battery charging process is considered as an interesting way to implement LM improvement measures. For instance, if the user provides a time period in which the EV is not needed and the desired state of charge at the end of this period, then a charging management system can control the energy delivered to the battery in order to e.g. improve the LM of a specific building (strategy A in Figure 3.7). Furthermore, if a Vehicle-to-Grid (V2G) concept is considered, the battery can also provide energy to satisfy demand surplus (strategy B in Figure 3.7). Regarding LM in residential buildings equipped with PV systems, the literature shows that improvement using EVs is limited due to the mismatch between the availability of the primary energy resource and the charging patterns (Munkhammar, Grahn and Widén, 2013). (Garcia-Valle and Lopes, 2013) provide additional information on EVs and their important role in the near future of the electrical power systems.

3.4. Discussion

Four types of devices are normally considered to improve LM in residential buildings (i.e. EB devices, TC devices, ES devices, and EVs). A common characteristic is shared among these devices: they can offer a certain degree of Energy Flexibility to the respective building. EB devices can have their electrical consumption decoupled from the need for the service they provide, which sets the possibility to delay their electrical consumption during a user defined shifting window (24 h shifting windows are normally considered). TC devices use the respective thermal properties to store energy and therefore delay or anticipate some of a building's electricity demand while taking into consideration the users' comfort needs. ES devices allow generation surplus shifting (delay) to periods with excessive electricity demand, offering flexibility to buildings' on-site generation. EVs can offer Energy Flexibility to buildings' electricity demand by i) allowing smart charging strategies over user defined charging windows and ii) offering energy storage services while connected to buildings' electrical circuit.

From a technical point of view, EB devices are the best suited for LM improvement systems. The reason for this is twofold: i) they exhibit a time invariant load diagram; and ii) EB devices do not need complex automatic control systems (they can be controlled manually or controlled by simple relays that implement the computed operation starting times (D'hulst *et al.*, 2015)). Another advantage of EB devices is related with the fact that any operation time shifting will not result on an energy losses increase. Additionally, high ownership rates of some EB devices are commonly observed – e.g. 92% of Portuguese households have washing machines (INE and DGEG, 2011). TC devices can operate with no user mediation as long as users' comfort needs are satisfied. However, large investments in dedicated temperature sensors and actuators are normally required. Still on the demand side, EVs present great potential to be controlled by LM improvement systems but strong mismatch normally exists between the periods with generation surplus and the charging patterns in residential buildings (Munkhammar, Grahn and Widén, 2013). ES devices are the most effective solution to improve LM in residential buildings. These devices can shift generation surplus to periods with excessive demand with no concerns about users' comfort needs and using dedicated State of Charge controllers already available in the market. However, due to the large investment required, these devices are only profitable in locations where the existing power system is based on e.g. expensive diesel generators operation as it has been the case of the island of Ta'u in American Samoa (SolarCity, 2017). As new players start to introduce more ES devices in the market and the demand for LM improvement systems increases, the prices are expected to decrease. The resulting energy losses should also be taken into consideration when using ES devices to improve LM. These losses should not be considered as a contribute to increase LM since the referred energy is not used to satisfy the buildings' electricity demand.

At the moment, LM improvement systems based on information reported by existing monitoring systems can already be profitable since short to no investment is needed (this is the case of LM improvement systems based on EB devices manually controlled by users). In the future, mixed approaches, in which ES devices are used together with electricity demand devices, can be implemented to decrease the initial investment on ES devices (i.e. smaller storage devices are needed if demand surplus decreases through the operation shifting of some electricity demand devices). Some studies, where ES devices are used together with electricity demand devices to improve LM in residential buildings, can already be found in the literature (Castillo-Cagigal *et al.*, 2010, 2011; Matallanas *et al.*, 2012; Nicola, Toledo and Zamb, 2013; Widén and Munkhammar, 2013). The LM improvement values registered in these studies are always higher when EB devices are also controlled, comparing with initial scenarios with only ES devices.

When electricity demand devices are considered, the reviewed works implement LM improvement measures in individual buildings without taking into consideration the demand and generation profiles of the other buildings that are connected to the same LVG (i.e. Building-Level LM improvement measures). In line with this, the reviewed works do not assess the benefits introduced to LVG operators, assuming that LM improvement implemented at Building-Level is always benefic to this entity. In the research work presented in this dissertation, such assumption is considered as a knowledge gap, being addressed by hypothesis H #1. Additionally, no Community-Level LM improvement measure, using electricity demand devices, was found in the literature. This second knowledge gap is addressed by hypothesis H #2, aiming to improve the benefits offered to building owners and LVG operators (comparing to Building-Level approaches). For this purpose, the concept of Cooperative Net-Zero Energy Community (CNet-ZEC) is introduced in Chapter 4.

CHAPTER 4

Cooperative Net-Zero Energy Community

The Community-Level LM Improvement (CL-LMI) measure used to assess hypothesis H #2 is presented in this chapter. This measure is based on the Cooperative Net-Zero Energy Community (CNet-ZEC) concept whose main components are described in the following sections.

4.1. Conceptual Vision

Under the new organization of the electrical power system, LVGs have not only to supply the consumption entities but also to receive electricity from the existing generation devices. Additionally, as illustrated in Figure 4.1, both types of devices (consumption and generation) can be associated with the supplied buildings or directly connected to the distribution feeder. Therefore, at the distribution transformer output, which represents the interface between the MV and LV parts of the respective distribution grid, the LVG electricity demand $\boldsymbol{LVG\_D}$ and generation $\boldsymbol{LVG\_G}$ profiles are given by Equations 4.1 and 4.2, respectively. $\boldsymbol{idd}$ and $\boldsymbol{idg}$ refer to the electricity demand and generation profiles of each individual device i directly connected to the distribution feeder, respectively. Street lighting, EVs charging stations or PV covered parking structures are examples of such devices. Still in Equations 4.1 and 4.2, $\boldsymbol{BD}$ and $\boldsymbol{BG}$ represent the electricity demand and on-site generation profiles of each building b, while N_B and N_id refer to the number of buildings and individual devices connected to the LVG.

$$\mathbf{LVG\_D}(\mathrm{n}) = \sum_{\mathrm{b}=1}^{\mathrm{N\_B}} \mathbf{BD}_{\mathrm{b}}(\mathrm{n}) + \sum_{\mathrm{i}=1}^{\mathrm{N\_id}} \mathbf{idd}_{\mathrm{i}}(\mathrm{n}) \tag{4.1}$$

$$\mathbf{LVG\_G}(\mathrm{n}) = \sum_{\mathrm{b}=1}^{\mathrm{N\_B}} \mathbf{BG}_{\mathrm{b}}(\mathrm{n}) + \sum_{\mathrm{i}=1}^{\mathrm{N\_id}} \mathbf{idg}_{\mathrm{i}}(\mathrm{n}) \tag{4.2}$$

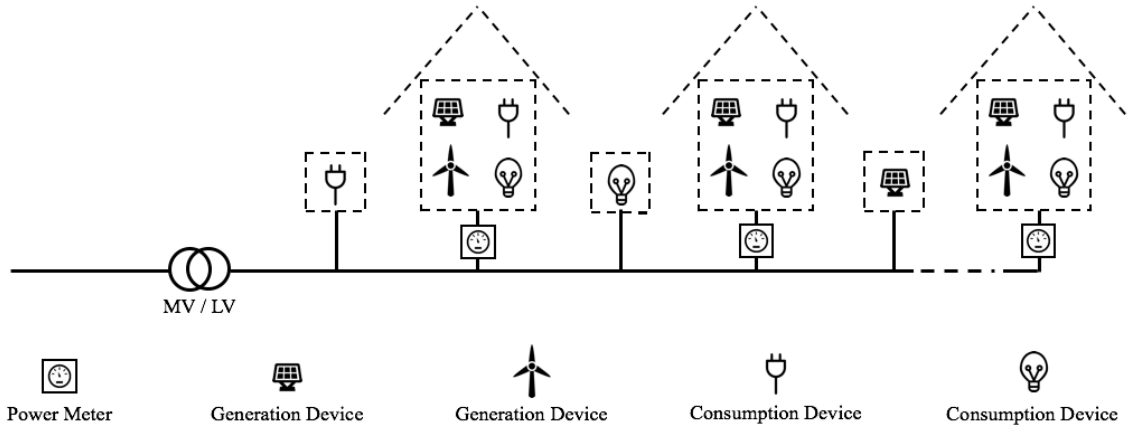

Figure 4.1 – Illustrative representation of entities interacting with a specific LVG.

In the reviewed literature, the Energy Flexibility offered by electricity demand devices is used to improve LM only at Building-Level (see Section 3.3). Following this approach, Building-Level Load Matching Improvement (BL-LMI) measures are conducted at each individual building without taking into consideration the demand and on-site generation profiles of the remaining buildings that are connected to the same LVG or the contribution of the individual devices directly connected to the LVG, as illustrated in Figure 4.2. Therefore, according to hypothesis H #1, despite the fact that a LM optimization may be achieved at each individual building's point of common coupling, it is not guaranteed that such optimization is benefic to the considered LVG's operation.

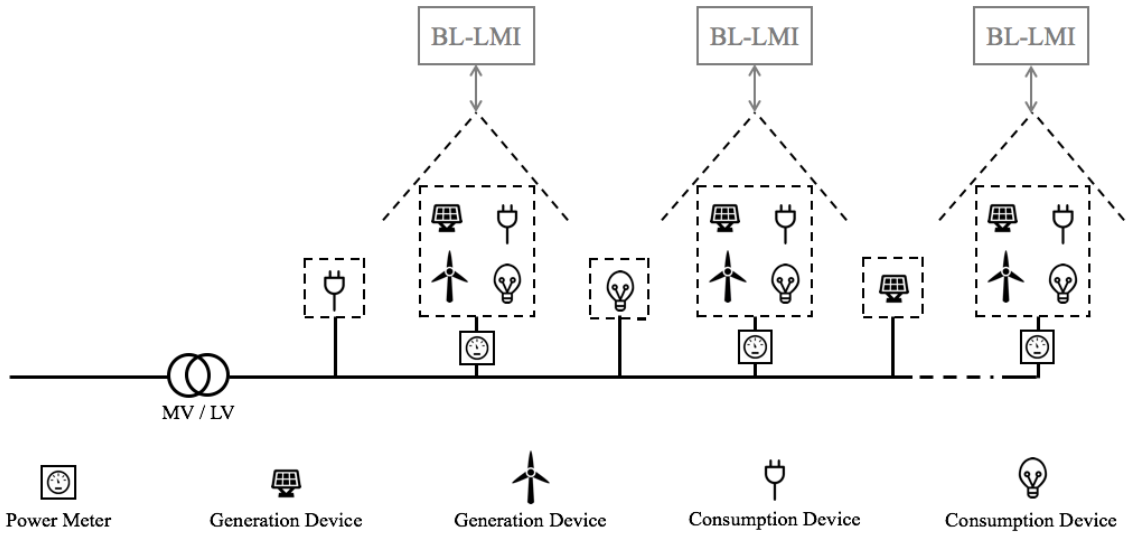

Figure 4.2 – Illustrative representation of Load Matching improvement measures conducted at Building-Level.

Taking into consideration hypothesis H #2, the Cooperative Net-Zero Energy Community concept is introduced in this work in order to extend the LM improvement field to the Community-Level and thus improving the benefits offered to both LVG operators and building owners. A CNet-ZEC is composed by N_B buildings fed by the same LVG that, together with the individual devices directly connected to the grid, cooperate to improve LM values at LVG's MV/LV transformer output. This cooperation is managed by the Community Energy Manager (C-EM) using the Energy Flexibility available in the entire community (i.e. the aggregated flexibility). Additionally, in order to improve the benefits offered to building owners, community's buildings share a common meter located at the transformer output instead of being charged individually by the electricity retailer. The relationship between the CNet-ZEC and the external entities, such as the electricity retailer, is managed by the Community Administrator (C-ADMIN). The proposed CL-LMI measure is conceptually represented in Figure 4.3.

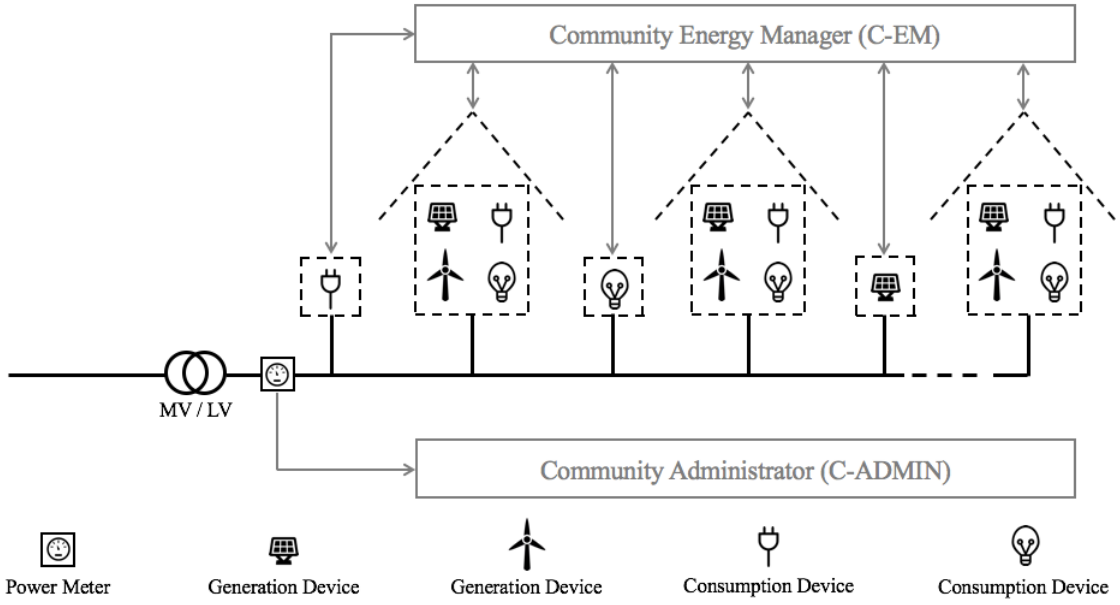

Figure 4.3 – Illustrative representation of the proposed Community-Level Load Matching improvement measure.

The term "Net-Zero" is used to underline the fact that, over a specific period of time, a zero NB is achieved by a CNet-ZEC. In this case, the NB refers to the difference between the energy imported and exported by the entire community. Nevertheless, if a NB lower/higher than zero is registered, the cooperative community under analysis is defined as a nearly/plus CNet-ZEC. As in Net-ZEBs, Balance Boundary, Balance Period, and Balance Metric concepts are used to compute a CNet-ZEC's NB. Among these, only the Balance Boundary differs from the ones addressed in Sections 2.1.1 – 2.2.3 as follows: for each Energy Carrier, demand and generation devices are considered to be within CNet-ZEC's Balance Boundary if the respective buildings are

supplied by the LVG. Additionally, electrical devices directly connected to the LVG are also considered to be within CNet-ZEC's Balance Boundary. Therefore, considering the Balance Boundary, Balance Period, and Balance Metric, the CNet-ZEC's NB is given by Equation 4.3, where $\boldsymbol{CD}_{EC}$ and $\boldsymbol{CG}_{EC}$ refer to the community's energy demand and generation associated to each one of the N_EC Energy Carriers. If only electricity is considered as Energy Carrier, Equations 4.1 and 4.2 represent $\boldsymbol{CD}_{EC}$ and $\boldsymbol{CG}_{EC}$, respectively.

$$\mathrm{NB} = \sum_{\mathrm{EC}=1}^{\mathrm{N\_EC}} \sum_{\mathrm{n}=1}^{\mathrm{T}} \mathbf{M}_{\mathrm{EC,E}}(\mathrm{n}) \times \mathbf{CG}_{\mathrm{EC}}(\mathrm{n}) - \sum_{\mathrm{EC}=1}^{\mathrm{N\_EC}} \sum_{\mathrm{n}=1}^{\mathrm{T}} \mathbf{M}_{\mathrm{EC,I}}(\mathrm{n}) \times \mathbf{CD}_{\mathrm{EC}}(\mathrm{n}) \tag{4.3}$$

4.2. Community Administrator (C-ADMIN)

The C-ADMIN is in charge of managing the relationship between the CNet-ZEC and the respective external entities while ensuring benefits to building owners and the LVG operator. Although this document can support the respective negotiations, details about them are out of scope. Nevertheless, in the following paragraphs three examples of interested external entities are provided, namely, LVG operator, electricity retailer, and owners of individual devices directly connected to the grid.

The LVG operator's main goal concerns the reduction of its operation costs while ensuring satisfactory levels of reliability and quality of supply. Therefore, the LVG operator benefits from the CNet-ZEC concept due to an improvement of the considered Performance Indicators. In return, the C-ADMIN asks the LVG operator for a common and shared metering point located at the transformer output. Due to this metering location transition, building owners benefit from generation surplus sharing and a consequent reduction of the electricity costs (assuming that the value paid by the electricity imports is always higher than the value received by the electricity exports). At a specific time-step, the on-site generation surplus of a certain building can be consumed by another building to satisfy its electricity demand surplus and only net import/export values are charged/paid to the CNet-ZEC[10]. It is important to note that by following this type of metering, Joule Effect energy losses occurring throughout the LV distribution feeder are reflected on the CNet-ZEC's electricity bill.

Another interested external entity is the Electricity Retailer, which aims at maximizing the profit obtained from each celebrated contract. For this entity, the CNet-ZEC is seen as a single costumer. Under the current regulatory framework in countries like Portugal, where electricity selling is open for competition, the C-ADMIN role concerns the constant search for better market conditions.

[10] The CNet-ZEC's electricity net profile is given by subtracting Equation 4.2 to Equation 4.1. Electricity importing/exporting periods are associated with net positive/negative values.

Since the LVG feeding the CNet-ZEC may comprise individual devices directly connected to the grid, which are not associated to any building of the community, owners of such devices may also represent interested external entities. The reason for this relies on the fact that the operation of these devices impacts the CNet-ZEC's electricity bill due to the Community-Level metering. Using dedicated meters to measure the electricity consumption/generation of these devices, their impact on the CNet-ZEC's electricity bill could be assessed and mitigated through a monetary compensation. If those devices could offer some degree of Energy Flexibility, then the C-EM could also control their operation to improve CNet-ZEC's LM values and therefore increase the benefits offered to building owners and the LVG operator.

Last but not least, C-ADMIN is in charge of distributing the resulting monetary benefits by the building owners. Several models can be followed to conduct this profit distribution. If all buildings integrating the cooperative community are Net-ZEBs, then a simple equal division among them could be considered. Another scenario concerns the existence of some nZEBs within the community that present a NB lower than zero. In this case a weighted distribution taking into consideration the NB of these buildings could be carried out. These two examples are just illustrative of a wider range of possible models to distribute the monetary benefits.

Another benefit offered to building owners, by the CNet-ZEC concept, concerns the privacy of data metering information. The recent replacement of traditional electromechanical meters, that were used to measure the electricity consumption over long periods (e.g. one month), by smart meters capable of providing up-to-date and accurate information about buildings' electricity consumption, raises privacy concerns since they may leak detailed information about household activities. For instance, in (Molina-Markham *et al.*, 2010) the potential for consumption patterns to reveal private information about buildings' users (e.g. buildings' occupancy or users' eating and sleeping routines) is demonstrated. Therefore, due to the Community-Level metering, the CNet-ZEC offers an extra level of protection against electricity metering related privacy issues. By following this Community-Level metering, only the total community's electricity consumption is available, reducing the chances to gather detailed information about specific users' activities.

4.3. Community Energy Manager (C-EM)

Using the community's aggregated Energy Flexibility, which is offered by controllable devices that can be found within CNet-ZEC's Balance Boundary, C-EM manages the cooperation conducted by the buildings in order to improve the LM at LVG's MV/LV transformer output. This section details different aspects of the C-EM operation, giving a special focus to the community's aggregated Energy Flexibility computation in Section 4.3.1 and to the Cooperation Mechanism, which uses this flexibility, in Section 4.3.2.

To compute the community's aggregated Energy Flexibility and to implement the referred Cooperation Mechanism, C-EM should be supported by enabling technology that, at least, satisfies the following requirements:

- Controllable devices receive and apply the control variable computed values;
- C-EM acquires all users' comfort preferences regarding the controllable devices;
- C-EM acquires controllable devices' power consumption and all physical quantities related with their operation;
- C-EM acquires non-controllable devices' power consumption;
- C-EM acquires generation devices' power output; and
- C-EM implements or uses electricity demand and generation forecast services.

4.3.1. Aggregated Energy Flexibility

In terms of electricity consumption, a specific electrical device is considered to be flexible if the respective demand profile can be modified without compromising users' expected comfort levels. Therefore, considering a period of analysis P, the Energy Flexibility profile $\boldsymbol{f}_c(n)$ offered by a single device c can be predicted by subtracting the predicted original electricity demand profile $\boldsymbol{d}_c(n)$ to the predicted modified electricity demand profile $\boldsymbol{d}_c^*(n, x_c)$ as described by Equation 4.4, where $\boldsymbol{X}_c$ is a matrix containing the N_V control variables x that can be controlled at each time-step n in order to modify the device's electricity demand profile. A positive value of $\boldsymbol{f}_c$ is associated with a future increase on the electrical device's electricity consumption whereas a negative value indicates a future electricity demand decrease. The period of analysis P should be large enough to accommodate possible rebound effects. This is of special importance in Thermostatically-Control devices where large electricity demand increases may be registered after turning off the controllable devices' operation for a specific period. The severity of the rebound effect increases with the interruption duration due to the impacts introduced in the respective system's temperature (Zehir and Bagriyanik, 2012).

Each line of a matrix $\boldsymbol{X}_c$ (see Equation 4.4), is associated with a specific control variable whereas each column is associated with a certain time-step. To use the Energy Flexibility offered by a specific controllable device, in order to achieve a certain objective, the value of each control variable during each time-step of the period of analysis should be defined accordingly. The compressor state (ON or OFF) of a controllable refrigerator is an example of control variable. In this case, the refrigerator's compressor state would have to be defined for each time-step of the period P, taking into consideration the minimum and maximum temperature set-points defined by the user. To compute the refrigerator's predicted modified electricity demand profile, considering the compressor state at each future time-step, a model describing its thermal behavior

would be necessary, which, in addition to the compressor state, would also receive the predicted refrigerator outside temperature as an input.

$$\mathbf{f}_c(\mathrm{n}, \mathbf{X}_c(\mathrm{n})) = \mathbf{d}_c^*(\mathrm{n}, \mathbf{X}_c(\mathrm{n})) - \mathbf{d}_c(\mathrm{n}) \tag{4.4}$$

$$\mathbf{X}_c(\mathrm{n}) = \begin{bmatrix} x_{1,1} & x_{1,2} & \cdots & x_{1,P} \\ x_{2,1} & x_{2,2} & \cdots & x_{2,P} \\ \vdots & \vdots & \vdots & \vdots \\ x_{N\_V,1} & x_{N\_V,2} & \cdots & x_{N\_V,P} \end{bmatrix}$$

The CNet-ZEC's aggregated Energy Flexibility $\boldsymbol{F}(n, \boldsymbol{X})$ is then obtained by adding the Energy Flexibility profiles $\boldsymbol{f}_c(n)$ of the N_C controllable devices that can be found within the Balance Boundary, as described by Equation 4.5, where the matrix $\boldsymbol{X}$ aggregates the N_C $\boldsymbol{X}_c$ matrices. To compute each entry of the the N_C $\boldsymbol{X}_c$ matrices and, therefore, each entry of matrix $\boldsymbol{X}$, C-EM must take into consideration the comfort needs of all CNet-ZEC users, associated not only to the controllable devices found in each building but also to the controllable individual devices directly connected to the LVG (e.g. EV charging stations). For each type of controllable device, the following comfort requirements are required by C-EM in order to compute the Energy Flexibility profiles of the N_C controllable devices[11]:

- Event-Based devices – Instant when the service provided by the EB device must be completed.
- Thermostatically-Controlled devices – Minimum and maximum temperature set-points. For some TC devices (e.g. heat pumps), these requirements can be further defined for periods of time with and without building occupancy.
- Electric Vehicles – Instant when the EV charging must be completed and the respective State of Charge.

$$\mathbf{F}(\mathrm{n}, \mathbf{X}(\mathrm{n})) = \sum_{c=1}^{N\_C} \mathbf{f}_c(\mathrm{n}, \mathbf{X}_c(\mathrm{n})) \tag{4.5}$$

$$\mathbf{X}(\mathrm{n}) = \begin{bmatrix} \mathbf{X}_1(\mathrm{n}) \\ \mathbf{X}_2(\mathrm{n}) \\ \vdots \\ \mathbf{X}_{N\_C}(\mathrm{n}) \end{bmatrix}$$

For the sake of clarity, the remaining of this section details the aggregated Energy Flexibility computation when Event-Based devices are considered.

[11] The presented comfort requirements denote examples of a broader range of possible options.

Computing the Energy Flexibility offered by Event-Based Devices

Event-Based devices show electricity demand profiles that are independent of the time-step in which they are switched-on by the users. As a result, $\boldsymbol{d}_c^*(n, x_c)$ is identical to $\boldsymbol{d}_c(n)$ but shifted in time. Therefore, the matrix $\boldsymbol{X}_c(n)$ of a specific EB device c is composed by P columns and only one line representing the device state (ON or OFF) at each future time-step.

Due to the existing decoupling between EB devices' electricity consumption and the need for the provided services, their operation can be shifted within a user defined shifting-window. The initial time-step (n_i) of this window refers to the instant at which the device is predicted to start its operation according to $\boldsymbol{d}_c(n)$. Regarding the shifting-window's final time-step, it refers to the instant when the service provided by the controllable device must be completed (n_f) (which is informed by the users) minus the time-period necessary for the device's operation (n_o). For a specific time-step k, the following illustrates a matrix $\boldsymbol{X}_c(n)$ where the respective EB device's future states are represented by Boolean values:

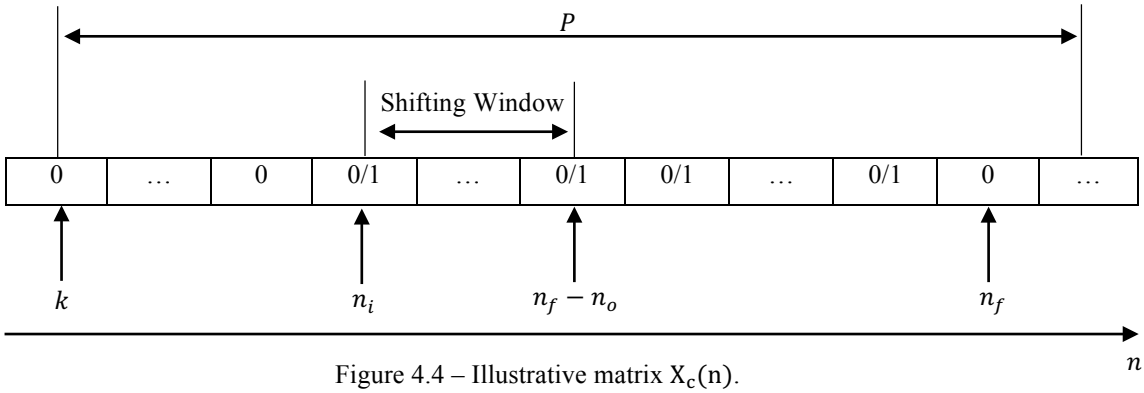

Figure 4.4 – Illustrative matrix $X_c(n)$.

Before the shifting window initial time-step, the EB device is always switched-off. The same occurs after the time-step when the service provided by the controllable device must be completed. Since the operation of the controllable device takes n_o time-steps, the controllable device operation can only be delayed by a maximum of $(n_f - n_o) - n_i$ time-steps. Therefore, between n_i and n_f the controllable device state can be either one or zero. The Energy Flexibility profile $\boldsymbol{f}_c(n)$ offered by a EB device, predicted at time-step k, is therefore given by Equation 4.6.

$$\mathbf{f_c}(\mathrm{n}) = \mathbf{X_c}(\mathrm{n}) \times \mathbf{d_c}\left(\sum_{\tau=\mathrm{k}}^{\mathrm{n}} \mathbf{X_c}(\tau) - 1 + \mathrm{n_i}\right) - \mathbf{d_c}(\mathrm{n}) \tag{4.6}$$

As an example, assuming $P = 10$ time-steps, one can consider a generic EB device c with the predicted original electricity demand profile $\boldsymbol{d}_c(n)$ depicted in Figure 4.6. In this case, $n_o = 3$ time-steps and $n_i = k + 2$. If the respective user only needs the service provided by this device

to be completed at time-step $k + 8$, then its operation can be delayed and start only at $k + 3$, $k + 4$, or $k + 5$. Assuming that the Energy Flexibility offered by this device is used to delay its operation by 1 time-step, the predicted modified electricity demand profile $\boldsymbol{d}_c^*(n, x_c)$ would be the one presented in Figure 4.7, being the respective matrix $\boldsymbol{X}_c(n)$ equal to:

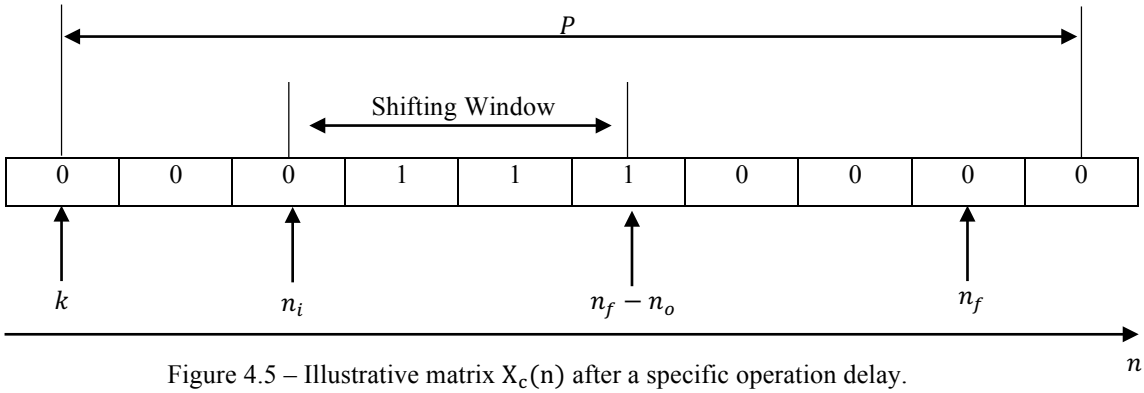

Figure 4.5 – Illustrative matrix $X_c(n)$ after a specific operation delay.

Considering the predicted original and modified electricity demand profiles presented in Figures 4.6 and 4.7, respectively, Figure 4.8 depicts the resulting Energy Flexibility profile according to Equation 4.4. The introduced delay would result on an electricity demand decrease at time-steps $k + 2$ and $k + 3$ and on an electricity demand increase at time-steps $k + 4$ and $k + 5$, which could be used to e.g. improve the LM values of a specific building. It is important to note that two other Energy Flexibility profiles could be obtained, which would result from delaying the device's operation by 2 or 3 time-steps. Therefore, as previously referred, the introduced delay should be chosen in accordance with the existing objectives as multiple options may exist.

In the context of the CNet-ZEC concept, the Energy Flexibility offered by the N_C controllable devices found within the Balance Boundary is aggregated and used to improve the LM values of the entire community. Through its Cooperation Mechanism, which is detailed in Section 4.3.2, C-EM is the entity in charge of finding the matrix $\boldsymbol{X}(n)$ that best suits this CNet-ZEC's objective.

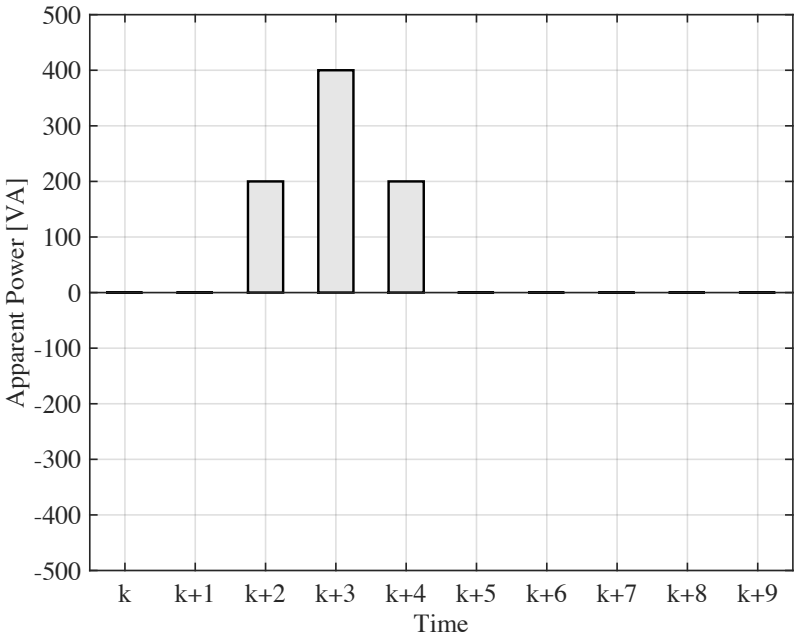

Figure 4.6 – Predicted original electricity demand profile for EB device *c*.

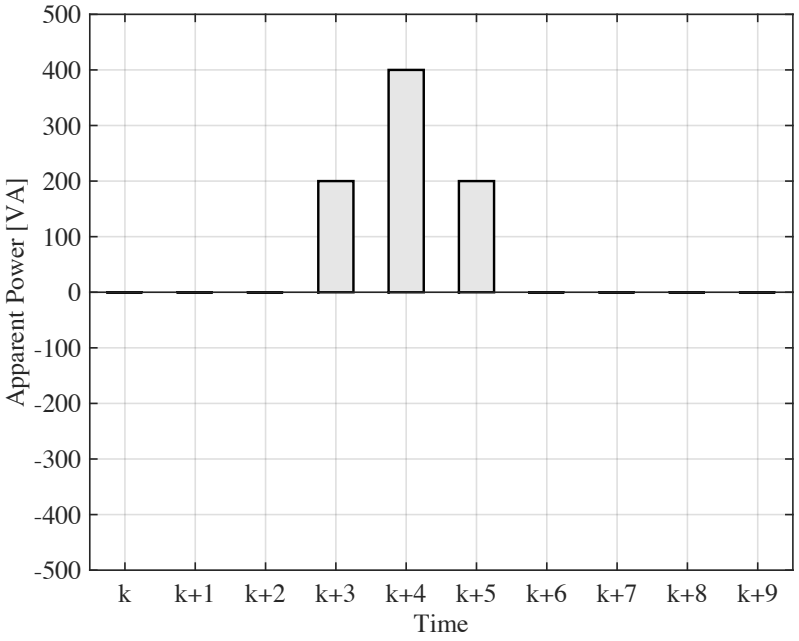

Figure 4.7 – Predicted modified electricity demand profile for EB device *c*.

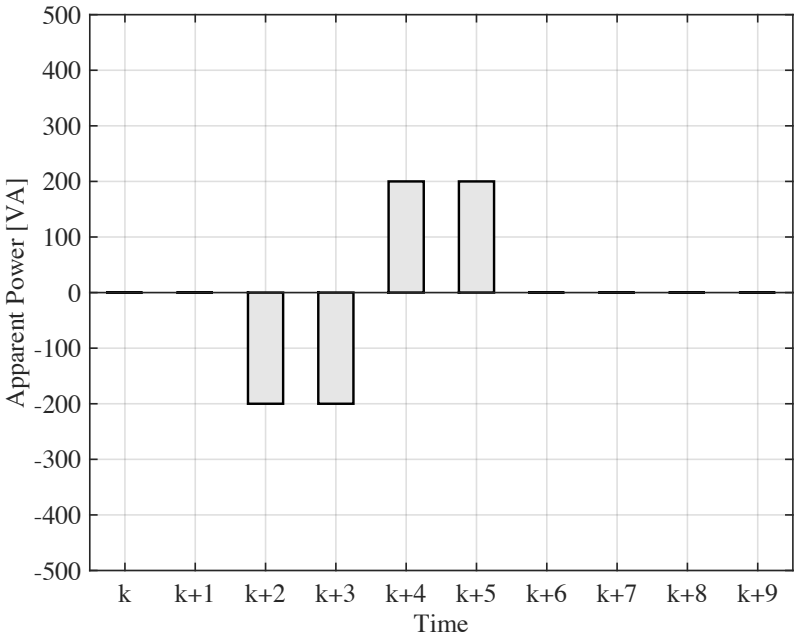

Figure 4.8 – Predicted Energy Flexibility profile for EB device *c* resulting from an operation delay of 1 time-step.

4.3.2. Cooperation Mechanism

The Cooperation Mechanism proposed in this work follows a predictive approach to find the controllable devices' operation that maximizes the CNet-ZEC's LM values. The goal is to find an optimal action plan which is updated at each time-step due to the acquisition of new measurements and predictions of the real world quantities that impact the LM optimization. Figure 4.9 presents the flowchart that describes this process.

At a specific time-step k, C-EM starts by measuring all real world quantities that are necessary for its operation. This includes the controllable and non-controllable devices' electricity consumption, electricity generation devices' power output, and other relevant quantities (e.g. buildings inner and outside temperatures or buildings occupancy). Then, community users' comfort preferences related with the controllable devices are updated. Using the measurements referred in first step and the updated users' comfort preferences, C-EM gets the predicted CNet-ZEC's electricity generation ($\boldsymbol{LVG\_G}(n)|k$) and original demand ($\boldsymbol{LVG\_D}(n)|k$) profiles over the prediction horizon. In ($\boldsymbol{LVG\_G}(n)|k$) and ($\boldsymbol{LVG\_D}(n)|k$), the parameter k is used to associate the predicted profiles to the time-step k. To obtain these profiles, C-EM uses forecast services provided by external entities or implemented by itself. The referred prediction horizon is equal to the period of analysis *P* described in Section 4.3.1. In the fourth step, C-EM uses the predicted CNet-ZEC's electricity generation and original demand, as well as the updated users' comfort preferences, to find the matrix $\boldsymbol{X}(n)$ that maximizes CNet-ZEC's LM values over the prediction horizon according to Expression 4.7, where $\boldsymbol{LVG\_D}^{*}(n, \boldsymbol{X}(n))|k$ is the CNet-ZEC's electricity

demand profile predicted at time-step k and modified using the aggregated Energy Flexibility $\boldsymbol{F}(n, \boldsymbol{X}(n))$ as described by Equation 4.8. The value of the control variables associated to time-step k, i.e. $\boldsymbol{X}(k)$, are subsequently applied to the respective controllable devices and the cycle is repeated in time-step $k + 1$.

$$\min_{\mathbf{X}(\mathrm{n})} [\mathbf{LVG\_G}(\mathrm{n})|\mathrm{k} - \mathbf{LVG\_D}^{*}(\mathrm{n}, \mathbf{X}(\mathrm{n}))|\mathrm{k}]^2 \tag{4.7}$$

$$\mathbf{LVG\_D}^{*}\big(\mathrm{n}, \mathbf{X}(\mathrm{n})\big)|\mathrm{k} = \mathbf{LVG\_D}(\mathrm{n})|\mathrm{k} + \mathbf{F}(\mathrm{n}, \mathbf{X}(\mathrm{n})) \tag{4.8}$$

By implementing the described predictive Cooperation Mechanism, C-EM is able to adapt the operation of controllable devices over the time in response to external events. In fact, according to Model Predictive Control theory (Lamoudi, 2012), the proposed Cooperation Mechanism consists of an implicit feedback-feedforward scheme. The feedforward feature results from the direct inclusion of the predicted CNet-ZEC's electricity generation and demand profiles in Expression 4.7, which provides the C-EM with the ability to optimize the controllable devices' operation taking into consideration future variations on CNet-ZEC's electricity generation and/or demand. Regarding the feedback feature, it results from updating the users' comfort preferences and the predicted CNet-ZEC's electricity generation and original demand profiles, which is translated on a reactive optimization of the controllable devices' operation in response to unpredicted disturbances. Such disturbances may comprise, for instance, users' comfort preferences changes or non-controllable devices unexpected operation.

Following the example provided in Section 4.3.1 to illustrate the Energy Flexibility profile computation, the remaining of this section illustrates the operation of the Cooperation Mechanism during two consecutive time-steps when EB devices are considered. In order to reflect the feedback-feedforward feature, it is considered that the predicted CNet-ZEC's electricity generation profile is modified between the referred time-steps (the predicted original CNet-ZEC's electricity demand profile and the users' comfort preferences remain unchanged).

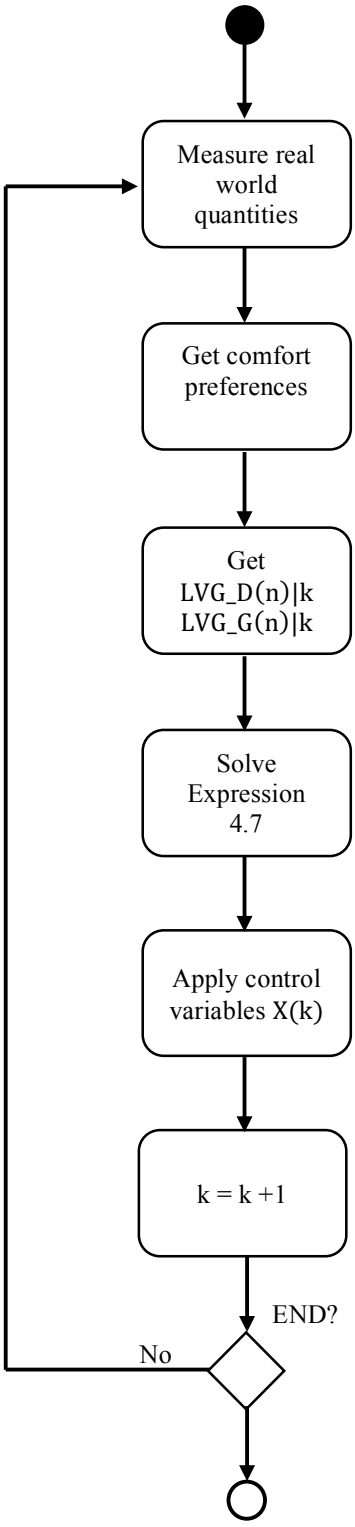

Figure 4.9 – Flowchart of the Cooperation Mechanism.

An Illustrative Example

This example considers two identical controllable EB devices, whose electricity demand profiles are identical to the one depicted in Figure 4.6. At time-step k, the predicted original CNet-ZEC's electricity demand profile is defined by the operation of these two controllable devices alone, considering that the respective users will complete the loading process at time-steps $k + 2$ and $k + 4$. Additionally, it is considered that both users only need the service provided by the EB devices at time-step $k + 9$. Therefore, assuming a period of analysis $P = 10$ time-steps, Figure 4.10 shows the predicted original electricity demand profile. Regarding the predicted CNet-ZEC's electricity generation profile, it is presented in Figure 4.11.

Considering these predicted CNet-ZEC's electricity demand and generation profiles and the comfort preferences of the users, the Cooperation Mechanism finds the matrix $\boldsymbol{X}(n)$ that minimizes the difference between the referred profiles, as described by Expression 4.7. In this case, Expression 4.7 is satisfied if the operation of both devices is delayed by 1 time-step, resulting on the predicted modified electricity demand profile presented in Figure 4.12. The 1 time-step delay was found to be the optimal solution by testing all the possible combinations. Then, the operation state of EB devices is defined according to $\boldsymbol{X}(k)$. Since the EB devices original operation is predicted to be started only at time-steps $k + 3$ and $k + 5$, the control variables associated to $\boldsymbol{X}(k)$ are both zero, meaning that the EB devices will remain turned off.

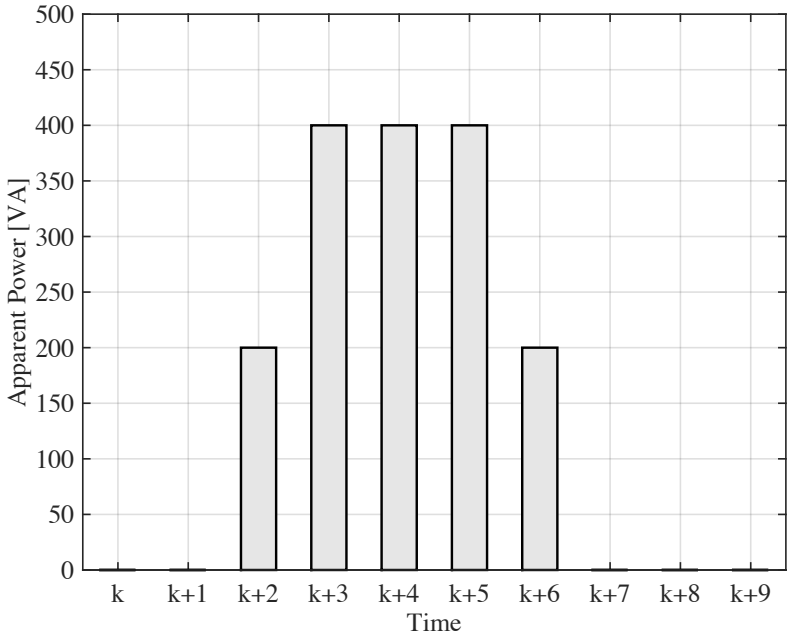

Figure 4.10 – Predicted original electricity demand profile at time-step k.

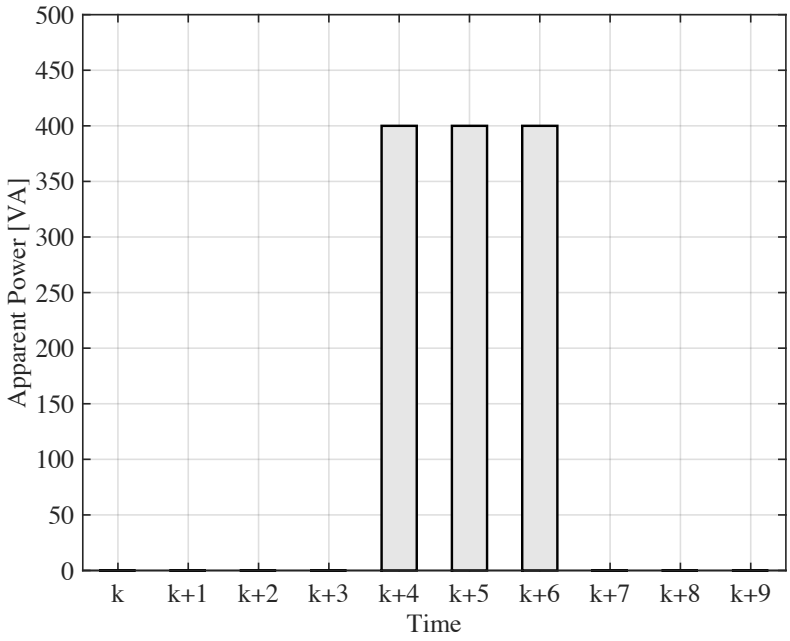

Figure 4.11 – Predicted electricity generation profile at time-step k.

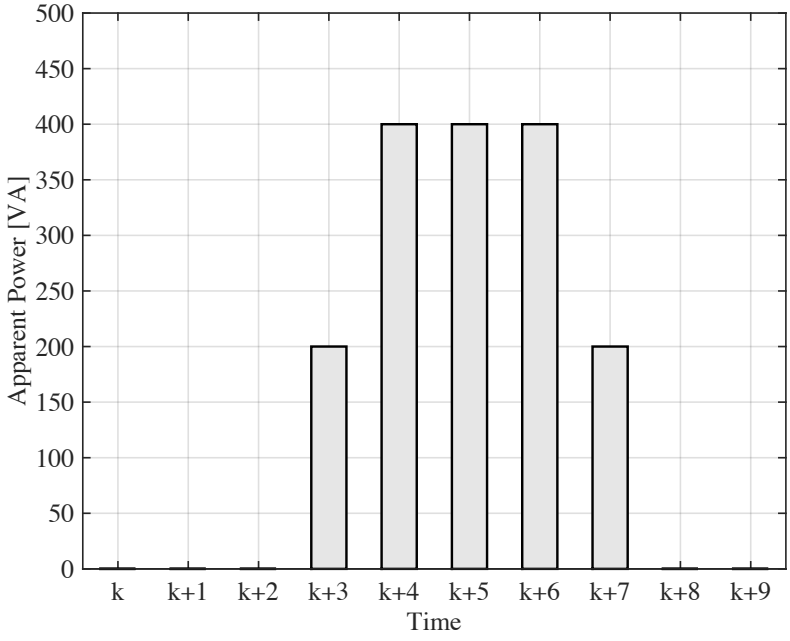

Figure 4.12 – Predicted modified electricity demand profile at time-step k using the Energy Flexibility offered by the controllable devices.

At time-step $k + 1$, it is considered that the predicted CNet-ZEC's electricity generation profile is modified due to a certain external event, resulting on the predicted profile depicted in Figure 4.13. Therefore, the matrix $\boldsymbol{X}(n)$ is updated in order to satisfy Expression 4.7 considering the new predicted generation profile. By computing all the possible solutions, the Cooperation Mechanism

finds that Expression 4.7 is satisfied if the EB devices' operation is delayed by 1 and 2 time-steps. Figure 4.14 presents the new predicted modified electricity demand profile. This iterative process is repeated until the operation of the Cooperation Mechanism is terminated.

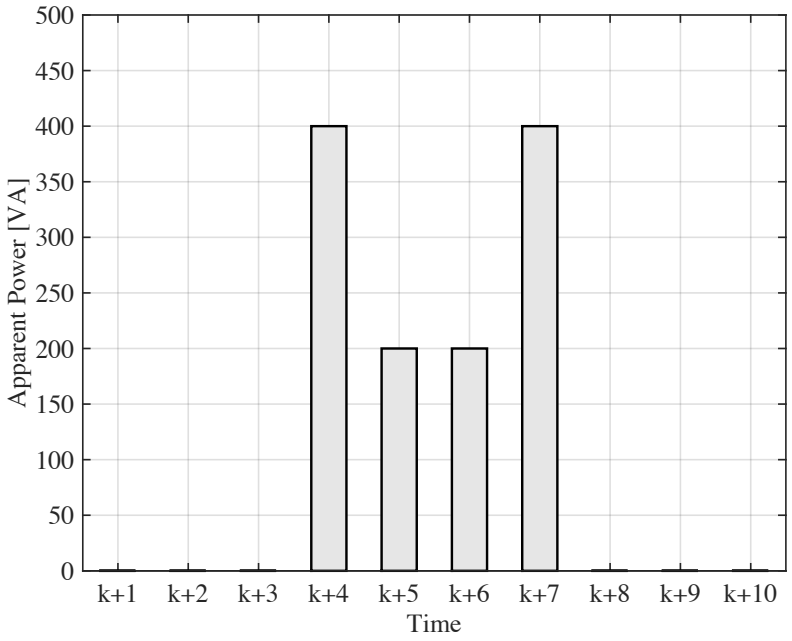

Figure 4.13 – Predicted electricity generation profile at time-step $k + 1$.

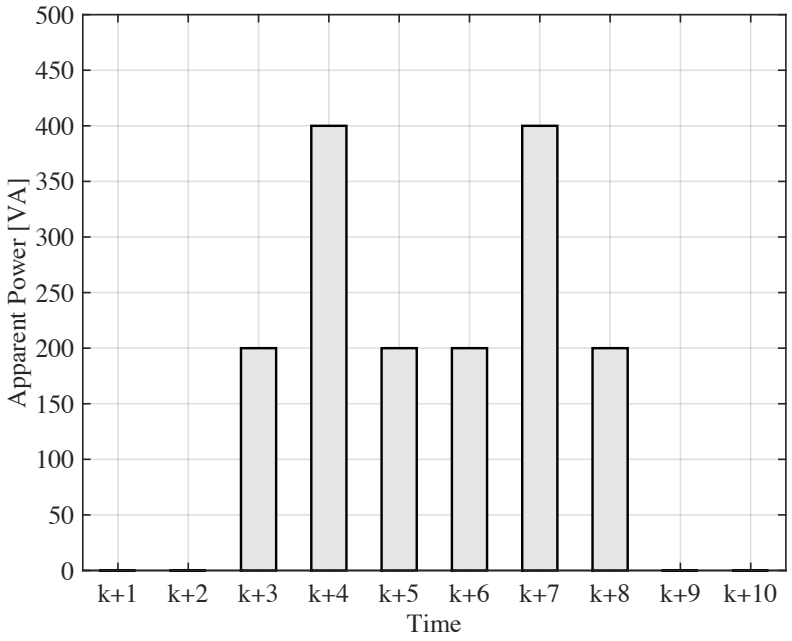

Figure 4.14 – Predicted modified electricity demand profile at time-step $k + 1$ using the Energy Flexibility offered by the controllable devices.

As in any scheduling problem involving finding an optimal time allocation for a large number of controllable units, the number of possible combinations of $\boldsymbol{LVG\_D}^*(n, \boldsymbol{X}(n))|k$ grows exponentially with the number of considered controllable devices. Therefore, finding the matrix $\boldsymbol{X}(n)$, testing all the possible combinations as in this illustrative example, might not be a reasonable option. For instance, to find the operation starting-times of N_C controllable devices, considering shifting windows of 24 h with a 1-min resolution, would require testing $1440^{\mathrm{N\_C}}$ combinations. Taking this into account, a Genetic Algorithm for Scheduling (GA4S) with reduced computational complexity was developed to find the EB devices' operation starting times that compose $\boldsymbol{X}(n)$.

GA4S is based on a selection process that mimics biological evolution, representing a vector of operation starting times as a chromosome composed by N_C genes, where each gene refers to a controllable device's operation starting-time. The algorithm starts by creating a random initial population of chromosomes (i.e. sets of operation starting-times with N_C elements). Then over a specified number of generations, GA4S creates a sequence of new populations with the objective of finding the chromosome that satisfies Expression 4.7. At each step, GA4S uses the individuals in the current generation to create the next population according to the following sequence:

1. Evaluating the quality of each chromosome in the current population by computing the fitness function, which measures how similar the resulting community demand $\boldsymbol{LVG\_D}^*(n, \boldsymbol{X}(n))|k$ is to the community generation $\boldsymbol{LVG\_G}(n)|k$;
2. Selecting the chromosomes of the current population that will produce the next generation (the Parents). The GA4S uses a "roulette wheel" based selection where the area of the section of the wheel corresponding to a parent is proportional to its result of the fitness function. Then, GA4S generates a random number to select one of the sections, resulting on a probability to select a specific chromosome equal to its section area.
3. Based on the results of step 1, selecting the chromosomes in the current population with the best quality to directly integrate the next generation. This process is known as Elitism and ensures that the results of the next generation are at least as good as the ones of the current population.
4. Generating the remaining individuals of the new generation through two distinct processes: crossover and mutation. In the first one, a chromosome of the new generation is formed by combining a pair of parents randomly chosen, resulting on a chromosome composed by operation starting-times of two distinct sets. In the second process, GA4S creates new chromosomes by randomly changing some operation starting-times of certain individual parents.

The following parameters are therefore necessary to describe the GA4S' operation: population size, number of generations, number of elite chromosomes, crossover rate, mutation rate, and mutation probability.

CHAPTER 5

Experiments Design

A neighborhood composed by 33 residential detached houses, fed by the same LVG, is used to assess the proposed hypotheses (number of buildings is aligned with the radial IEEE 34 Node Test Feeder (Kersting, 1991)). The experiments carried out consider a 1-year duration and comprise four distinct scenarios. Taking this 1-year time-scale, the referred experiments subject the 33 buildings to seasonal variation in solar irradiance and ambient temperature, which strongly affects the PV generation and thus the LVG Performance Indicators. In addition to the description of the referred scenarios in Section 5.1, this chapter also details the studied LVG in Section 5.2 and the applied electricity costs structure in Section 5.3.

5.1. The Scenarios

The considered scenarios address different building operation conditions, which result on distinct impacts on LVG Performance Indicators. For each scenario, buildings' electricity demand and generation profiles (if applied) are described in the following sections. In order to generate these profiles, models use real data gathered during 2013 from the meteorological station located at Faculty of Science and Technology of *Universidade Nova de Lisboa* (38º 39' 36'' N / 9º 12' 11'' W). These data cover the global irradiance at the horizontal plane ($\boldsymbol{G}$) and the ambient temperature ($\boldsymbol{\theta_a}$), obtained with 1-min resolution. Figures 5.1 and 5.2 present both data sets as a function of

the time of the day and month of the year (in both figures, each horizontal line is associated with a specific day, while each vertical line refers to a certain minute). Each of these figures comprise a total of 525,600 data points.

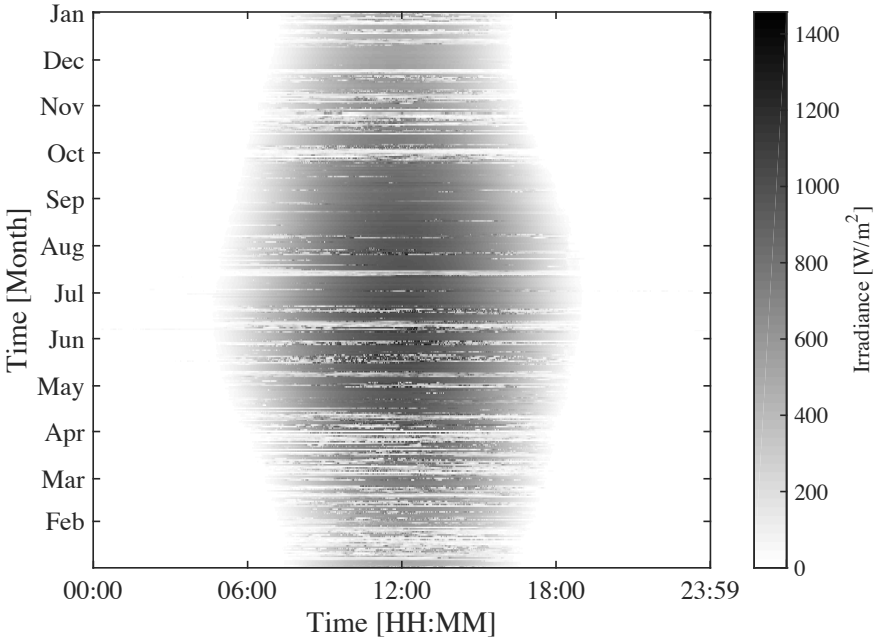

Figure 5.1 – Input data: global irradiance.

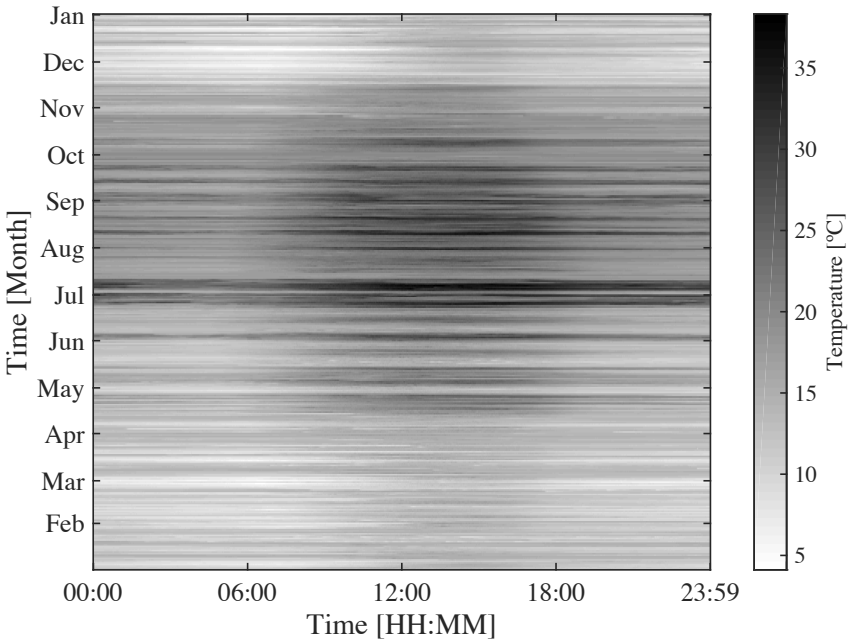

Figure 5.2 – Input data: ambient temperature.

5.1.1. Scenario #1

In this scenario only regular buildings that do not generate energy on-site compose the considered neighborhood. It aims to represent the current Portuguese residential building stock reality, where 68 % of the energy spent in space heating comes from biomass (see Figure 5.3) and 78 % of the energy spent in water heating comes from gas (see Figure 5.4), while summer thermal comfort is normally achieved through natural ventilation (INE and DGEG, 2011). Electricity is mostly used to power domestic appliances and lighting. To reflect this reality, in Scenario #1 it is assumed that all 33 buildings use wood for space heating, bottled gas for water heating and electricity to power domestic appliances and lighting. Therefore, all 33 buildings are only connected to one energy grid, i.e. the electricity grid.

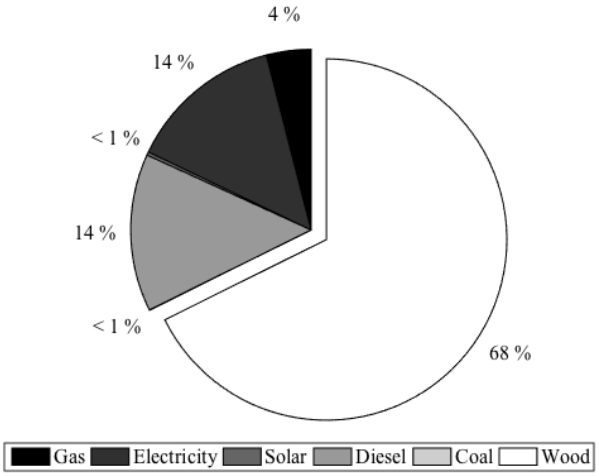

Figure 5.3 – Space heating energy consumption of the Portuguese residential building stock by energy source.

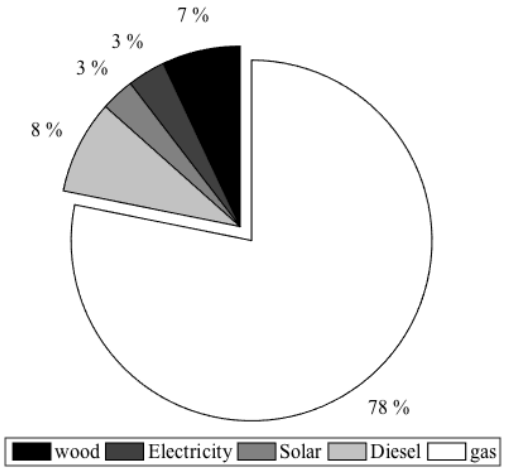

Figure 5.4 – Water heating energy consumption of the Portuguese residential building stock by energy source.

Amongst other possibilities, the electricity demand profiles of the 33 building are generated using the stochastic model developed by Richardson *et al.* (2010), considering that the buildings are equipped with the electrical devices presented in Table 5.1. This model follows a "bottom-up" approach where the individual domestic electricity loads are the basic building blocks. It uses stochastic occupancy profiles (Richardson, Thomson and Infield, 2008) and information related to the respective activities performed by a building's occupants when at home and awake to define, with 1-min resolution, the state of each load in the building. Additionally, such a model uses the meteorological data (i.e. incident solar radiation) to define the lighting electricity demand (Richardson *et al.*, 2009). In this work, the meteorological data described in Section 2.1 are used as input to this model.

Table 5.1 – Electrical devices considered in this study.

Device	**Mean Cycle Length [min]**	**Mean Cycle Apparent Power [VA]**	**Standby Apparent Power [VA]**	**Power factor**
Refrigerator	18	110	0	0,8
Iron	30	1000	0	1
Vacuum	20	2000	0	1
Personal computer	300	141	5	0,9
Printer	4	335	4	0,9
TV	73	124	3	0,9
Oven	27	2125	3	1
Microwave	30	1250	2	1
Dish washer	60	1131	0	0,8
Clothes Drier	60	2500	1	0,8
Washing Machine	138	406	1	0,8
Lighting	Usage Dependent	Usage Dependent	0	1

Due to the occupancy dependence of Richardson model, the probability that some devices have to operate depends on the number of occupants of the respective building. As a result, the annual electricity demand of a specific building is also dependent on its number of occupants. In this work it is considered that the number of residents in each building varies from 1 to 5. The occupancy is also used to define each building size, which is set according to the Portuguese general regulation of urban construction (Portuguese Directive 51/38382). Table 5.2 shows the main characteristics of all 33 building, focusing their position in the LVG, the considered number of occupants, the respective area, and the annual electricity consumption. A uniform distribution

was used to set the number of occupants for each building. The position of each building in the LVG was randomly selected.

Table 5.2 – Description of buildings position in the LVG, occupancy, area, and annual electricity demand (site energy consumption).

LVG's node	Occupants	Area [m^2]	Electricity Demand [kWh]
1	1	60	2141
2	1	60	2126
3	1	60	2121
4	2	80	2539
5	3	100	2836
6	3	100	2832
7	2	80	2634
8	5	140	3423
9	3	100	2842
10	1	60	2156
11	2	80	2641
12	2	80	2718
13	2	80	2676
14	1	60	2154
15	3	100	2760
16	4	120	2974
17	5	140	3546
18	1	60	2123
19	3	100	2922
20	5	140	3449
21	4	120	3010
22	3	100	2900
23	4	120	2634
24	4	120	2976
25	5	140	3416
26	2	80	2664
27	4	120	3152
28	5	140	3557
29	4	120	2924
30	3	100	2988
31	5	140	3365
32	4	120	2964
33	5	140	3486

5.1.2. Scenario #2

Aiming at assessing impacts introduced on LVG Performance Indicators due to the application of the EPBD 2010 recast, this scenario considers that all 33 original buildings are converted to Net-ZEBs. For the NB computation, a 1-year Balance Period is considered and the primary energy factors of Table 2.1 are chosen as Balance Metric. In order to reduce their primary energy demand, the converted buildings ensure their water and space heating by a solar thermal system composed by i) a solar collector; ii) a wood based auxiliary system; iii) a hot water storage tank; and iv) floor heat radiators. Buildings' electricity demand remains unchanged. Thereby, the Balance Boundary considers the electrical devices of Table 5.1 and the referred wood based auxiliary system.

T*SOL, a software tool developed by (Valentin Software, 2017), was used to compute water heating annual energy demand, considering a 40 l hot water consumption each day, per user, at a temperature of 45 ºC. After the renovation works take place, buildings' space heating annual energy demand is assumed to comply with the Passive House requirements, showing a reduced space heating annual energy demand of 8 kWh/m^2, in line with registered values for Portugal (Marcelino and Gavião, 2013).

The solar collector located at each building, together with the hot water storage tank, are not able to satisfy all water and space heating energy demand. The remaining part is satisfied by the wood based auxiliary system. Table 5.3 presents the annual wood and electricity related primary energy demand of each building[12], solar collectors' area, and the hot water storage tanks' size. Since the existing LVG is the only energy grid used, Net-ZEBs compensate all their annual energy demand using PV systems. It is important to note that to achieve a zero NB, these buildings have to compensate their electrical and wood energy demand (i.e. the involved Energy Carriers). Table 5.3 also presents the peak power of each PV system and the associated primary energy displaced by the on-site generation during the 1-year period.

The analytical model presented in Section 2.3 is used to generate the PV system output of each Net-ZEB. This model uses the meteorological data referred in Section 5.1 (i.e. the incident solar radiation and the ambient temperature) to produce a 1-min resolution data series for the power produced by a typical residential PV system. The modeled system has a rated peak power of 1.5 kW for $N = 10$ and $A = 1$. Table 5.4 presents the remaining values of Equations 2.8 and 2.9 parameters. To reach a zero NB over the 1-year period, the number of PV modules of each system was linearly scaled.

[12] According to Table 2.1, the conversion from site energy consumption to primary energy consumption is based on factors of 3.31 and 1.09 for electricity and wood, respectively.

Table 5.3 – Net-ZEB's primary energy demand and primary energy displaced by the PV on-site generation, together with the associated on-site energy conversion and storage systems summary.

LVG's node	Solar Collector Area [m^2]	Storage Tank Capacity [l]	PV peak power [kW]	Water Heating Demand [kWh]	Space Heating Demand [kWh]	Electricity Demand [kWh]	Primary Energy Displaced by the PV on-site Generation [kWh]
1	2	100	1,56	78,84	523,2	7085,9	7687,94
2	2	100	1,55	78,84	523,2	7037,6	7639,64
3	2	100	1,54	78,84	523,2	7018,9	7620,94
4	3	100	1,87	154,16	697,6	8404,9	9256,66
5	4	200	2,11	168,51	872	9387,6	10428,11
6	4	200	2,11	168,51	872	9375,4	10415,91
7	3	100	1,94	154,16	697,6	8718,2	9569,96
8	6	200	2,61	317,58	1220,8	11331	12869,38
9	4	200	2,12	168,51	872	9407,5	10448,01
10	2	100	1,57	78,84	523,2	7137,5	7739,54
11	3	100	1,94	154,16	697,6	8740,5	9592,26
12	3	100	1,99	154,16	697,6	8997,6	9849,36
13	3	100	1,96	154,16	697,6	8857,5	9709,26
14	2	100	1,57	78,84	523,2	7129,7	7731,74
15	4	200	2,06	168,51	872	9135,6	10176,11
16	5	200	1,96	238,47	1046,4	9844,7	11129,57
17	6	200	2,69	317,58	1220,8	11738	13276,38
18	2	100	1,54	78,84	523,2	7021,6	7623,64
19	4	200	2,17	168,51	872	9670,1	10710,61
20	6	200	2,62	317,58	1220,8	11416	12954,38
21	5	200	2,28	238,47	1046,4	9964,4	11249,27
22	4	200	2,15	168,51	872	9600,2	10640,71
23	5	200	2,37	238,47	1046,4	10427	11711,87
24	5	200	2,25	238,47	1046,4	9850,3	11135,17
25	6	200	2,6	317,58	1220,8	11307	12845,38
26	3	100	1,96	154,16	697,6	8818,8	9670,56
27	5	200	2,37	238,47	1046,4	10434	11718,87
28	6	200	2,69	317,58	1220,8	11774	13312,38
29	5	200	2,22	238,47	1046,4	9678,4	10963,27
30	4	200	2,21	168,51	872	9889,5	10930,01
31	6	200	2,57	317,58	1220,8	11137	12675,38
32	5	200	2,25	238,47	1046,4	9811,8	11096,67
33	6	200	2,65	317,58	1220,8	11537	13075,38

Table 5.4– Values for the PV system model's parameters.

Parameter	Value	Unit
η_E	0.9	-
η_{STC}	0.15	-
μ	-0.0045	$^oC^{-1}$
$\theta_{C,STC}$	25	^oC
$\theta_{C,NOCT}$	47	^oC
$\theta_{a,NOCT}$	20	^oC
G_{NOCT}	800	Wm^{-2}

5.1.3. Scenarios #3 and #4

BL-LMI and CL-LMI measures are applied to the described Net-ZEBs in Scenarios #3 and #4, respectively, aiming at collecting data to assess hypotheses H#1 and H#2. To obtain comparable results, the CNet-ZEC concept is used in both scenarios but with some modifications in Scenario #3. In this scenario, 33 instances of the CNet-ZEC concept, composed by a single building, are used to implement the BL-LMI measures. On the contrary, Scenario #4 considers a single instance of the CNet-ZEC concept, composed by 33 buildings. Additionally, in Scenario #3, instead of considering the electricity demand and generation profiles of the entire LVG, only the profiles associated to each building are used by the respective BL-LMI measures and the metering is conducted at each building's point of common coupling. Therefore, the resulting electricity costs are supported individually by the respective building owners, as in Scenarios #1 and 2, whereas in Scenario #4 all buildings share the electricity bill equally.

From the electrical devices referred in Table 5.1, the 33 BL-LMI measures and the CL-LMI measure use the Energy Flexibility offered by the EB devices; i.e. "Dish Washer", "Washing Machine", and "Clothes Drier". Therefore, when compared to Scenario #2, only the electricity demand profiles are modified in Scenarios #3 and #4. Nevertheless, the annual electricity demand of all 33 buildings remains unchanged since the considered controllable devices exhibit the time-invariant profiles depicted in Figure 5.5. To increase the controllable annual electricity demand, at least one controllable device operates per day in each building.

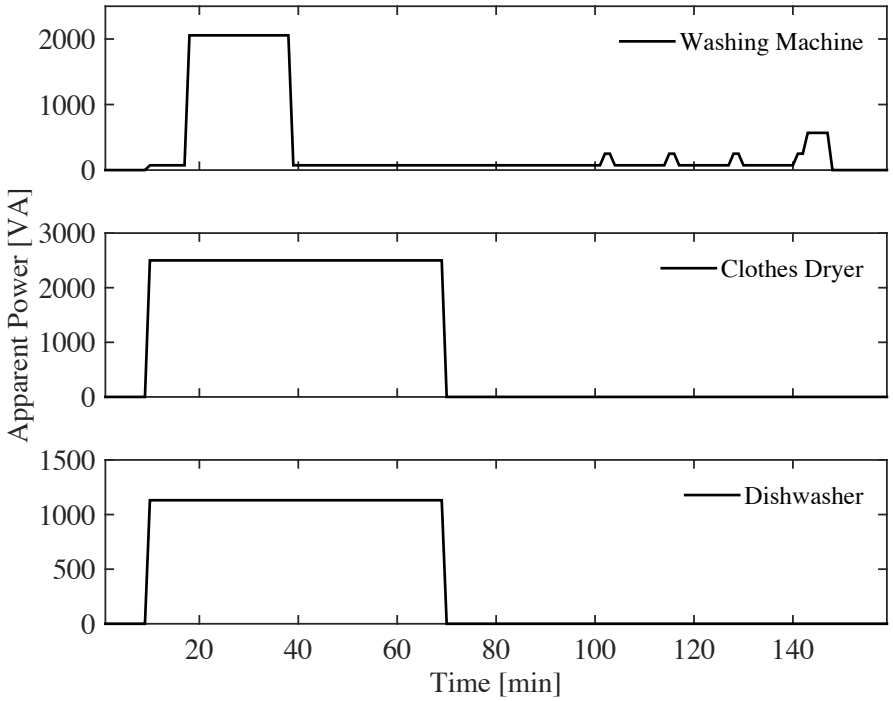

Figure 5.5 – Electricity demand profile of the considered EB devices.

According to the flowchart presented in Figure 4.7, the operation of the EB devices is controlled in Scenarios #3 and #4 as follows:

- Step 1 – The C-EM associated to a specific CNet-ZEC instance collects the electricity consumption of both controllable and non-controllable devices and the power output of the PV systems for time-step k.
- Step 2 – The comfort preferences of users are defined assuming that all users only need the service provided by the EB devices 24 h after the loading process has been finalized, which is in line with existing literature.
- Step 3 – Considering a 24 h period of analysis ($P = 24$ h), the predicted original electricity demand and generation profiles are obtained by observing the Richardson's model output and the PV systems' analytical model output for the period $k + P$. Note that time-step n_i associated to each controllable device (i.e. the moment when the device is loaded and ready to be switched-on) corresponds to the original predicted instant when the EB device starts consuming electricity.
- Step 4 – The operation starting-times of the controllable devices that maximize the LM values are found by C-EM. To obtain the matrix $\boldsymbol{X}(n)$ that conducts to such optimization, C-EM relies on the Genetic Algorithm for Scheduling described in Section 4.3.2, using the values of parameters presented in Table 5.5, and on the Energy Flexibility computation for EB devices described in Section 4.3.1.

- Step 5 – The control variables associated to $\boldsymbol{X}(k)$ - i.e. the state of each EB device at time-step k - are then applied to the 99 controllable devices (3 controllable devices per building), being the respective electricity demand profiles modified accordingly.

Table 5.5 – Values of the GA4S parameters.

Parameter	Value
Population size	100
Number of Generations	150
Number of elite chromosomes	2
Crossover Rate	0.8
Mutation Rate	0.2
Mutation Probability	0.01

5.2. Low Voltage Grid and Performance Indicators

This work considers the three-phase LVG presented in Figure 5.6. The chosen radial topology enables a better understanding of the voltage magnitude variations along the distribution feeder. It has a nominal voltage of 400 V (line to line voltage) and it is connected to a Medium-Voltage (MV) distribution grid through a three-phase oil-immersed distribution transformer. Additionally, the voltage applied to a specific electrical device is set equal to the point of common coupling voltage of the respective building.

The distribution feeder is considered to be of the underground type, based on a cooper cable with cross sections of 70, 50, and 25 mm^2. The sizing of the main cable was conducted iteratively with the objective of ensuring that the voltage along the LVG is kept within legal limits when none of the buildings generates on-site energy, i.e. in Scenario #1. This requires the voltage magnitude at any building's point of common coupling to be kept above 90 % and below 110 % of the nominal voltage value in agreement with EN 50160. To compensate the voltage drop along the distribution feeder, the voltage at the starting end of the main cable (i.e. at the distribution transformer output) is set 2 % above the nominal voltage, as it is common practice in low voltage distribution grids. Additionally, to replicate a typical residential district with detached houses, all buildings are located 50 meters apart from each other (Baetens *et al.*, 2012). Buildings are connected to the main cable by dedicated underground cooper cables with negligible resistance. It is also considered that the 33 building comprise all the electrical devices fed by the LVG.

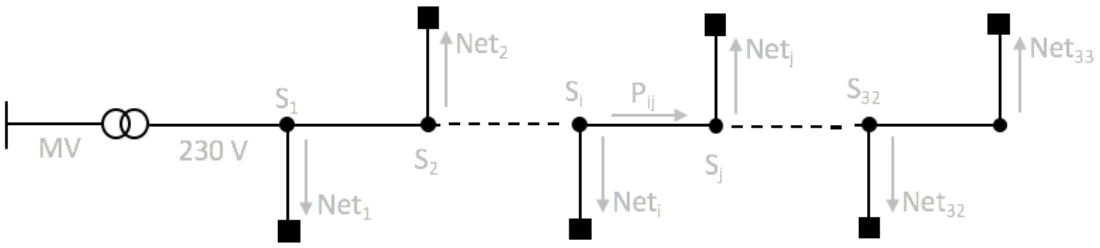

Figure 5.6 – Low Voltage distribution Grid considered for the experiments.

Buildings' on-site generation is considered for self-consumption and only the difference between demand and on-site generation is therefore imported/exported from/to the LVG. The load flow of this radial distribution network is computed using power flow analysis, where the considered radial grid has N_b branches, denoted by ij (with line impedance Z_{ij}), and $N_b + 1$ nodes. Each building is therefore connected to a grid node. The MV distribution grid point of common coupling (transformer) is considered to be node 0, being the reference node with imposed voltage level.

The power flow is iteratively computed for each time-step. At time-step n, the $\boldsymbol{Net}_i(n)$ load resulting from the operation of the building located at node i is given by Equation 5.1, where $\boldsymbol{BD}_i(n)$ and $\boldsymbol{BG}_i(n)$ denote building's electricity demand and generation, respectively. $\boldsymbol{Net}_i(n)$ can be either positive (importing energy from the LVG) or negative (exporting energy to the LVG). The iterative method then computes the power along the LVG and the voltage $\boldsymbol{V}$ at each node using Equations 5.2 and 5.3, where $\boldsymbol{S}_i$ denotes the power at each grid node i.

As described by Equation 5.3, the introduction of distributed generation into the LVG may result on voltage rising effects at the point of common coupling. To preserve voltage magnitude inside legal limits, it is assumed that the power inverters associated with each PV system curtail the energy generated on-site when building's point of common coupling voltage magnitude rises above the maximum allowed value (i.e. 110 % of the nominal voltage magnitude). Additionally, it is considered that these power inverters operate at a unitary power factor.

$$\mathbf{Net}_i(n) = \mathbf{BD}_i(n) - \mathbf{BG}_i(n) \tag{5.1}$$

$$\mathbf{S}_i(n) = \mathbf{Net}_i(n) + \mathbf{S}_j(n) + \mathbf{V}_{ij}(n)\left[\frac{\mathbf{V}_{ij}(n)}{Z_{ij}}\right]^* \tag{5.2}$$

$$\mathbf{V}_j(n) = \mathbf{V}_i(n) - Z_{ij}\left[\frac{\mathbf{S}_j(n)}{\mathbf{V}_j(n)}\right]^* \tag{5.3}$$

5.2.1. Peak Load

At time-step *n*, LVG's total load refers to $\boldsymbol{S}_0(n)$. In this work, the Performance Indicator related with peak load is the maximum value of $\boldsymbol{S}_0$ registered during the 1-year experiments (i.e. the yearly peak load). Peak loads registered at smaller time-scales and associated with specific LVG's branches could also be considered. However, smaller time-scales could not subject the 33 buildings to the yearly meteorological variations and different branches would not represent the entire LVG operation.

5.2.2. Energy Losses

Total energy losses by Joule effect, occurring at LVG's distribution feeder, are considered to assess the broader Energy Losses Performance Indicator. A set of resistance values are registered along the distribution feeder as the main underground cooper cable is composed by different cross sections, as presented in Table 5.6. The resulting total energy losses by Joule effect, over the time interval defined by minutes n_1 and n_2, are expressed by Equation 5.4 in kWh, considering 1-min resolution data series.

$$\mathrm{E} = \frac{1}{60000} \sum_{\mathrm{n}=\mathrm{n}_1}^{\mathrm{n}_2} \sum_{\mathrm{i,j}=1,2}^{32,33} \mathrm{Re}\{ \mathbf{V}_{\mathrm{ij}}(\mathrm{n}) \left[\frac{\mathbf{V}_{\mathrm{ij}}(\mathrm{n})}{\mathrm{Z}_{\mathrm{ij}}} \right]^* \} \tag{5.4}$$

Table 5.6 – LVG's distribution feeder characteristics.

Point of common coupling	Cross section (mm2)	Line impedance (Ω)
1 to 11	70	0.0120
12 to 23	50	0.0168
24 to 33	25	0.0336

5.2.3. Transformer Aging

The end of life of Distribution transformers is usually due to winding insulation failure. Generally, the major conductor insulation material is cellulose, an organic compound whose degradation is affected by three mechanisms: (i) hydrolysis, (ii) oxidation and (iii) pyrolysis (Shroff and Stannett, 1985; IEEE, 2002). Responsible agents for each of these mechanisms are water, oxygen and heat, respectively. These agents have distinct effects on the cellulose degradation rate so they should be individually controlled. Effects introduced by water and oxygen can be controlled by the transformer's oil preservation system (IEEE, 2002). On the other hand, heat is related with transformers' load and surrounding temperature. Therefore, subjecting the transformer to very high loads (larger than nameplate rating) or high ambient temperatures (higher than the ones

considered during the transformers' design) may increase the temperature inside the transformer and reach levels that accelerate its windings insulation aging.

The temperature distribution inside the transformer often exhibits a non-uniform pattern. The insulation section operating at the highest temperature is subjected to the greatest deterioration. Therefore, the considered temperature for the purpose of this work is the winding insulation highest temperature, known as hot-spot temperature ($\boldsymbol{\theta_h}$). Following the IEC 60076-7 Loading Guide For Oil-immersed Power Transformers (IEC, 2005), the heat transfer differential equations' block diagram presented in Figure 5.7 is used to estimate the winding hot-spot temperature at each time-step. Transformer aging model parameters' description and respective values used in this work are addressed in Table 5.7, which are according to IEC 60076-7 for a typical oil-immersed transformer with natural ventilation. The inputs to calculate the transformer aging are the LVG's total load, $\boldsymbol{S}_0$, and the ambient temperature, $\boldsymbol{\theta_a}$, which refers to the air in contact with the transformer's heat exchangers. This temperature is an important factor to establish the load capacity of the transformer under analysis because the temperature rising inside the transformer, for any load, shall be added to the ambient temperature.

The heat effect on the lifespan of a cellulose based insulation material can be estimated considering benchmark values. Experimental tests established that a normal insulation life time for a well-dried, oxygen-free insulation system is 180,000 hours or 20.55 years, considering a constant hot-spot temperature of 110 ºC (IEEE, 2002). These benchmark values allow the computation of the aging acceleration factor ($\mathbf{F_{AA}}$), at a specific time-step, as presented in Equation 5.5.

$$\mathbf{F_{AA}}(\mathrm{n}) = \mathrm{e}^{\left(\frac{15000}{110+273} - \frac{15000}{\boldsymbol{\theta_h}(\mathrm{n})+273}\right)} \tag{5.5}$$

Equation 5.5 specifies how the winding insulation aging is accelerated beyond normal for hot-spot temperatures above the reference temperature (110 ºC), and how it is reduced for temperatures below 110 ºC. The aging acceleration factor is unitary when the hot-spot temperature is 110 ºC. The equivalent aging of the winding insulation (EA) in minutes, over the time interval defined by n_1 and n_2, is then computed using Equation 5.6. In this work, the equivalent aging of the winding insulation over the 1-year experiment is considered as a Performance Indicator. Transformer sizing was conducted with objective of obtaining a 1-year equivalent aging for Scenario #1, resulting on a rated load of 21.4 kVA.

$$\mathrm{EA} = \sum_{\mathrm{n}=\mathrm{n}_1}^{\mathrm{n}_2} \mathbf{F_{AA}}(\mathrm{n}) \tag{5.6}$$

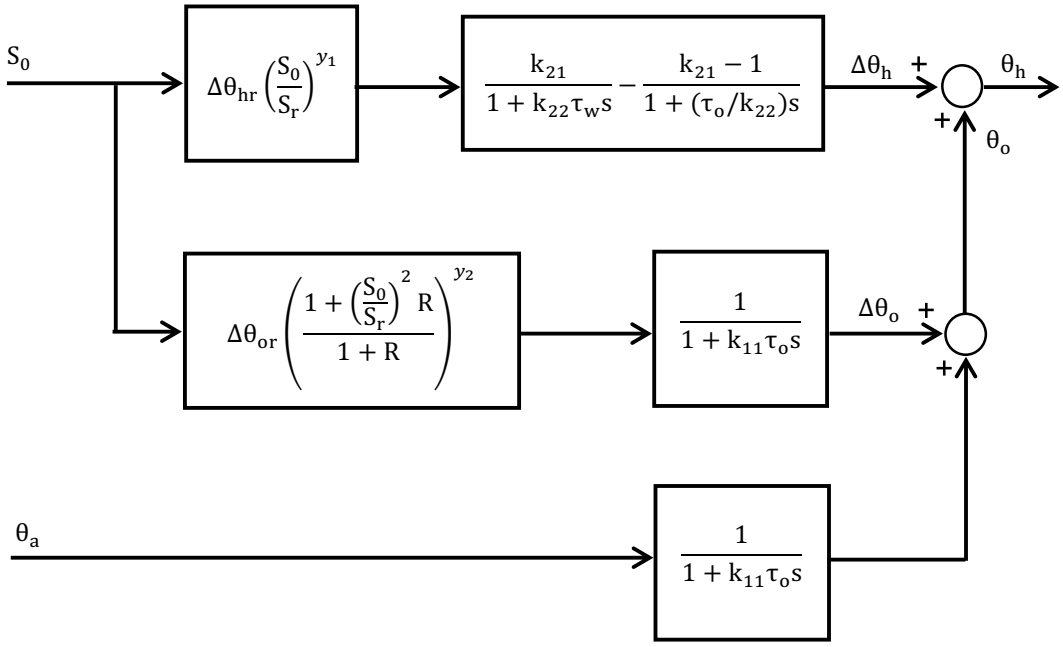

Figure 5.7 – Heat transfer differential equations' block diagram.

Table 5.7 – Description and values of transformer aging model parameters.

Parameter	Description	Value
S_0	LVG's total Load	-
θ_a	Ambient temperature	-
θ_h	Hot-spot temperature	-
$\Delta\theta_h$	Hot-spot to top-oil gradient at the load considered	-
θ_o	Top-oil temperature at the load considered	-
$\Delta\theta_o$	Top-oil temperature rise at the load considered	-
$\Delta\theta_{or}$	Top-oil temperature rise in steady state at rated losses (no-load losses + load losses)	45 K
$\Delta\theta_{hr}$	Hot-spot-to-top-oil gradient at rated current	35 K
τ_o	Average oil time constant	150 min
τ_w	Winding thermal time constant	7 min
y_1	Exponential power of current versus winding temperature rise	1,3
y_2	Exponential power of total losses versus top-oil temperature rise	0,8
R	Ratio of load losses at rated current to no-load losses	8
k_{11}	Thermal model constant	0,5
k_{21}	Thermal model constant	2
k_{22}	Thermal model constant	2
s	Laplace operator	-
S_R	Rated load	21.4 kVA

5.3. Electricity Cost

In the first three scenarios, the monetary costs associated with the electricity consumed in the 33 buildings are computed for each building, while in Scenario #4 power metering is executed at a single aggregated point (i.e. at LVG's distribution transformer output). This quantification is conducted under the Portuguese electricity market context and consists in subtracting the monetary benefits of selling electricity to the monetary costs related with electricity importing.

According to Directive 153/2014, the price to be paid for the exported electricity is 90 % of the monthly average price of the Portuguese spot electricity market (MAOTE, 2014). In order to quantify this price, data registered in 2014 was used (Figure 5.8) (Iberian Electricity Market, 2014), resulting in the electricity exporting prices expressed in Table 5.5. Regarding the price paid for the imported electricity, EDP Comercial 2017 tariffs were used as presented in Table 5.6 (EDP Comercial, 2017). Due to the different number of meters required among the considered scenarios, only the variable component of the referred tariffs are considered. Apart from these tariffs, DGEG exploitation rate (0.07 EUR/month) and IECE tax (0.001 EUR/kWh) were applied. To compute the final price paid for the imported electricity, a 23 % VAT is added to the referred values. As an example, consider a consumer with simple tariff (TOU 1 in Table 5.9) and annual electricity consumption of 10,000 kWh. The annual electricity cost supported by this consumer would be 2183 EUR (0.2183 EUR/kWh).

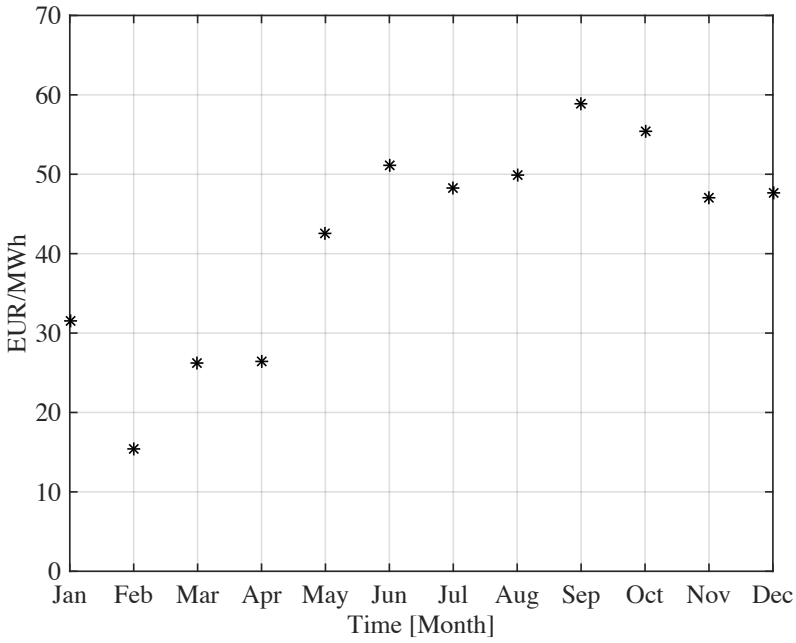

Figure 5.8 – Monthly average price of the Portuguese spot electricity market in 2014.

Table 5.8 – Price paid by the exported electricity in 2014.

Month	Exported Electricity [EUR/kWh]
January	0.0283
February	0.0139
March	0.0236
April	0.0237
May	0.0382
June	0.0461
July	0.0434
August	0.0449
September	0.0530
October	0.0499
November	0.0423
December	0.0429

Table 5.9 – Price paid by the imported electricity in 2017 according to (EDP Comercial, 2017).

	Season	Time	Tariff		
			TOU 1	TOU 2	TOU 3
Imported Electricity (EUR/kWh)	Winter	00:00 – 08:00 22:00 – 24:00	0.1652	0.0921	0.0930
		08:00 – 09:00 10:30 – 18:00 20:30 – 22:00	0.1652	0.1997	0.1681
		09:00 – 10:30 18:00 – 20:30	0.1652	0.1997	0.3326
	Summer	00:00 – 08:00 22:00 – 24:00	0.1652	0.0921	0.0930
		08:00 – 10:30 13:00 – 19:30 21:00 – 22:00	0.1652	0.1997	0.1681
		10:30 – 13:00 19:30 – 21:00	0.1652	0.1997	0.3326
Key: TOU – Time-of-Use.					

CHAPTER 6

Results and Analysis

The data collected during the previously described experiments are presented and analyzed in this chapter. All data processing was performed using MATLAB commercial software package (The Mathworks Inc, 2017). This chapter starts by the collected load profiles and resulting LM values. Following, in Sections 6.3 and 6.4, the considered Performance Indicators and the electricity costs associated to each experiment are addressed, respectively. With the information acquired in the previous sections, the proposed hypotheses are assessed in Section 6.5.

6.1. Load Profiles

Figure 6.1 presents the LVG's average load profile for each scenario, taking into consideration the results acquired during the 1-year experiments. The data presented in this figure result from averaging the LVG's load registered at node 0 for each minute of the 1-year experiments.

For Scenario #1, LVG's load typically follows a 24 h duration cycle that approximately reflects households' daily activity. This load cycle is characterized by a reduced electricity consumption value during night followed by a morning peak at breakfast time. During the day, it shows a relatively leveled power consumption until mid-afternoon, when it rises towards the evening peak. After this second peak, neighborhood's electricity demand falls again reaching the night-time lower values. Still for Scenario #1, Figure 6.2 presents the LVG's instantaneous load for

each 1-min time-step, where the described load cycle can be observed by analyzing each horizontal line of the surface (Figure 6.1 is obtained from Figure 6.2 by averaging all values obtained for each minute of the day along the 365 days of the experiment).

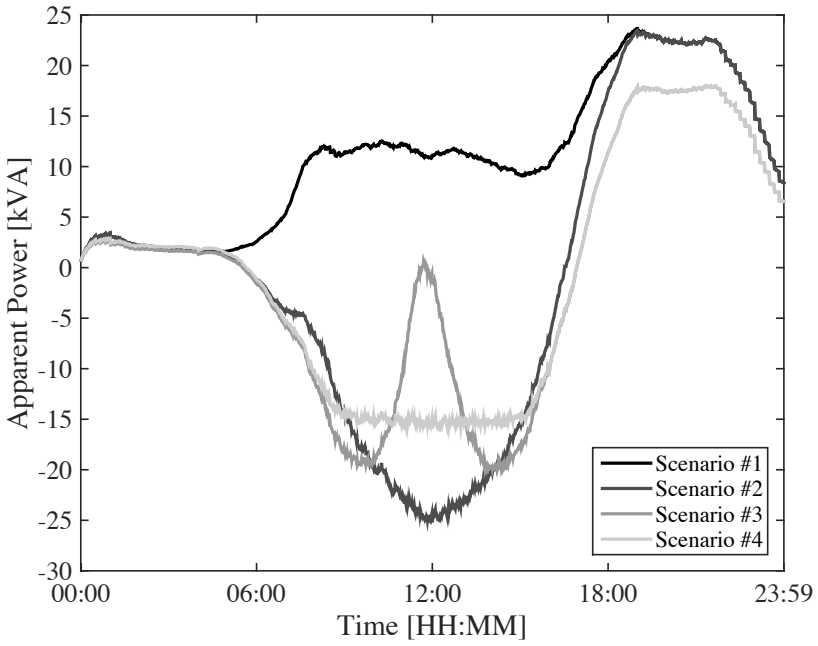

Figure 6.1 – Average load profiles at LVG's node 0 for the 1-year experiments.

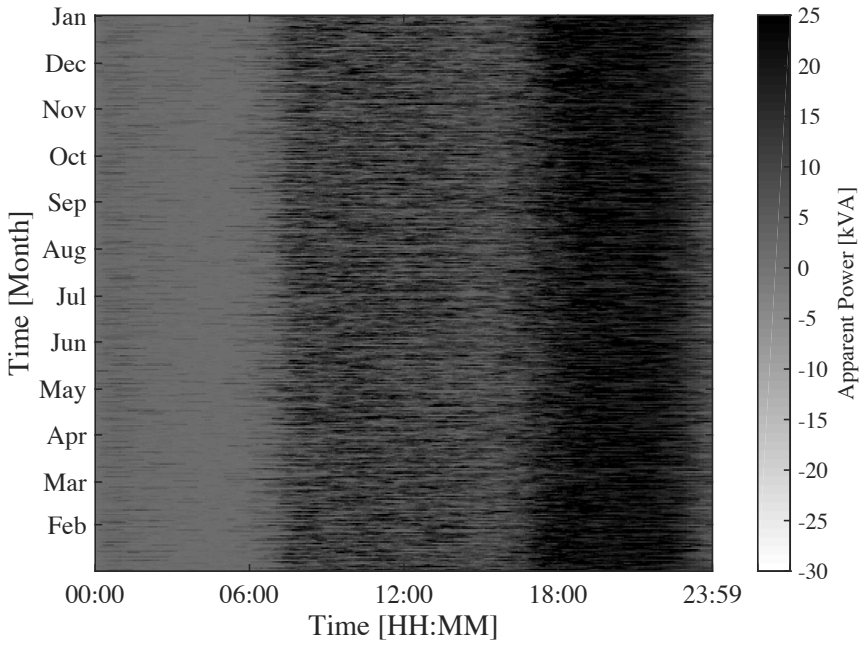

Figure 6.2 – LVG's node 0 load for Scenario #1.

When all 33 buildings are renovated and converted to Net-ZEBs, the described load cycle is deeply affected during daytime as it can be observed in Figure 6.1 for Scenario #2. The introduction of PV systems on the studied LVG results on reverse power flows whose magnitudes are higher than the evening peak load of Scenario #1. Due to the occurrence of these reverse power flows, the distribution transformer is forced to shift its operation to step-up transformer (in this operation the medium-voltage distribution grid receives energy from the LVG). When the solar resource is not available, the average load profile for the 1-year experiment shows no differences between the first two scenarios.

Figure 6.3 details the LVG's instantaneous load during the 1-year Balance Period for Scenario #2. Even with the curtailment mechanism present in each PV inverter, reverse power flows achieve values much higher than evening load peaks, reflecting the oversized and coincident PV systems operation (note that PV systems were designed to compensate not only buildings' electricity demand but also wood based energy demand). Effects of the seasonal radiance variation can also be observed in Figure 6.3. During the summer, reverse power flows occur for longer time periods and present higher magnitudes, while, during the winter, intermittent PV generation is relatively common reflecting the impacts introduced by cloud cover. During spring/autumn, an increasing/decreasing number of hours where reverse power flows occur can be observed, reflecting the solar resource variation in these transition periods.

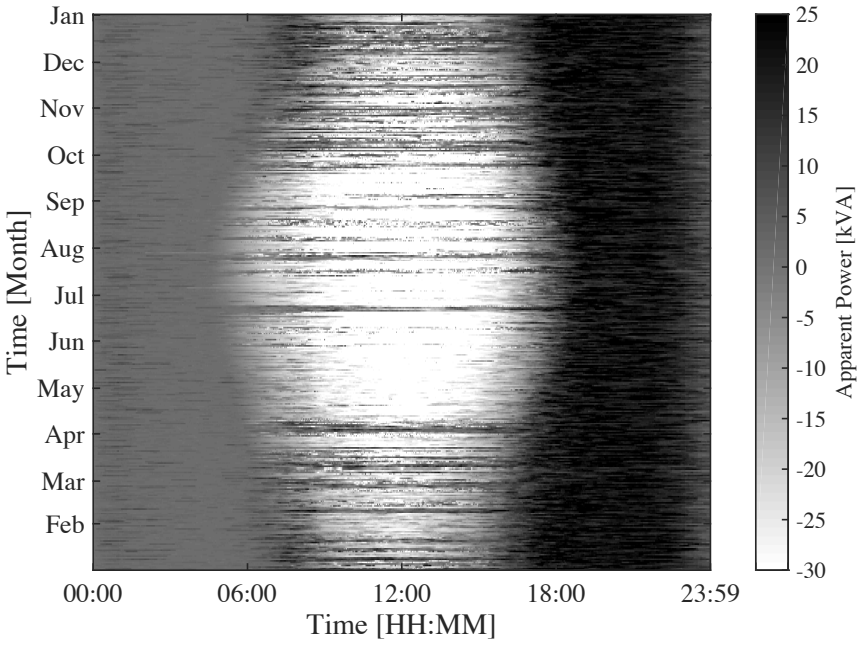

Figure 6.3 – LVG's node 0 load for Scenario #2.

The results depicted in Figure 6.1 for Scenario #3 show lower electricity demand values for periods with no solar energy availability (comparing to the first two scenarios) and lower reverse

power flow values during periods around midday (comparing to Scenario #2). The reason for these changes is related with the BL-LMI measures applied at an individual basis. The Energy Flexibility offered by the controllable devices is used to shift their operation from periods with demand surplus to time-intervals with excessive on-site generation. Figure 6.4 addresses this demand shifting at Building-Level for a specific day of the 1-year experiment, where the Energy Flexibility offered by 1 controllable device (clothes drier) is used to improve the LM of the building located at LVG's node 7. The controllable device's operation was delayed by 177 minutes so the building's SC and SS ratios were increased by 7.59 % (from 18.12 to 25.71 %) and 8.28 % (from 19.76 to 28.04 %) in this specific day, respectively. To delay the operation of this controllable device, the BL-LMI measure only considered the demand and generation profiles of the respective building. It is important to note that, even by shifting the operation of the controllable device to noon, a considerable amount of the controllable device's electricity demand is still not covered by building's on-site generation.

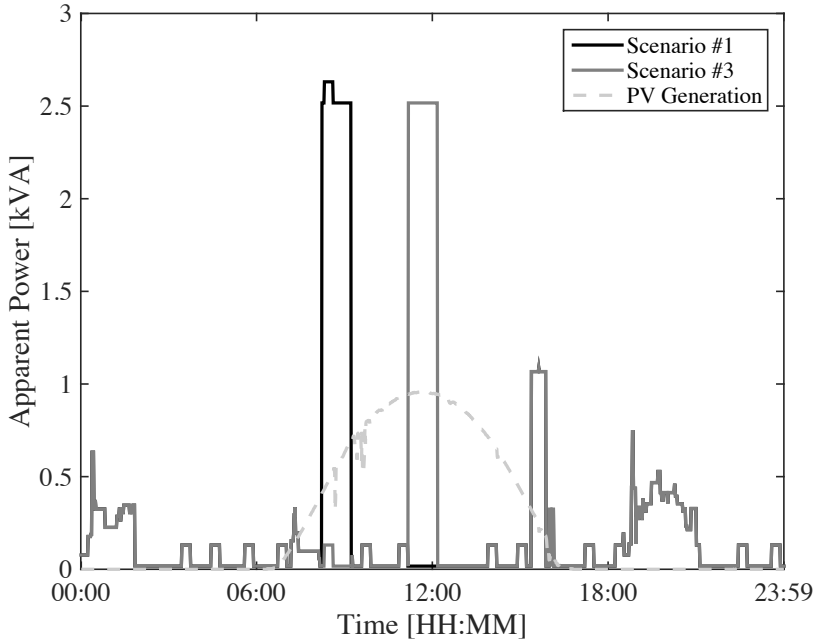

Figure 6.4 – Electricity demand and PV generation at LVG's node 7 for a specific day of the 1-year experiment.

Still for Scenario #3, Figure 6.5 presents the respective LVG's instantaneous load registered during the 1-year experiment. In this figure, a coincident demand shifting from evening to periods around midday (i.e. to periods with higher solar resource availability) is evident. In fact, during periods of the year with lower solar energy availability, the midday demand peak created by the coincident demand shifting are large enough to absorb all neighborhood's on-site generation and even to create positive loads higher than the ones observed during the evening. This reflects the

"greedy" approach followed by the implemented 33 BL-LMI measures, whose operation does not use information related with other buildings' electricity demand and on-site generation profiles, creating, as a result, new electricity demand peaks due to the coincident controllable devices' demand that is not directly covered by the respective buildings' on-site generation.

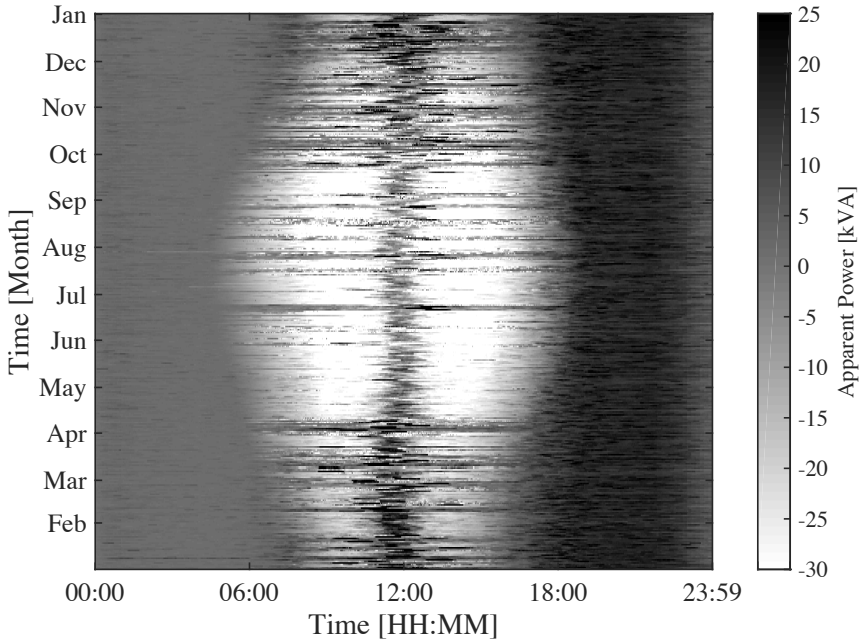

Figure 6.5 – LVG's node 0 load for Scenario #3.

In Scenario #4, the Energy Flexibility offered by the controllable devices is used on an aggregated and cooperative way, considering the electricity demand and generation profiles of all buildings fed by the LVG under analysis. As a result, the reverse power flow amplitude is decreased equally during daytime, as illustrated in Figure 6.1. When no solar energy is available, Scenarios #3 and #4 show no difference, indicating that all the Energy Flexibility offered by the controllable devices is used in both scenarios. Figure 6.6 presents the LVG's electricity demand for Scenarios #1 and #4 during the specific day also addressed in Figure 6.4. The controllable electricity demand is spread along daytime so the difference between CNet-ZEC's electricity demand and generation is reduced according to Expression 4.7. LVG's SC and SS ratios were increased by 24.73 % (from 49.97 to 74.70 %) and 18.10 % (from 35.65 to 53.75 %) in this specific day, respectively. By analyzing the LVG's instantaneous load depicted in Figure 6.7, the following is observed: i) the LVG's load around midday is relatively leveled and lower than in Scenarios #2 and #3; ii) the LVG's evening peak load is lower than in Scenarios #1 and #2; and iii) no additional peak load is created by the CL-LMI measure.

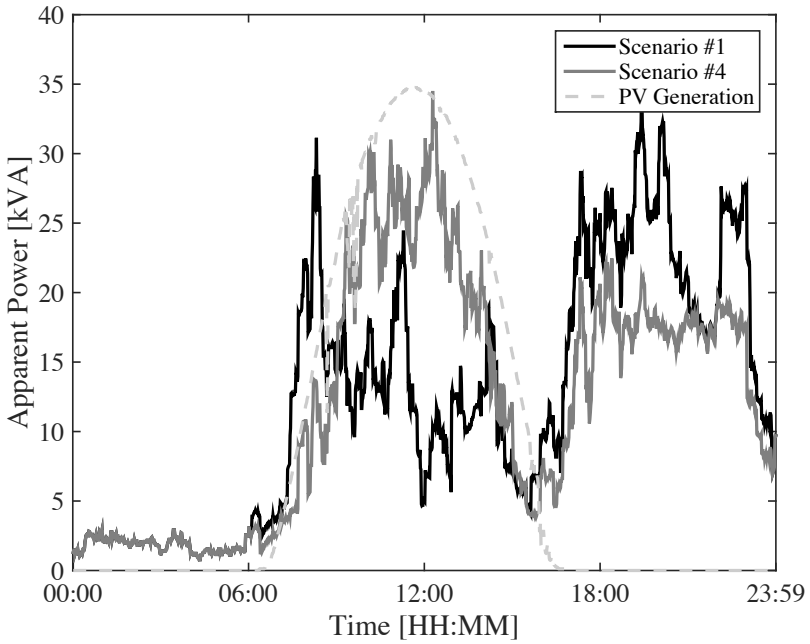

Figure 6.6 – Electricity demand at LVG's node 0 for a specific day of the 1-year experiments.

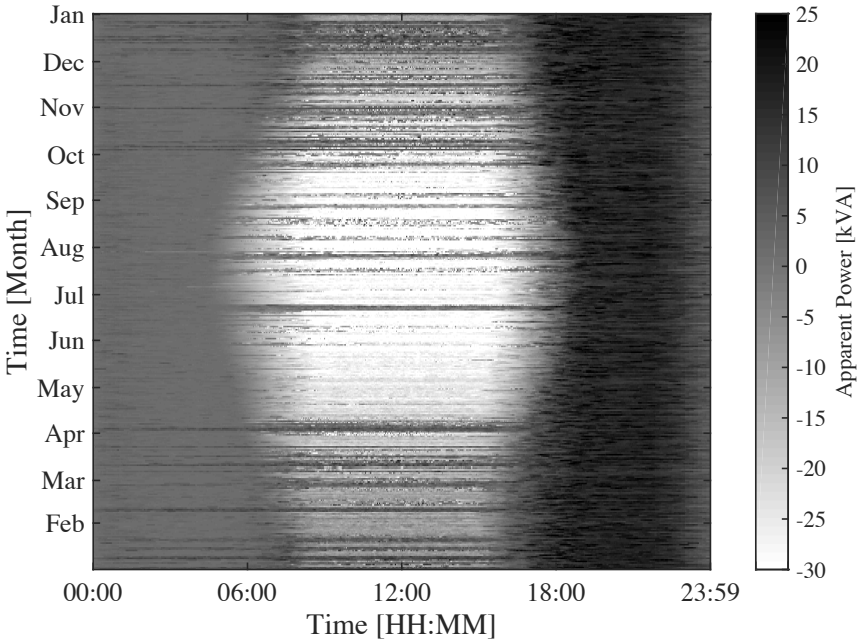

Figure 6.7 – LVG's node 0 load for Scenario #4.

For Scenarios #3 and #4, a variable number of controllable devices is available during each day. This is due to the stochastic behavior of the model used to generate the electricity demand profiles (i.e. Richardson model), in which every individual device has a certain probability to operate during a day as it is commonly observed on real world residential scenarios. As a consequence, there was not a single day where the controllable devices of the 33 buildings were all active (i.e.

the 99 controllable devices). Figure 6.8 presents the total number of controllable devices operating in each day of the 1-year experiments. On average, the Energy Flexibility offered by 48 controllable devices was available. The operation of the controllable devices accounts for 31.13 % of the neighborhood's annual electricity demand. However, this controllable electricity demand is not directly reflected into LM increasing because e.g. part of it is already observed during periods with PV generation.

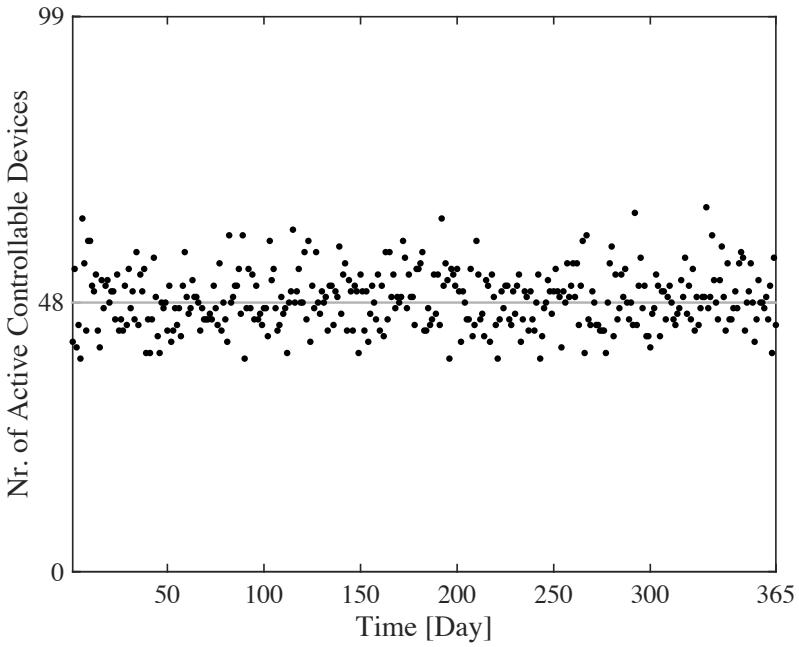

Figure 6.8 – Number of active controllable devices during each day of the 1-year experiments.

6.2. Load Matching

Despite the zero NB (computed on a yearly basis), the instantaneous LM of a Net-ZEB is normally far from being perfect. Net-ZEBs use the supply grid as an unlimited virtual storage system to achieve such NB not taking into consideration their instantaneous LM. Figure 6.9 presents the yearly SC and SS ratios of all 33 buildings for Scenario #2, considering the instantaneous LM between Net-ZEBs' on-site generation and electricity demand as described by Equations 3.2 and 3.3 (1-min resolution data is used). Yearly SC ratio values vary from 20.04 % to 28.66 %, while, SS ratio values vary from 21.86 % to 28.61% (both at Building-Level). The reason for these low values is related with the mismatch between the solar resource availability and the residents' daily routines and, consequently, their need for the services provided by household electrical devices. Analyzing the results obtained for Scenario #3, which are presented in Figure 6.10, it is evident that the yearly SC and SS ratios are increased when the 33 BL-LMI measures are applied. On

average these two metrics are improved by 9.50 and 10.68 %, respectively. Table 6.1 provides the data depicted in Figures 6.9 and 6.10.

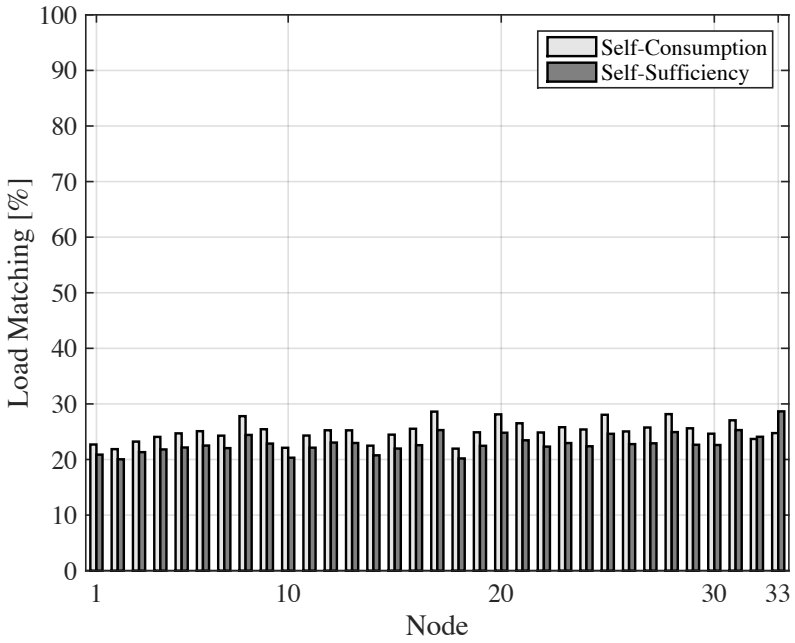

Figure 6.9 – Yearly load matching computed at each LVG's node for Scenario #2.

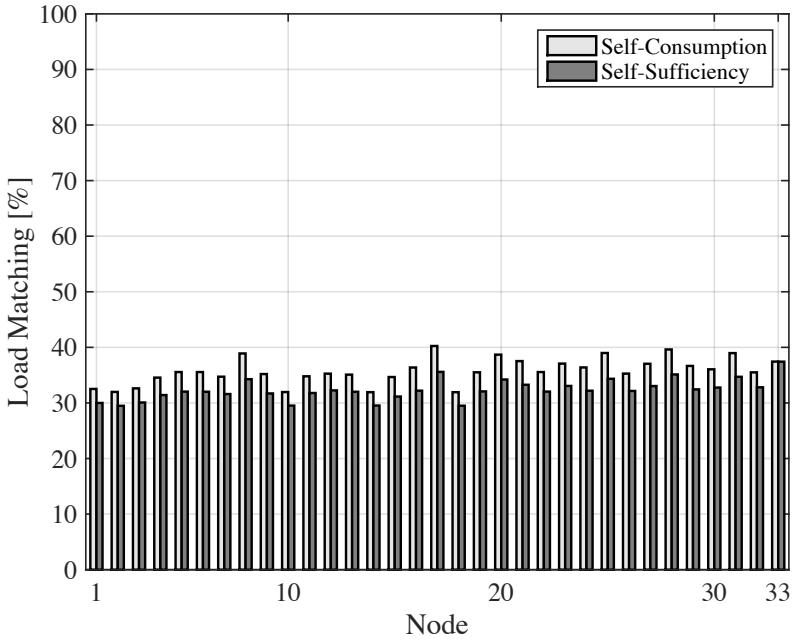

Figure 6.10 – Yearly load matching computed at each LVG's node for Scenario #3.

Table 6.1 – Yearly load matching computed at each LVG's node for Scenarios #2 and #3.

LVG's Node	Scenario #2		Scenario #3	
	SC [%]	SS [%]	SC [%]	SS [%]
1	20.88	22.70	30.00	32.52
2	20.04	21.86	29.48	31.98
3	21.32	23.22	30.08	32.62
4	21.81	24.07	31.42	34.56
5	22.16	24.70	32.04	35.56
6	22.51	25.09	32.02	35.56
7	22.05	24.29	31.60	34.72
8	24.42	27.80	34.27	38.90
9	22.86	25.45	31.71	35.20
10	20.32	22.11	29.52	31.96
11	22.12	24.31	31.79	34.79
12	23.05	25.26	32.26	35.27
13	22.97	25.25	32.01	35.09
14	20.75	22.49	29.53	31.94
15	21.97	24.47	31.15	34.66
16	22.58	25.53	32.21	36.38
17	25.29	28.61	35.59	40.24
18	20.19	21.95	29.50	31.93
19	22.46	24.89	32.08	35.51
20	24.82	28.12	34.21	38.69
21	23.46	26.52	33.27	37.53
22	22.32	24.86	32.04	35.56
23	22.96	25.81	33.06	37.08
24	22.38	25.40	32.20	36.39
25	24.62	28.05	34.34	38.98
26	22.77	25.05	32.16	35.28
27	22.92	25.76	33.04	37.05
28	24.93	28.16	35.12	39.62
29	22.65	25.62	32.44	36.66
30	22.61	24.64	32.76	36.05
31	25.29	27.05	34.70	38.97
32	24.09	23.69	32.81	35.50
33	28.66	24.75	37.42	37.44
Average	22.86	25.08	32.36	35.76

The value of the aforementioned ratios for Scenarios #2 and #3 is significantly increased when computed at LVG's node 0 (i.e. SC and SS ratios of the entire neighborhood), as depicted in Figure 6.11. This is due to the instantaneous matching between the generation surplus of some buildings and the electricity importing needs of others. Higher LM values at LVG's node 0 mean lower interaction between LV and MV distribution grids. Scenarios #3 and #4 reveal comparable yearly LM values at LVG's node 0 but with the later exhibiting higher values due to the superior instantaneous matching between CNet-ZEC's electricity generation and demand. The importing periods registered in Scenario #3 around noon are responsible for this difference as described further ahead in this section.

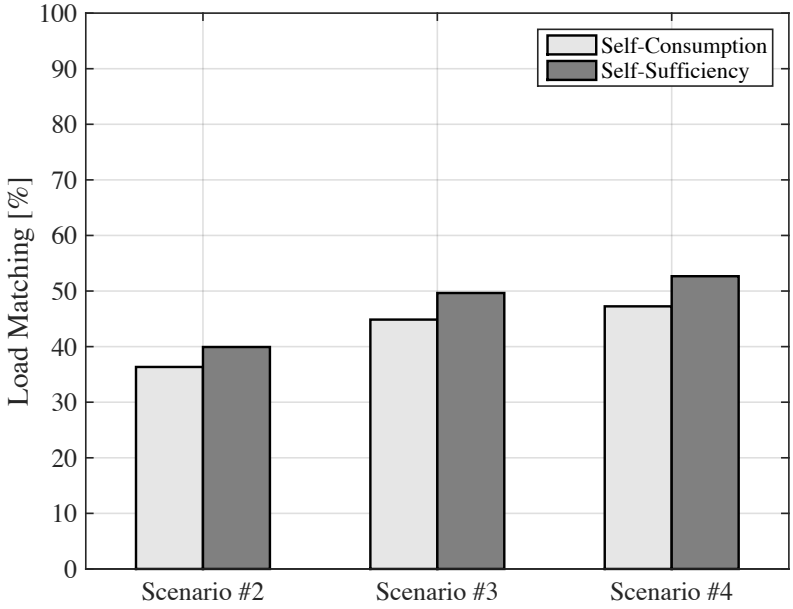

Figure 6.11 – Yearly load matching computed at LVG's node 0. Scenario #2: SC = 36.34 %, SS = 39.93 %. Scenario #3: SC = 44.86 %, SS = 49.65%. Scenario #4: SC = 47.25 %, SS = 52.67 %.

To understand the seasonal variation of the SC and SS ratios, the monthly values of these metrics were computed (see Figure 6.12). During the months with lower irradiance, monthly SC ratio values are higher, reflecting the existence of lower generation surpluses, while, the monthly SS ratio values are lower as a result of the decreased demand instantaneous matched by the electricity generated within the LVG. Regarding the summer months, the behavior of these metrics is exactly the opposite, with the monthly SS ratio achieving the highest values, due to the increased demand instantaneously matched by the PV generation, and the monthly SC reaching the lowest values due to the excessive PV generation. As expected, Scenario #2 presents the poorest monthly SC and SS ratios since no LM improvement measures are applied. Scenarios #3 and #4 exhibit similar values during the summer but differ in months with lower irradiance. The reason for this

difference is related with the type of load shifting applied – while in Scenario #3 the operation of all controllable devices is typically delayed to periods around noon, in Scenario #4 the operation of these devices is spread along the day, resulting in lower demand and generation surpluses when the availability of the solar resource is lower.

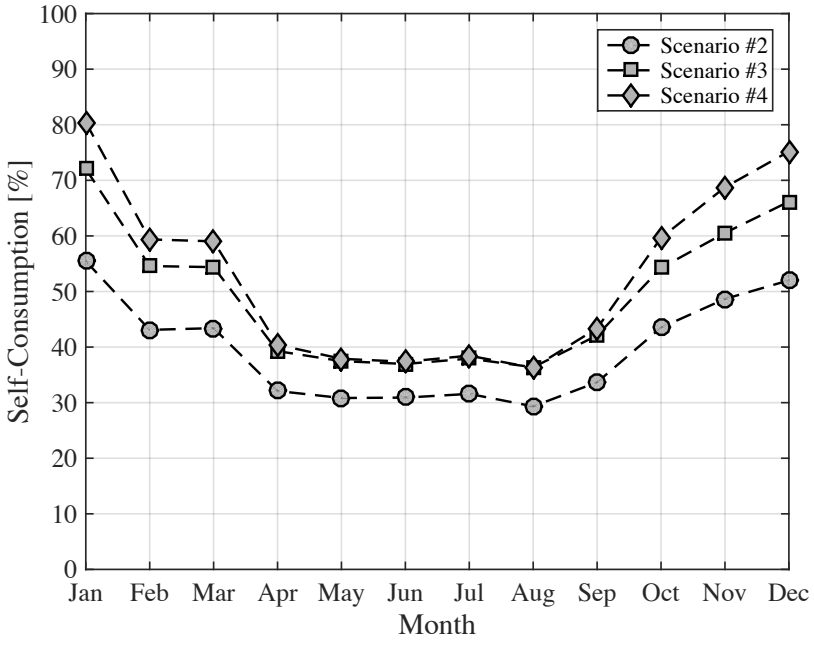

a)

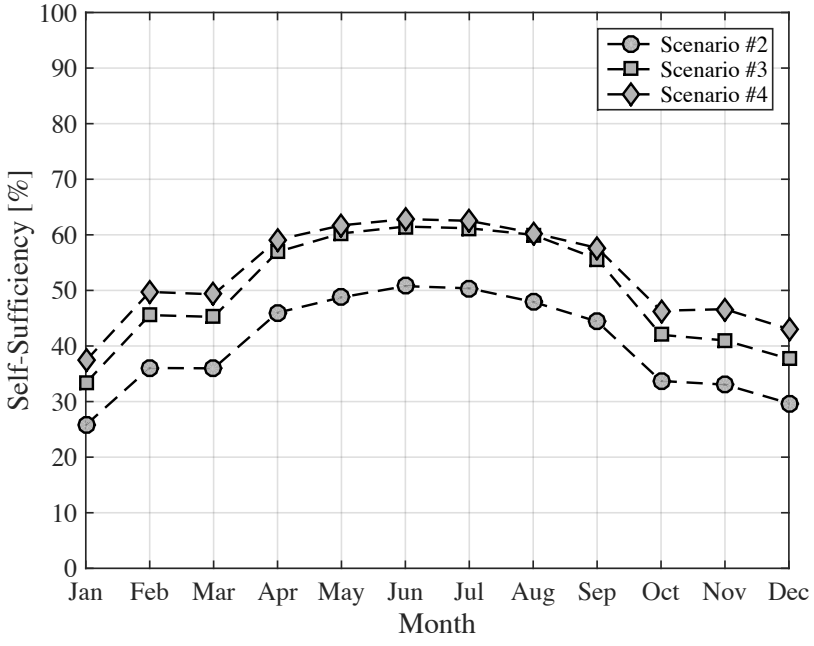

b)

Figure 6.12 – Monthly load matching computed at LVG's node 0. a) Self-Consumption. b) Self-Sufficiency.

The impacts introduced on SC and SS ratios by the application of different LM improvement measures are evident when the hourly values of these metrics are analyzed. Figures 6.13-6.16 present the average hourly LM values over four months (January, April, July, and October) representing the different seasons of the year. While in Scenario #3, the average hourly SC ratio has its peak during the 12th hour of the day, in Scenario #4 the improvement of this metric is reasonably distributed along the day (still with the maximum value typically occurring during the 12th hour of the day). Regarding the hourly SS ratio, the application of the BL-LMI measures (Scenario #3) results on decreased values around midday, even when compared to Scenarios #2. These reduced values reflect the demand surplus originated by controllable devices' operation delay to a coincident period. The applied CL-LMI measure (Scenario #4) does not suffer from this drawback since the operation of the controllable devices is spread along the day. In harmony with the results previously analyzed, the average hourly SC ratio values are higher during January and lower during July for all the considered scenarios, in opposition to the average hourly SS ratio values, that are higher in July and lower in January. In fact, SS ratio values close to 100 % are common for all scenarios, particularly in April and July, as a result of the oversized PV systems installed in each building. As expected, SS ratio is 0 % during the night, reflecting the lack of solar energy. By convention, SC ratio is 100 % during this period.

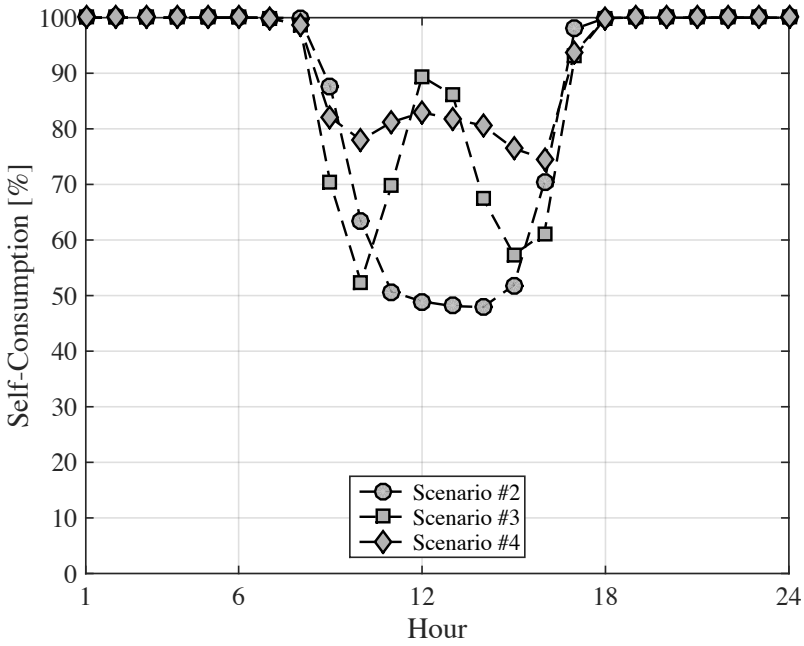

a)

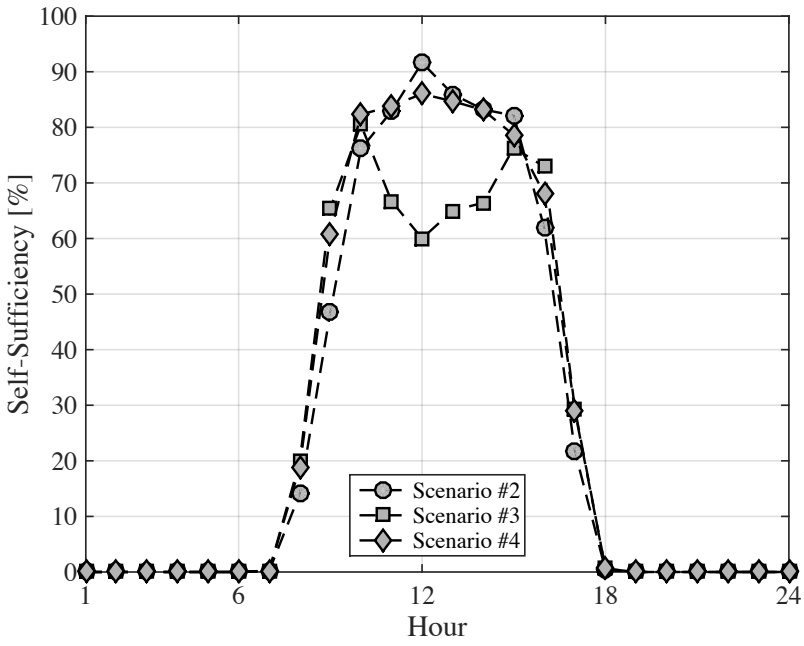

b)

Figure 6.13 – Hourly average load matching computed at LVG's node 0 for January. a) Self-Consumption. b) Self-Sufficiency.

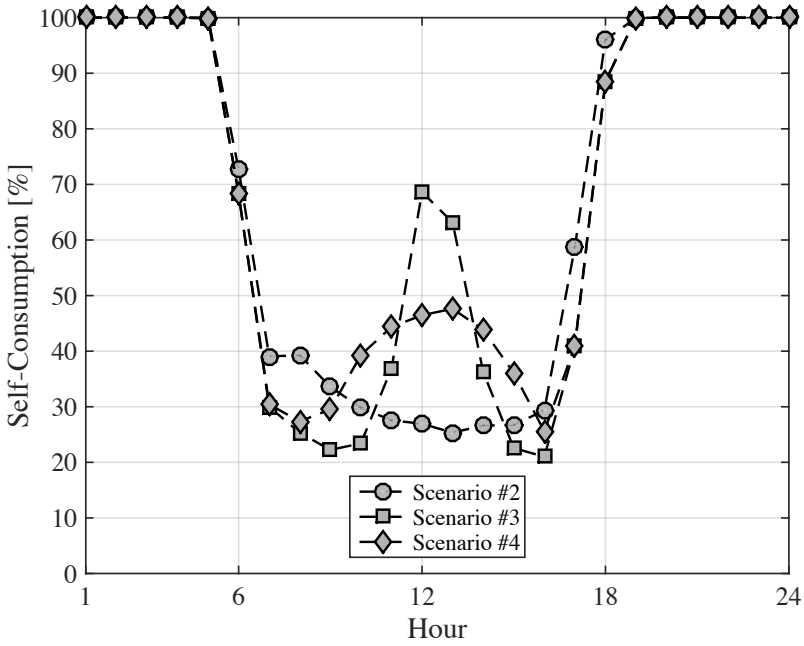

a)

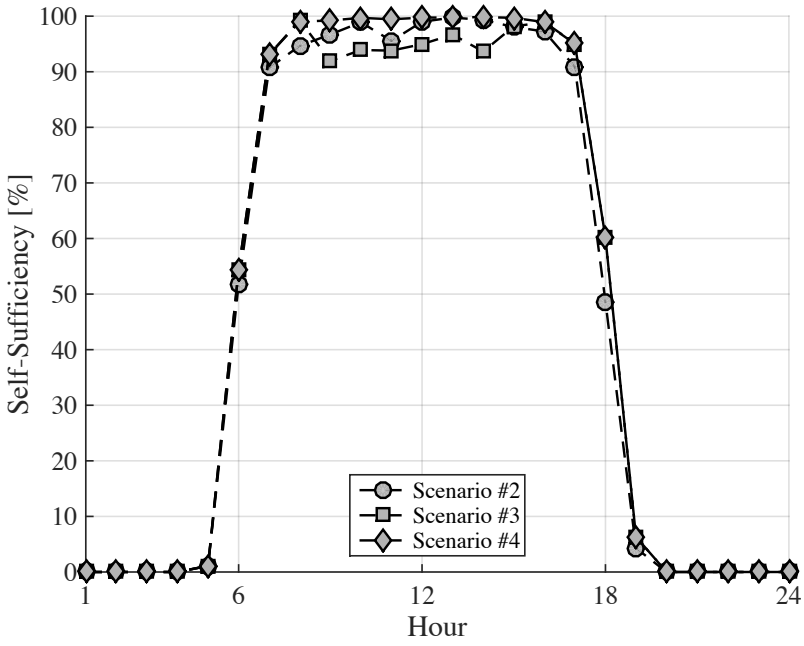

b)

Figure 6.14 – Hourly average load matching computed at LVG's node 0 for April. a) Self-Consumption. b) Self-Sufficiency.

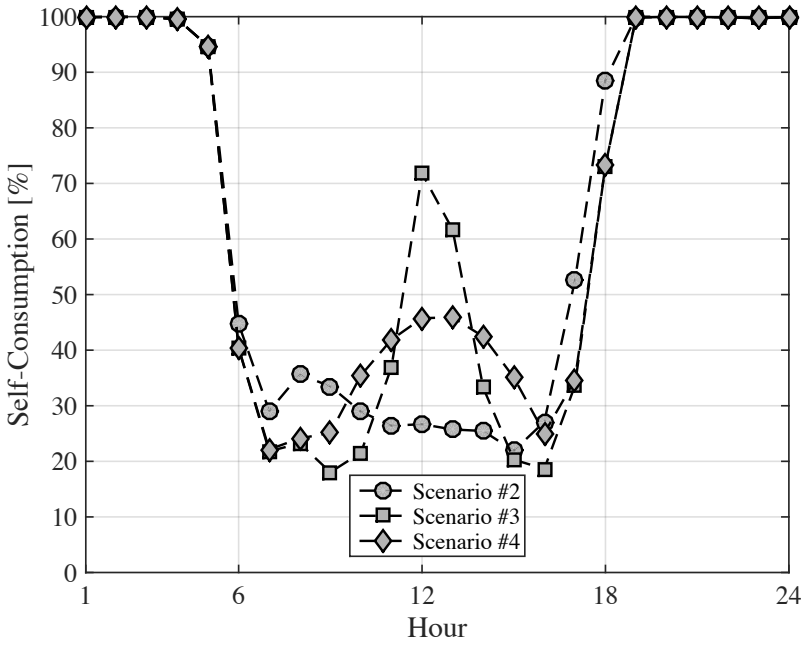

a)

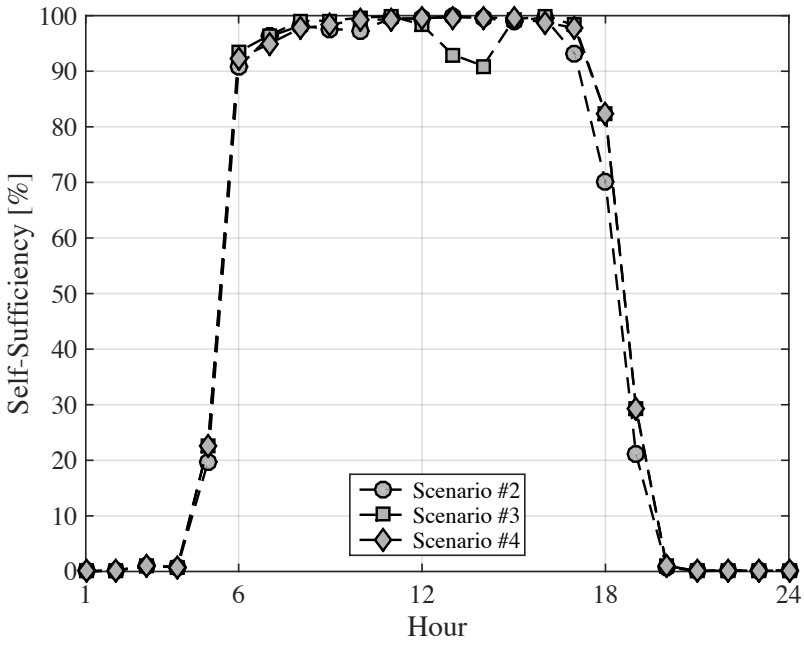

b)

Figure 6.15 – Hourly average load matching computed at LVG's node 0 for July. a) Self-Consumption. b) Self-Sufficiency.

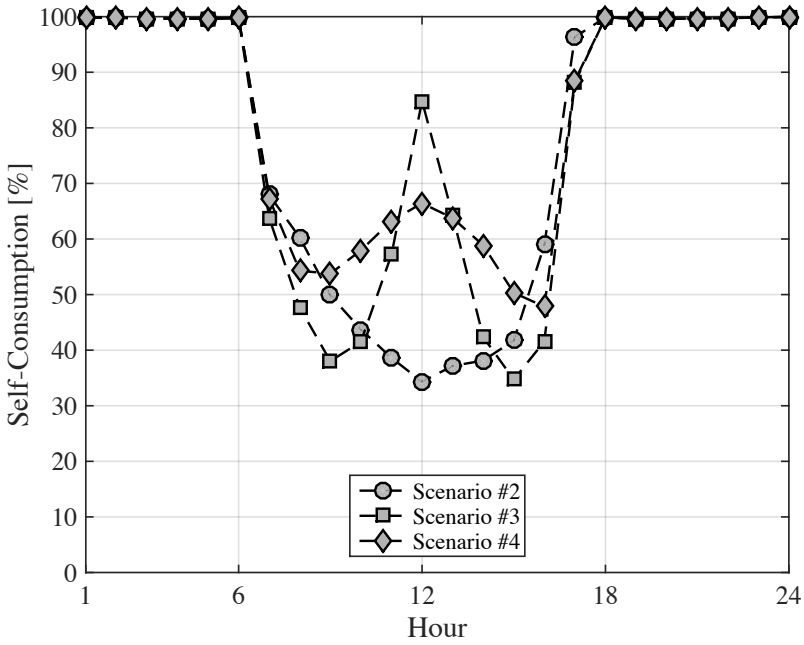

a)

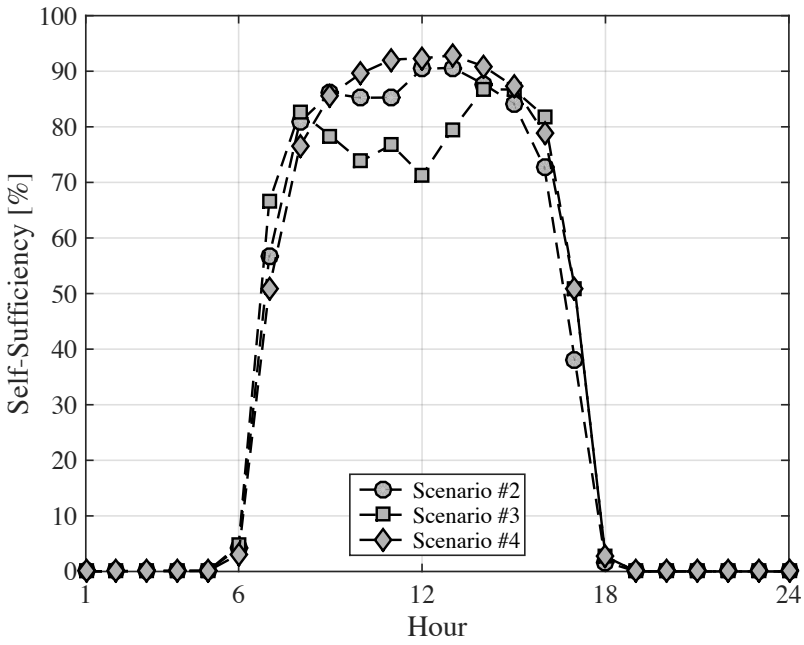

b)

Figure 6.16 – Hourly average load matching computed at LVG's node 0 for October. a) Self-Consumption. b) Self-Sufficiency.

6.3. Performance Indicators

The following sections present and analyze the results obtained for the Performance Indicators associated to each scenario, which are summarized in Table 6.2. These Performance Indicators were described in Section 5.2. Since on a real world situation the renovation works necessary for the transition between Scenario #1 and Scenario #2 would probably not occur simultaneously in all buildings, an additional scenario is considered in this work, where the number of buildings converted to Net-ZEBs varies over time. These results are presented and analyzed in Annex B.

Table 6.2 – Performance Indicators for the experiments carried out.

Scenario	**Peak Load [kVA]**	**Energy Losses [kWh]**	**Transf. Aging [days]**
#1	49.6	2308	365
#2	51.6	3821	32377
#3	72.3	2923	17338
#4	49.5	2678	1342

6.3.1. Peak Load

According to the data provided in Table 6.2, the yearly peak load registered in each scenario during the conducted experiments is depicted in Figure 6.17. The gathered values vary from 49.5 kVA in Scenario #4 to 72.3 kVA in Scenario #3. These results show that the 33 BL-LMI (isolated) measures deteriorate this Performance Indicator, when compared to Scenario #2, as a result of controllable devices' operation shifting to coincident periods. In addition to the yearly peak load, the daily peak load is also considered in this analysis to support the collected findings.

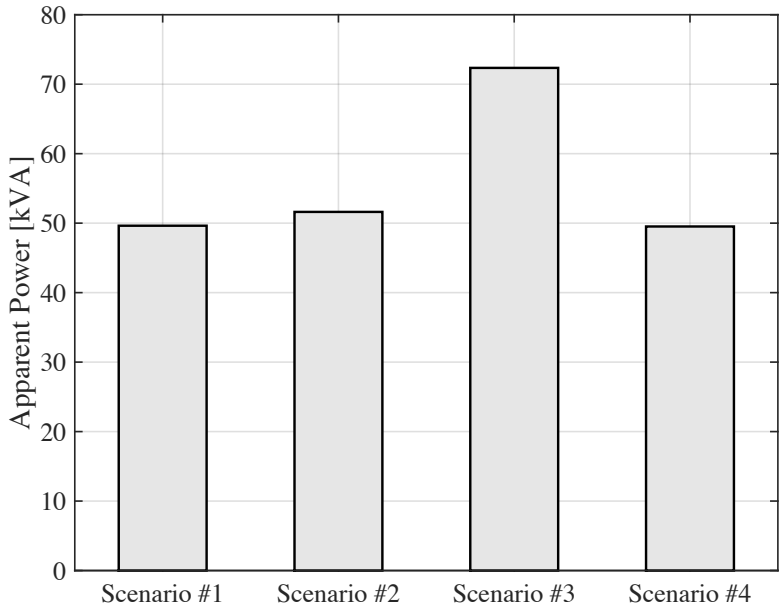

Figure 6.17 – Yearly peak load at LVG's node 0.

Figure 6.18 depicts the peak load registered at LVG's node 0 during each day of the 1-year experiments for the four considered scenarios, while Figure 6.19 shows the average daily peak load for each scenario, according to the data presented in Figure 6.18. These figures show that the daily peak load at LVG's node 0 is strongly affected by the scenario considered in the analysis, reflecting, as expected, the results presented in Sections 6.1 and 6.2. The main differences among scenarios concern the instant of the daily peak load occurrence and its amplitude.

In Scenario #1, the daily peak load typically occurs during the early-evening, with a few exceptions occurring around breakfast time. On lower irradiance days, Scenarios #2 and Scenario #1 show similar maximum loads. During the remaining days, Scenario #2 is characterized by strong reverse power flows that originate peak loads around noon. From Scenario #1 to Scenario #2, the average daily peak load is increased by 18 %.

Regarding Scenario #3, the obtained results show that the 33 BL-LMI measures originate the highest daily peak loads of all the considered scenarios with an average value of 40 kVA (22 % higher than in Scenario #1). The reason for this performance is related with the previously referred coincident demand shifting to periods with maximum on-site generation (i.e. each BL-LMI measure delays the operation of its controllable devices without taking into consideration the demand and on-site generation profiles of the remaining buildings, resulting in new peak loads at the referred time periods). Additionally, Scenario #3 also presents peak loads around noon in days with higher irradiance due to excessive PV generation (in these days, neighborhood's PV generation is higher than the demand peak originated by the BL-LMI measures).

Last but not least, Scenario #4 is characterized by daily peak loads occurring during the early-evening and around noon, depending on the amount of solar energy available. For lower irradiance days, SC ratios close to 100 % are achieved due to the applied CL-LMI measure. As a consequence, in these days, the peak load occurs during the early-evening, as in Scenario #1, but with smaller amplitudes since the electricity demand of the controlled devices is shifted to periods that improve the LM values of the entire LVG. In days with higher irradiance, the shifted electricity demand is not sufficient to avoid the occurrence of reverse power flows with higher amplitude than the demand registered during the early-evening. It should be noted that no additional demand peaks are originated by the CL-LMI measure. This scenario presents the best results with an average daily peak load at LVG's node 0 of 31 kVA.

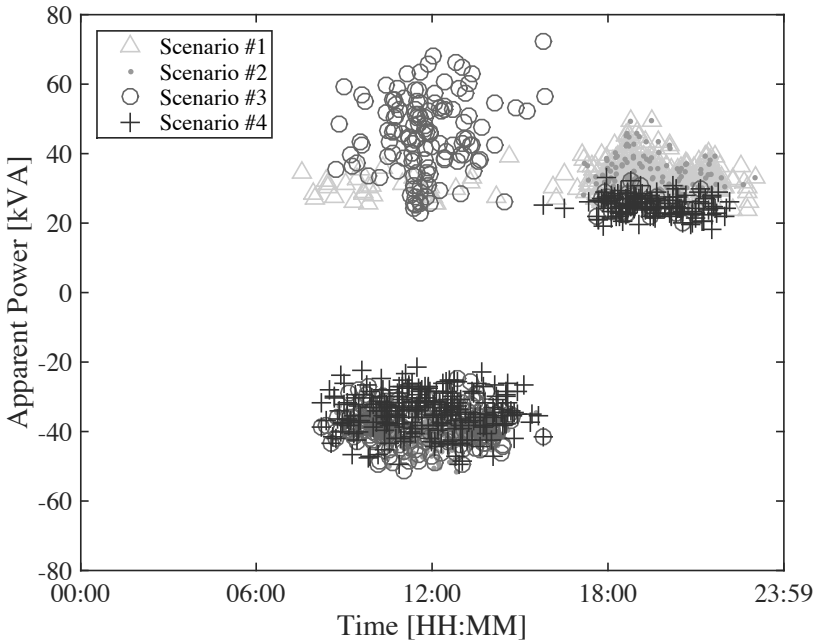

Figure 6.18 – Daily peak load at LVG's node 0.

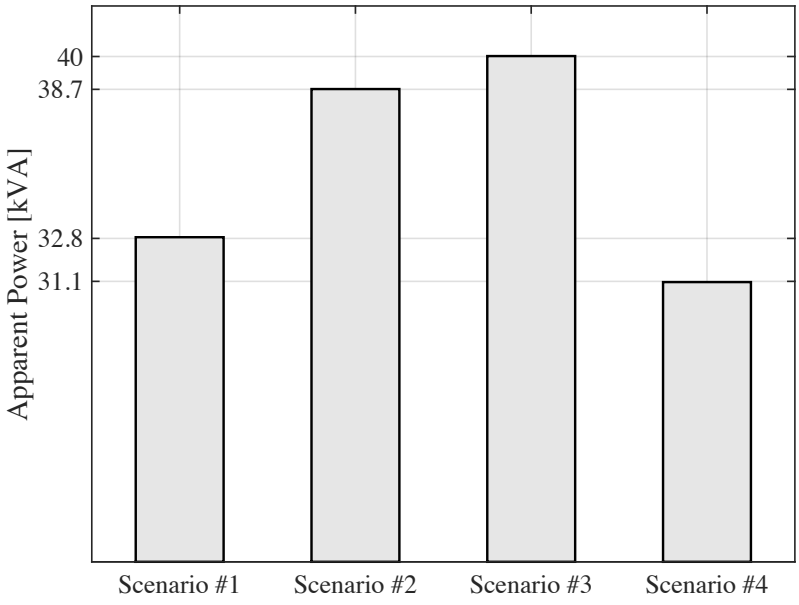

Figure 6.19 – Average daily peak load at LVG's node 0.

6.3.2. Energy Losses

The registered resistive losses have a cumulative nature both in time and location if the entire LVG is considered. Increasing losses of a specific section can be compensated by a reduction at another time-period or at another grid section. The annual losses by Joule Effect occurring along the entire LVG were computed for all the considered scenarios using Equation 5.4. The obtained results, presented in Figure 6.20, show that resistive losses are comparable with the annual electricity demand of a single building (see Table 5.2). Scenario #2 presents the worst performance, followed by the scenario where the BL-LMI measures are implemented (Scenario #3). Despite presenting the lowest yearly and average daily peak load at LVG's node 0, Scenario #4 shows higher annual resistive losses than Scenario #1. The reason for this is related with the cumulative nature of Equation 5.4 and with the fact that, in total, due to the PV generation, Scenario #4 still has higher LVG's load values than Scenario #1. Comparing to the electricity demand of the 33 buildings, the registered resistive losses vary from 2.47 % in Scenario #1 to 4.1 % in Scenario #2.

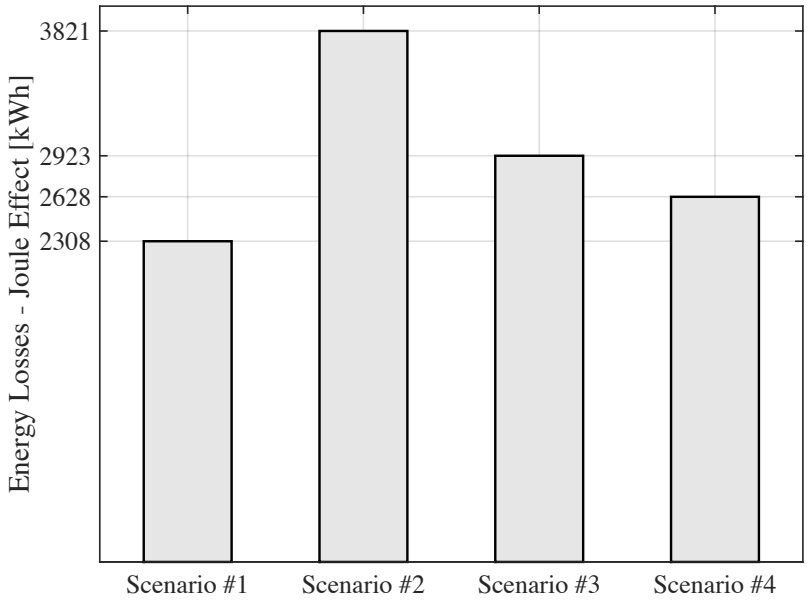

Figure 6.20 – Energy losses due to Joule effect during the 1-year experiments.

6.3.3. Transformer Aging

The model used in this work considers that the ambient temperature and the LVG's load impact the winding hot-spot temperature, which, consequently, sets the pace at which the winding insulation ages compared to a reference scenario where the transformer operates at rated load and temperature. To illustrate the aging process, this section starts by analyzing the transformer's

relative aging for Scenario #1 during a specific day of the 1-year experiment (the respective LVG's load and ambient temperature registered are depicted in Figure 6.21). The resulting transformers' hot-spot temperature and aging acceleration factor values are presented in Figure 6.22.

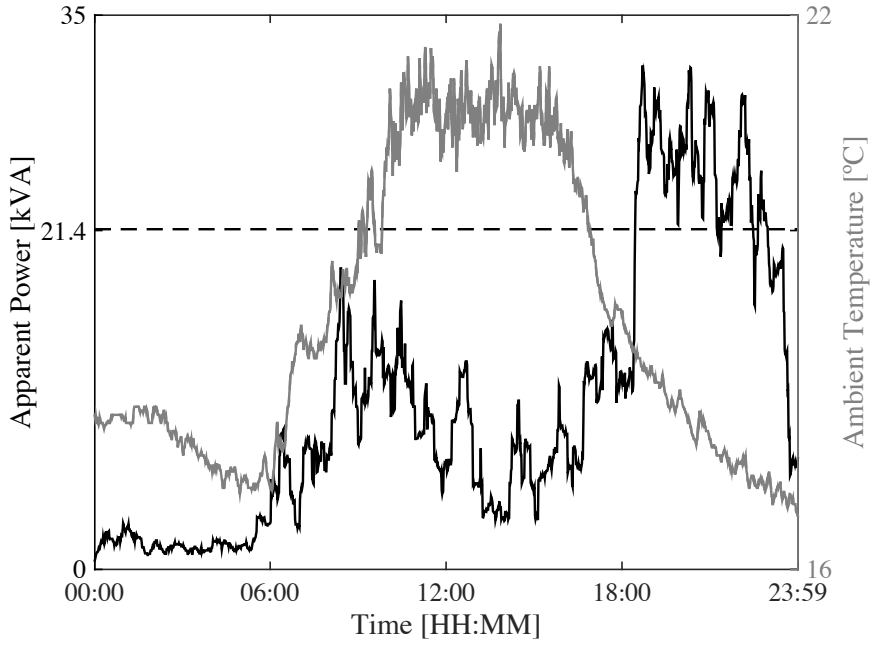

Figure 6.21 – Electricity demand at LVG's node 0 during a specific day of the 1-year experiment and the respective ambient temperature (Scenario #1).

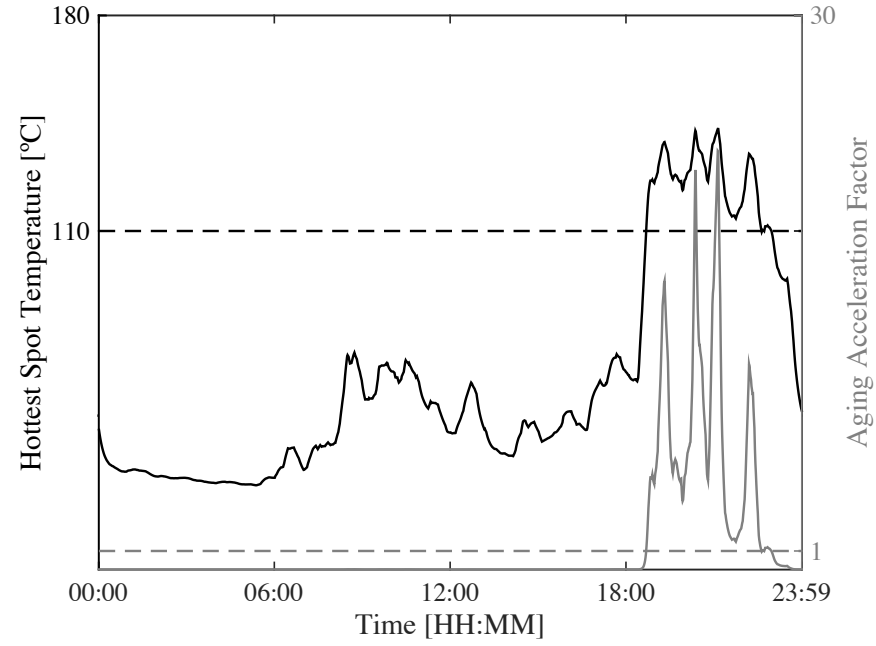

Figure 6.22 – Hot-spot temperature and aging acceleration during a specific day of the 1-year experiment (Scenario #1).

The obtained hot-spot temperature profile (Figure 6.22) follows the transformer's load, exhibiting slower dynamics essentially due to the thermal inertia of the mineral oil and windings. During the evening load peak, the hot-spot temperature reaches values higher than 110 ºC resulting in aging acceleration factor values greater than 1 (grey curve of Figure 6.22). During the rest of the day, the hot-spot temperature is smaller than 110 ºC resulting in reduced aging acceleration factor values. For this specific day, the equivalent aging of the transformer was 30.3 hours. This value indicates that the transformer aged 6.3 hours more when compared to the reference 24 h operation at hot-spot temperature of 110 ºC.

The normal life expectancy loading considers occasional LVG's loads higher than transformer's rated values. In fact, according to IEC 60076-7, during a normal cycle, transformer's load can reach values 50% higher than rated load. As long as these operation periods at higher than rated loads have a relatively short duration, comparing to the entire operation cycle, the transformer's winding insulation aging can still be unitary (i.e. operation periods with excessive aging are compensated by longer periods operating with lower loads). This is the case of Scenario #1, where the considered transformer suffered a unitary relative aging over the 1-year experiment despite the fact that in some time-steps its aging acceleration factor assumed values higher than 1 (see Figure 6.23).

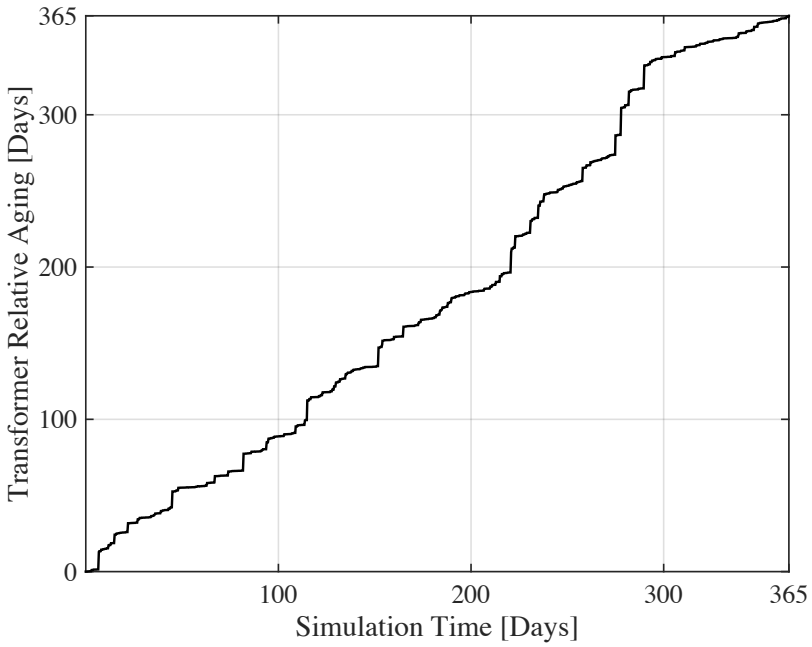

Figure 6.23 – Cumulative equivalent transformer aging for Scenario #1.

As addressed in Sections 6.1 and 6.3.1, the conversion of the original buildings to Net-ZEBs strongly impacts LVG's load profiles and peak load values (i.e. the transition from Scenario #1 to Scenario #2). Taking this into consideration, the results for Scenario #2 show that the 21.4 kVA

transformer suffered an unacceptable aging of 32,377 days during the 1-year experiment (see Figure 6.24). For Scenarios #3 and #4, the relative aging of the considered transformer was 17,338 and 1342 days, respectively. These results show that the simple transition of the 33 buildings to Net-ZEBs (Scenario #2) or the transition assuming the application of the BL-LMI measures (Scenario #3) result in prohibitive equivalent transformer aging values. In these cases, (Scenarios #2 and #3), the transformer would have to be replaced by a larger one. More specifically, the 21.4 kVA transformer would have to be replaced by a 28.5 kVA transformer in Scenario #2 and by a 27.3 kVA transformer in Scenario #3 in order to achieve a unitary aging over the 1-year experiments. If a unitary aging over a 1-year period would also be a requirement for Scenario #4, a 23.4 kVA transformer would be needed.

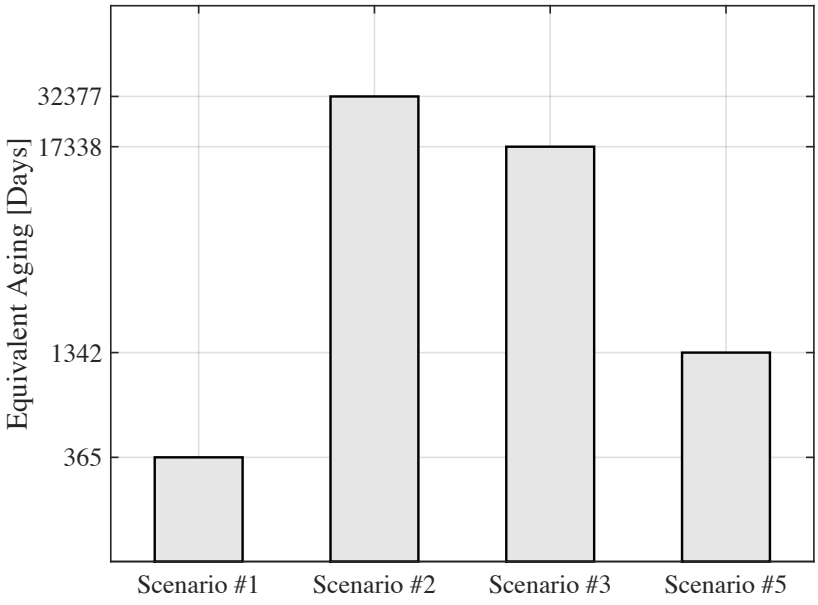

Figure 6.24 – Equivalent transformer aging during the 1-year operation (logarithmic scale).

The rate at which the transformer aging occurs is completely different when comparing Scenario #1 with the remaining scenarios. This difference is related with the operation of the introduced PV generation systems. For instance, Figure 6.25 depicts the cumulative equivalent transformer aging for Scenario #4, where it can be seen that periods associated to lower equivalent aging are not enough to compensate the equivalent aging induced by the reverse power flows and higher ambient temperatures registered during the summer.

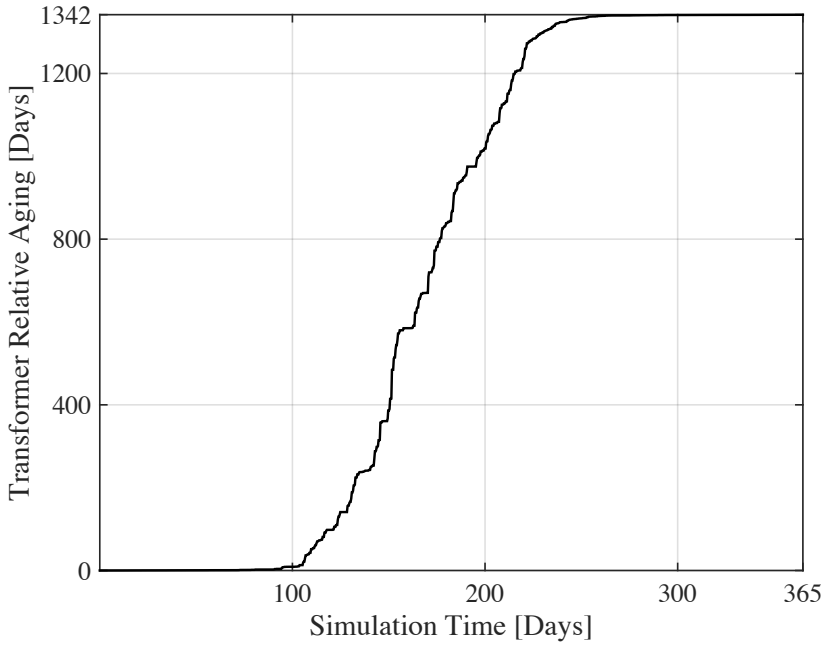

Figure 6.25 – Cumulative equivalent distribution transformer aging for Scenario #4.

The variance introduced in the transformer's relative aging by the different scenarios can be assessed in more detail by analyzing the hot-spot temperature during the 1-year experiments, as depicted in Figures 6.26-6.29. In all scenarios, the hot-spot temperature reveals a 24 h duration cycle, following the LVG's load and ambient temperature profiles, as expected from the results presented in Figures 6.21 and 6.22. For Scenarios #2, #3 and #4, the highest hot-spot temperatures are normally registered around noon, when the PV generation is more effective and the ambient temperature is higher, while, for Scenario #1, the highest hot-spot temperatures occur during the evening when LVG's load reaches its higher values.

The highest hot-spot temperatures reached in Scenarios #2 and #3 are higher than 180 ºC for long periods of time, which are well above the maximum value suggested by IEC 60076-7 (in such extreme conditions, transformer's winding insulation would most probably decay and the transformer would fail). When compared to Scenario #2, Scenario #3 presents reduced values during the evening and around noon due to the delayed operation of the controllable devices. It is important to note that in periods with lower irradiance, additional hot-spot temperature peaks occur around noon as a consequence of the coincident demand shifting induced by the BL-LMI measures. Regarding the results obtained for Scenario #4, these show that the CL-LMI leads to the lower hot-spot temperature peak values as a result of the evenly distributed demand of the controllable devices during periods with solar energy availability. However, on average, the hot-spot temperature registered in Scenario #4 is still higher than the one of Scenario #1. As in Scenario #3, the CL-LMI measure also conducts to reduced hot-spot temperatures during the evening, reflecting the delay applied to the operation of the controllable devices.

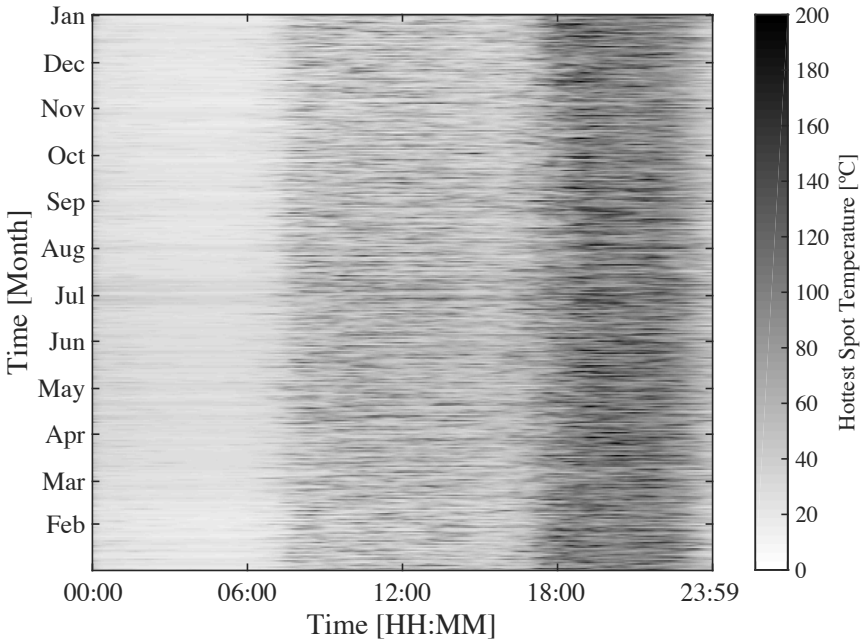

Figure 6.26 – Hot-spot temperature during each minute of the 1-year experiment (Scenario #1).

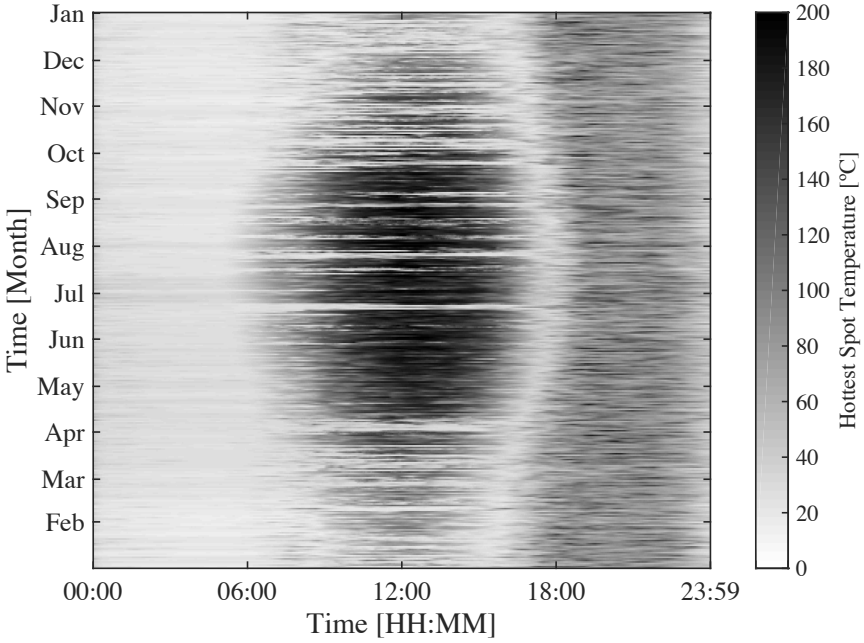

Figure 6.27 – Hot-spot temperature during each minute of the 1-year experiment (Scenario #2).

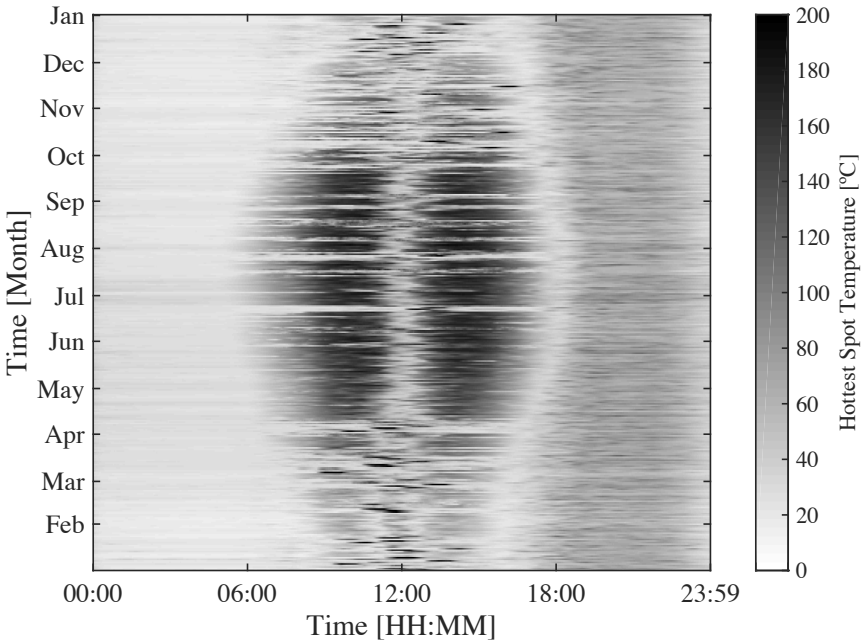

Figure 6.28 – Hot-spot temperature during each minute of the 1-year experiment (Scenario #3).

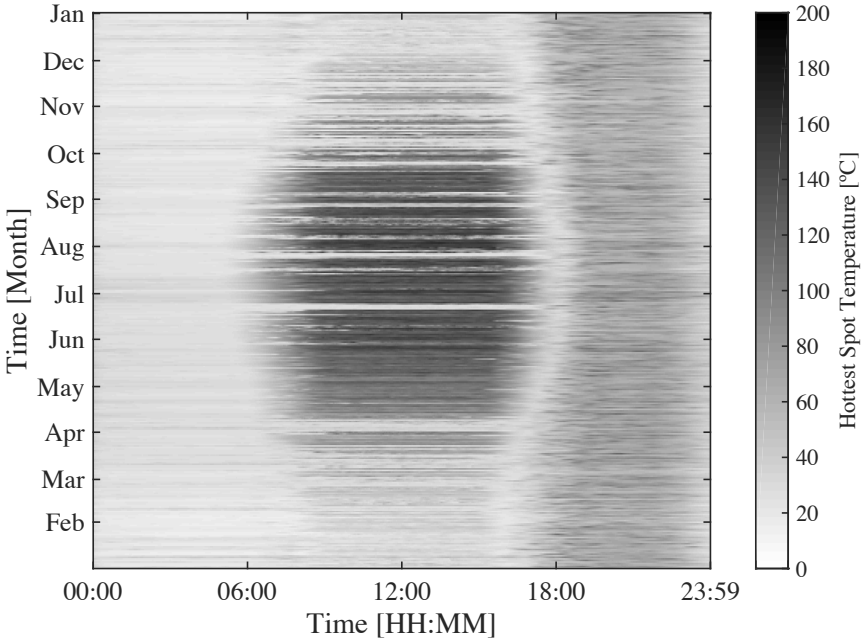

Figure 6.29 – Hot-spot temperature during each minute of the 1-year experiment (Scenario #4).

6.4. Electricity Costs

Electricity costs associated with each tariff vary significantly among the considered scenarios. This can be observed in Figure 6.30, where the average annual electricity cost, supported by building owners in each scenario, is depicted for TOU 1, 2, and 3. Table 6.3 aggregates the data presented in this figure. For the three types of tariffs, Scenario #4 presents the lowest annual electricity costs. On average, the CNet-ZEC leads to annual electricity cost reductions of 63 %, 38 %, and 27 % when compared to Scenarios #1, #2, and #3, respectively. Three factors contribute for the difference observed among the considered scenarios, namely: i) type of power metering; ii) load profiles associated with each scenario; and iii) amount of curtailed energy. These factors are analyzed in the following sections.

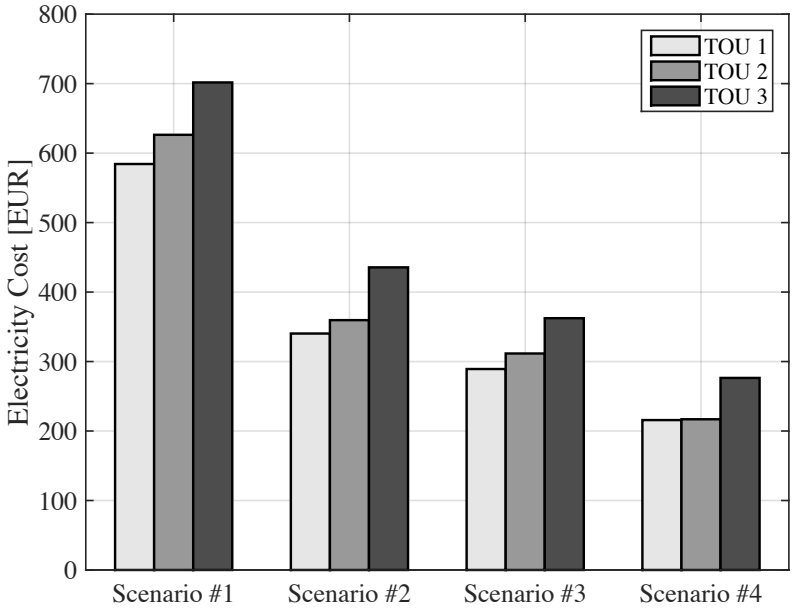

Figure 6.30 – Average annual electricity cost supported by building owners.

Table 6.3 – Annual electricity bill paid by each building owner (values in EUR).

Node	Scenario #1			Scenario #2			Scenario #3			Scenario #4		
#	T. 1	T. 2	T. 3	T. 1	T. 2	T. 3	T. 1	T. 2	T. 3	T. 1	T. 2	T. 3
1	438	471	526	266	282	338	232	256	284	216	217	276
2	434	466	523	265	282	341	232	255	285	216	217	276
3	434	468	523	261	279	335	229	253	282	216	217	276
4	520	561	633	308	329	401	265	288	330	216	217	276
5	580	621	697	339	358	435	290	313	362	216	217	276
6	579	620	696	336	355	430	289	312	363	216	217	276
7	538	576	645	318	335	404	274	295	336	216	217	276
8	700	756	850	389	415	508	327	351	419	216	217	276
9	582	623	696	336	354	427	292	314	367	216	217	276
10	441	470	527	269	284	342	236	259	288	216	217	276
11	541	580	651	320	338	408	275	298	342	216	217	276
12	557	604	675	325	350	424	281	308	357	216	217	276
13	547	588	650	319	338	401	276	300	341	216	217	276
14	442	473	529	269	284	341	236	259	288	216	217	276
15	566	608	687	332	353	430	286	308	360	216	217	276
16	610	650	724	350	367	442	297	317	372	216	217	276
17	727	784	871	399	424	513	331	353	419	216	217	276
18	435	466	521	266	282	339	232	255	286	216	217	276
19	599	640	717	350	367	445	299	318	371	216	217	276
20	708	756	848	392	410	505	332	351	423	216	217	276
21	617	660	729	349	367	439	295	315	362	216	217	276
22	592	635	713	345	364	443	295	318	372	216	217	276
23	646	693	786	370	392	484	312	336	400	216	217	276
24	608	647	727	349	365	445	297	317	373	216	217	276
25	699	748	838	386	404	496	326	346	416	216	217	276
26	545	587	653	318	339	407	274	297	341	216	217	276
27	646	690	780	371	390	478	312	337	401	216	217	276
28	729	782	878	404	426	523	337	359	431	216	217	276
29	598	641	718	343	362	438	291	311	361	216	217	276
30	611	652	739	360	380	468	304	328	387	216	217	276
31	688	735	820	395	415	500	323	343	407	216	217	276
32	609	650	728	376	396	474	307	327	378	216	217	276
33	715	768	859	453	480	570	360	386	458	216	217	276
AVG	584	626	712	340	360	436	289	312	365	216	217	276
Total	19 k	21 k	23 k	11 k	12 k	14 k	10 k	10 k	12 k	7 k	7 k	9 k
Key: AVG – Average; T.1 – TOU 1; T.2 – TOU 2; T.3 – TOU 3.												

6.4.1. Type of Power Metering

As previously referred, Scenarios #1, #2, and #3 implement power metering at each building's point of common coupling, while, in Scenario #4, power metering is conducted at LVG's transformer output. This metering paradigm shift reduces the costs spent on electricity imports and increases the value of the electricity generated within the CNet-ZEC's Balance Boundary due to the generation surplus sharing among the 33 buildings. This generation surplus sharing effect can be observed if an extra scenario is considered, where the referred power metering transition is applied to Scenario #2 and the resulting electricity costs are equally shared by the 33 building owners. In this extra scenario, the annual electricity cost supported by each building owner would be 283, 290, and 369 EUR, for TOU 1, TOU 2, and TOU 3, respectively. Therefore, comparing to Scenario #2, where power metering is conducted at each building's point of common coupling, average reductions of 17, 19, and 15 % would be achieved by implementing the referred metering paradigm shift. However, it should be noted that no benefit would result for the LVG operator since the electricity demand and generation profiles would remain unchanged.

6.4.2. Load Profiles Associated with Each Scenario

Based on Table 5.9, Figure 6.31 presents the price of each tariff throughout the day. Taking into consideration the load profiles associated with each scenario, analyzed in Section 6.1, considerable cost differences are observed among the scenarios, as depicted in Figures 6.32-6.34, where the resulting annual cost for each time-step (365 values added per time-step) is provided for the average of the 33 buildings. In Figures 6.31-6.34 only electricity bill's variable component, without taxes applied, is considered.

The electricity cost profiles obtained for TOU 1 (Figure 6.32) approximately follow the LVG's average load profiles presented in Figure 6.1. However, negative electricity cost values assume reduced magnitudes, while importing periods show amplified values. This discrepancy is related with asymmetric electricity importing and exporting costs (i.e. for each time-step, energy import values are multiplied by a factor of 0.1652 EUR/kWh, while energy export values are multiplied by a factor raging from 0.0139 to 0.0530 EUR/kWh, depending on the considered month – see Tables 5.8 and 5.9). The electricity cost profiles associated to the remaining tariffs (i.e. TOU 2 and 3) also follow this trend but with higher importing costs in some periods (e.g. from 18:00 to 20:30 for TOU 3) resulting in large cost increases. Note that TOU 2 and 3 most costly time-periods are coincident with LVG's peak periods, specially the one registered in the evening.

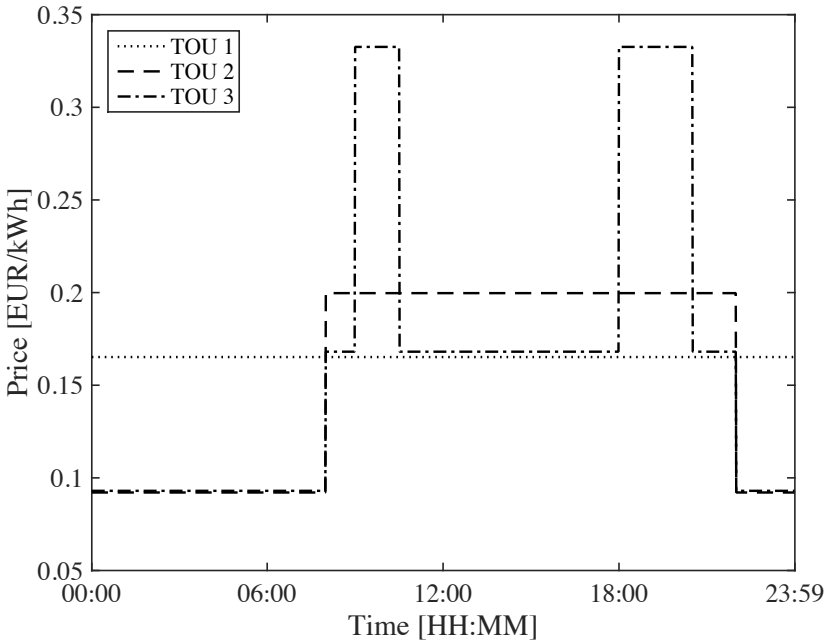

Figure 6.31 – Electricity tariffs without taxes (values based on Table 5.9).

The asymmetry between import and export prices is of special importance for Scenario #3 since the electricity demand originated around noon by the BL-LMI measures in days with lower solar resource availability results on considerable costs. Scenario #4 does not suffer from this phenomenon due to the following: i) the CL-LMI considers the on-site generation of the 33 buildings and therefore it is normally higher than the electricity demand of the controllable devices; and ii) the operation of the controllable devices is spread throughout the day.

It should be noted that in Scenario #4, since power metering is conducted at LVG's transformer output, energy losses due to Joule Effect are charged equally to building owners. Such losses are responsible for the differences registered between Scenarios #3 and #4 during evening and yearly morning. As analyzed in Section 6.3.2, losses due to Joule effect are comparable to a single building's annual electricity demand.

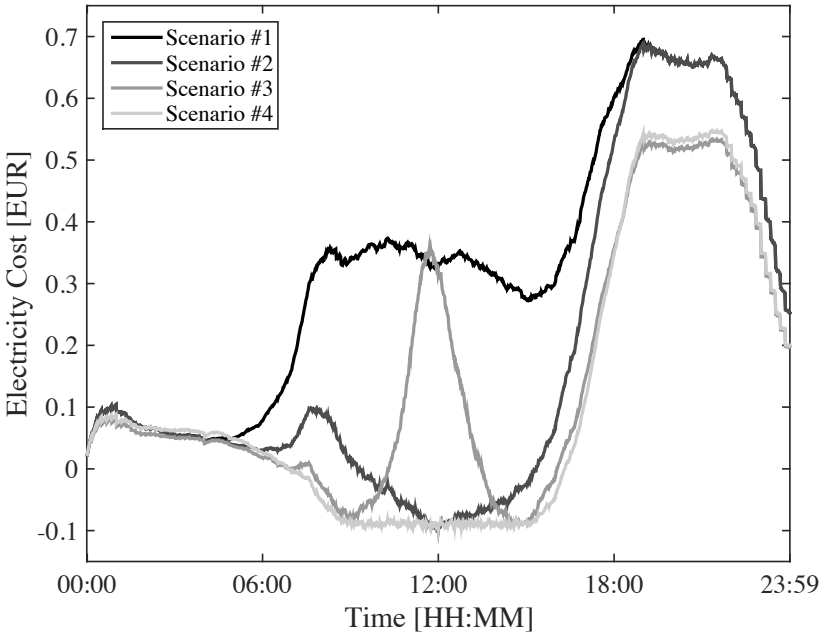

Figure 6.32 – Annual electricity cost for each time-step when TOU 1 tariff is applied without taxes (neighborhood average values).

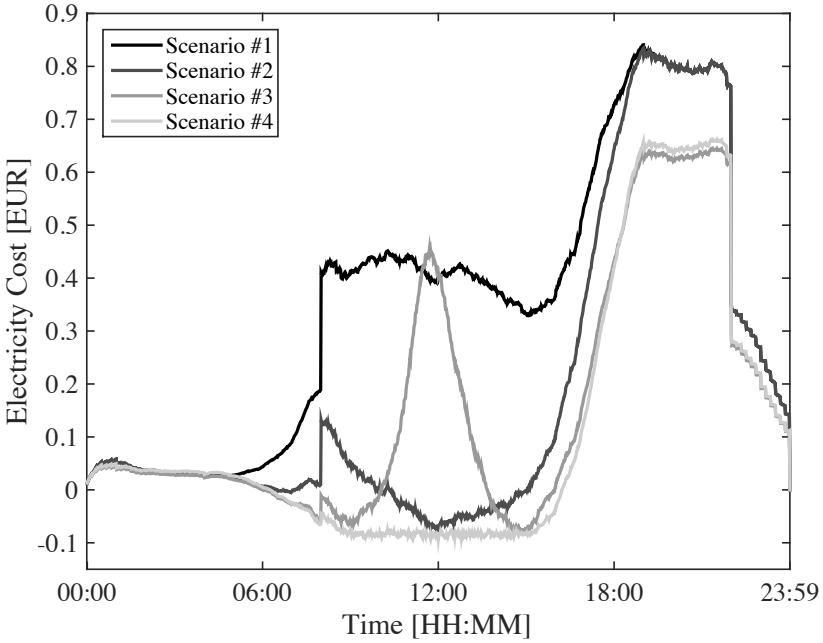

Figure 6.33 – Annual electricity cost for each time-step when TOU 2 tariff is applied without taxes (neighborhood average values).

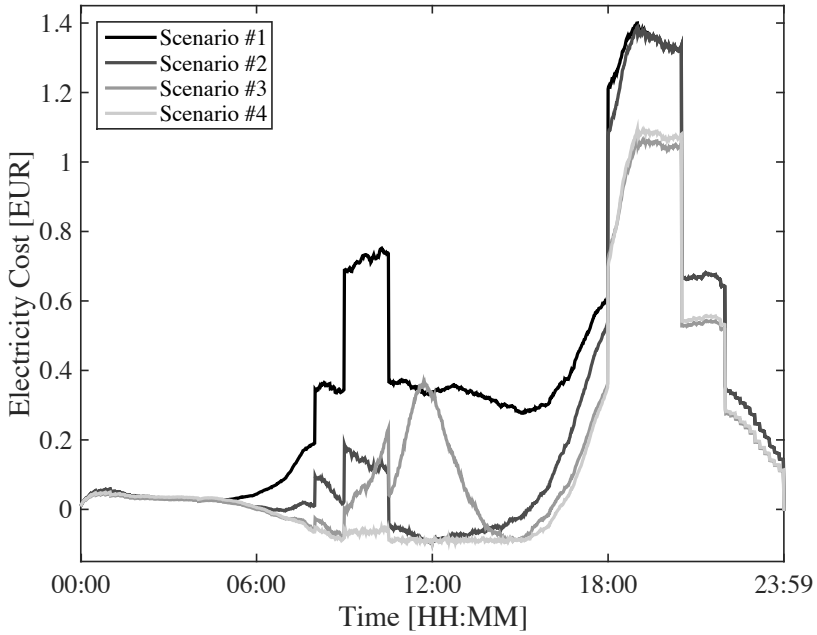

Figure 6.34 – Annual electricity cost for each time-step when TOU 3 tariff is applied without taxes (neighborhood average values).

6.4.3. Amount of Energy Curtailed

Curtailment is applied when building's point of common coupling voltage magnitude is 10 % higher than the nominal value. The amount of energy curtailed impacts building owners' annual electricity costs because less energy is exported to the LVG in the first three scenarios or to the MV distribution grid in Scenario #4 and less energy is available on-site to satisfy buildings' electricity demand. Figure 6.35 presents the amount of energy curtailed in each scenario, where Scenario #4 exhibits the best result, followed by Scenarios #3 and #2.

LVGs are traditionally seen as passive networks with radial configuration where power flows from higher to lower voltage levels (i.e. from the transformer output to consumers), leading to voltage drops along the distribution feeder. However, the integration of distribution generation in LVGs changes this paradigm resulting in reverse power flows and voltage rises along the distribution feeders. Therefore, the results presented in Figure 6.35 reflect the lower LVG's loads for Scenario #4, as analyzed in Sections 6.1 and 6.3.1, followed by the remaining two scenarios.

Impacts caused by PV generation systems on LVG's voltage magnitude levels strongly change along the day, following the availability of the solar resource. For illustration purposes, Figure 6.36 shows the line to line voltage magnitude at each LVG's node during a specific day of the 1-year experiment for two different instants (12h00 and 20h00) when the 33 buildings are converted to Net-ZEBs (Scenario #2), where the dashed lines refer to the voltage magnitude limits. At 20h00 the voltage drop along the distribution feeder is identic to Scenario #1, as the PV systems have no influence on LVN's operation. However, at 12h00, when the solar resource is available and

all Net-ZEBs are generating electricity on-site, the voltage profile is strongly modified, showing a rising effect along the grid, which is truncated due to the curtailment mechanism.

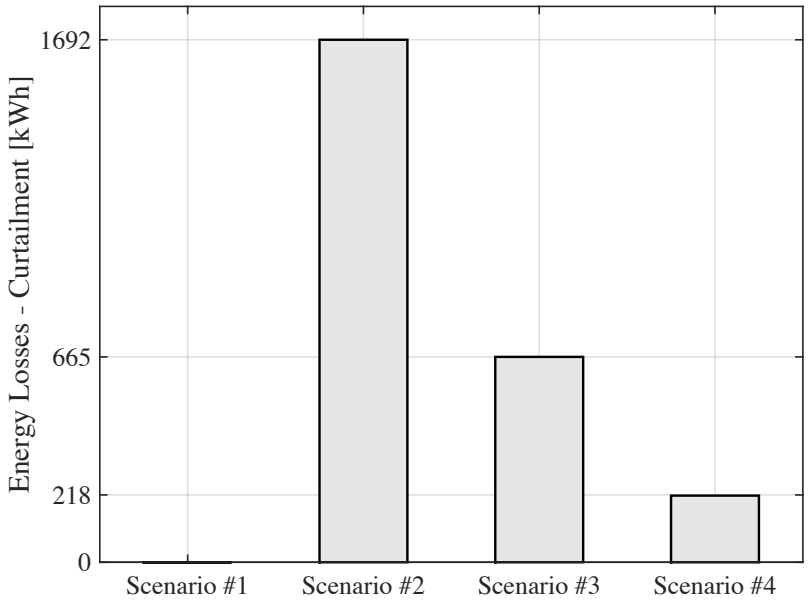

Figure 6.35 – Total Energy losses due to curtailment during the 1-year experiments.

Buildings at the end of the LVG suffer the larger voltage magnitude variations. Figure 6.37 presents the percentage of annual on-site generation curtailed by each building for the considered scenarios (buildings located between LVG's nodes 1 and 27 show no energy curtailment). It is clear that buildings at the end of the LVG suffer the biggest curtailment losses. This fact results from the voltage rising effect previously addressed. Curtailment losses also impact buildings' *NB*. As a result, buildings located between LVG's nodes 28 and 33 are no longer Net-ZEBs but nearly Net-ZEBs. To mitigate energy curtailment effects on buildings' *NB*, the number of PV modules present in each building would have to be increased. However, this change would further increase curtailment losses and, therefore, deteriorate expected ROIs.

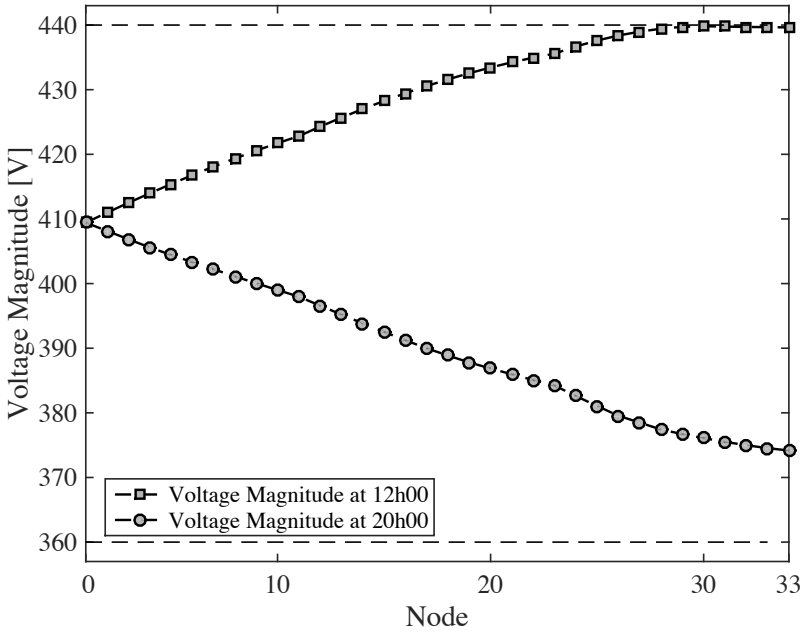

Figure 6.36 – Line to line voltage magnitude throughout the LVG at 12h00 and 20h00 during a specific day of the 1-year experiment for Scenario #2.

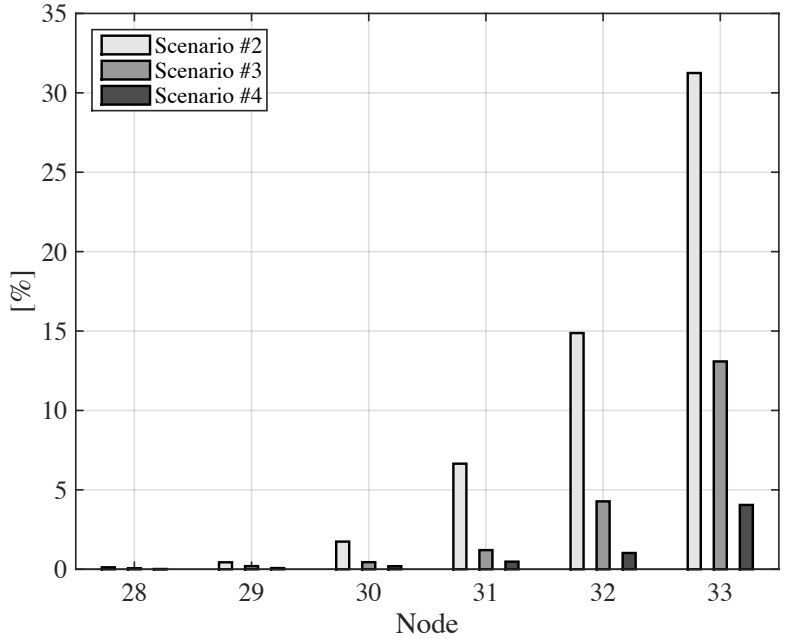

Figure 6.37 – Percentage of annual on-site electricity generation curtailed by each building during the 1-year experiments.

6.5. Hypotheses Assessment

To assess the proposed hypotheses, results gathered from different scenarios are compared. Since the BL-LMI measures are implemented with the objective of improving the benefits offered to LVG operators and building owners when the 33 buildings are converted to Net-ZEBs, hypothesis H #1 is assessed by comparing the Performance Indicators associated to Scenarios #2 and #3. Regarding hypothesis H #2, it addresses the improvement of benefits offered to LVG operators and building owners resulting from implementing LM improvement at Community-Level rather than at Building-Level. Therefore, to assess this second hypothesis, results obtained for the considered Performance Indicators and for the electricity costs associated to Scenarios #4 and #3 are compared. The results gathered through the conducted experiments validate both hypotheses H #1 and H #2.

In the case of hypothesis H #1, results show that one of the Performance Indicators (i.e. yearly peak load at LVG's node 0) was deteriorated when the 33 BL-LMI measures were implemented. Concretely, as a result of the controllable devices' operation delay to coincident instants, the yearly peak load for Scenario #3 was increased by 40 %, when compared to Scenario #2. Additionally, during 278 distinct time-steps, the load registered at LVG's node 0 (see Figure 6.5) for Scenario #3 achieved higher values than the yearly peak load registered for Scenario #2, which was 51.6 kVA. Figure 6.38 depicts the load registered at LVG's node 0 for Scenario #3 during these time-steps, where the dashed gray line refers to the yearly peak load registered for Scenario #2, denoted as $Lmax$.

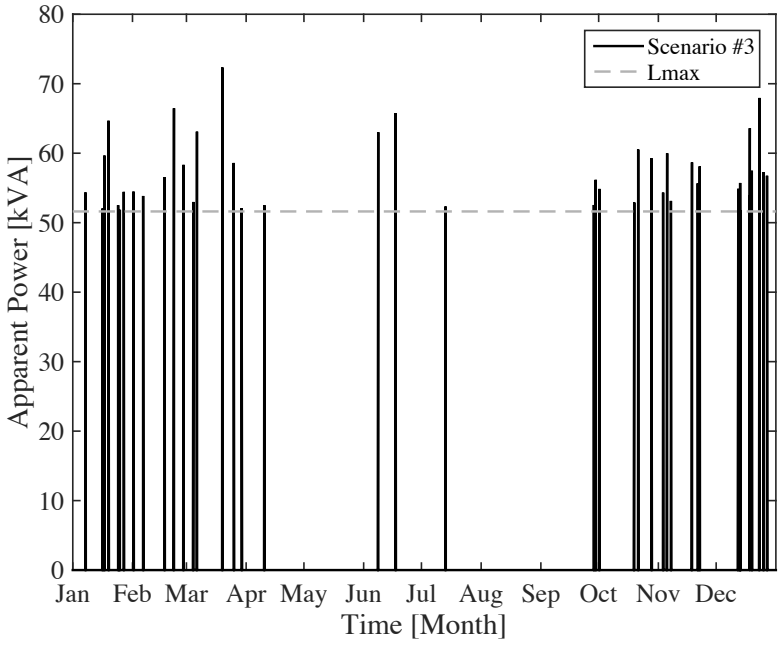

Figure 6.38 – LVG's load at node 0 for Scenario #3 during the 278 time-steps in which the 33 BL-LMI measures have a negative impact on LVG's operation.

The above mentioned results for the specific case of the load registered at transformer's output for the studied LVG validate hypothesis H #1. These findings can be extended for any branch β of a generic radial distribution grid as follows:

Considering a period of analysis T, BL-LMI measures have a negative impact at a specific branch β, defined by nodes v and $v+1$, of a generic radial distribution grid, if the difference between buildings' on-site electricity generation downstream that branch at any time-step n and the buildings' controllable electricity demand, in addition to the non-controllable buildings' electricity demand and the electricity losses occurring at LVG's distribution feeders, is higher than the maximum peak load observed before the BL-LMI measures take place, as described by Expression 6.1.

$$\forall\, n \in T, \tag{6.1}$$

$$\left| \sum_{b=b_\beta}^{N\_B} C\_BD_b(n) + \sum_{b=b_\beta}^{N\_B} NC\_DB_b\,(n) + \sum_{i=\beta,j=\beta+1}^{N\_b-1,N\_b} V_{i,j}(n) \left[\frac{V_{i,j}(n)}{Z_{i,j}(n)}\right]^* - \sum_{b=b_\beta}^{N\_B} BG_b(n) \right| > Lmax_\beta$$

In Expression 6.1, the first term refers to the controllable electricity demand associated to all buildings downstream branch β (i.e. from building b_β to building N_B). For each building b, the controllable demand ($\boldsymbol{C\_BD}$) at time-step n is defined by the operation of the respective controllable devices. The second term is the non-controllable electricity demand downstream the concerned branch, which is obtained by adding the non-controllable electricity demand ($\boldsymbol{NC\_BD}$) associated to the previously referred buildings. The third term concerns the energy losses occurring from branch β to branch N_b, where N_b is the total number of branches. The fourth term refers to the total electricity generation occurring downstream branch β. The only term in the right-hand side of Expression 6.1 is the maximum peak load registered at branch β before the BL-LMI measures take place. $Lmax_\beta$ should be associated to a period of analysis equivalent to T so the conducted analysis is associated to similar conditions (e.g. 1-year analysis in order to subject the LVG to similar meteorological conditions).

Concerning hypothesis H #2, the collected results show that all Performance Indicators and the electricity costs supported by building owners for the three considered tariffs are improved in Scenario #4, when compared to scenario #3. According to Expression 4.7, the proposed CL-LMI measure distributes the controllable devices' operation throughout the day, which results on higher LM values at LVG's node 0 and a consequent decreasing of LVG's peak load, resistive losses, and transformer aging. Regarding the electricity costs, these are decreased due to the three factors described in Sections 6.4.1 – 6.4.3.

CHAPTER 7

Conclusions

This last chapter concludes the dissertation. In Sections 7.1 and 7.2 an overview of the work undertaken and a description of the resulting main findings and contributions are provided, respectively. Section 7.3 concludes this chapter by listing a set of future research directions left opened by this work.

7.1. Research Work Overview

European Union EPBD 2010 recast targets 31st December 2020 as the time-horizon when all new buildings shall be, at least, nZEBs. Furthermore, the same directive recommends member states to promote the transformation of regular building into nZEBs when renovation works take place. Net-ZEBs, a specific type of nZEB, rely on energy grids to achieve a zero NB over the Balance Period. These buildings are often equipped with PV systems to compensate their energy demand and use LVGs as virtual unlimited storage systems to achieve such NB. However, the instantaneous matching between Net-ZEBs' electricity demand and on-site generation is often far from being perfect, which can introduce negative impacts on LVGs' operation.

In order to mitigate the aforementioned mismatch in buildings equipped with distributed generation systems in general, and in Net-ZEBs in particular, LM improvement incentives are being introduced worldwide. These incentives are based on two assumptions: i) LVG operators

benefit from lower building-LVG interaction and, therefore, improved Performance Indicators; and ii) building owners benefit from lower electricity bills due to a reduction of both high cost electricity imports and low cost electricity exports. The assumption that LM improvement measures are always benefic to LVG operators is questioned in this work, leading to RQ #1. Additionally, a second Research Question was introduced (i.e. RQ #2) with the objective of finding a novel LM improvement approach to enhance the benefits offered to LVG operators and building owners.

The reviewed literature shows that LM improvement measures, based on the Energy Flexibility offered by electricity demand devices, are implemented only at Building-Level without taking into consideration the demand and on-site generation profiles of other buildings. Moreover, these studies do not consider impacts introduced by the implemented LM improvement measures on LVGs Performance Indicators, assuming that benefits are always offered to LVG operators. Therefore, based on the conducted literature review, hypotheses H #1 and H #2 were formulated to address RQs #1 and #2, respectively.

Experiments were carried out during this work aiming at collecting data to test the proposed hypotheses. These experiments focused a neighborhood composed by 33 residential detached houses fed by the same LVG and comprised four distinct scenarios. Scenario #1 represents the current state of the Portuguese building stock. Scenario #2 illustrates a worst case situation to LVG operators, where the 33 buildings are renovated and converted to Net-ZEBs, introducing negative impacts on LVG operation. Scenario #3 aims to test hypothesis H #1 and, therefore, BL-LMI measures are implemented at the 33 Net-ZEBs. Last but not least, Scenario #4 implements a CL-LMI measure with the objective of testing hypothesis H #2.

In the referred experiments, both LVG Performance Indicators and annual electricity costs per building are used to assess the benefits offered to the LVG operator and to building owners, respectively. LVG yearly peak load, annual energy losses due to Joule Effect occurring throughout the distribution feeder, and transformer aging are used as Performance Indicators. Regarding the annual electricity costs, three distinct tariffs were considered to quantify importing costs, while exporting costs are computed according to Portuguese legislation. Table 6.1 summarizes the results obtained for each scenario.

Table 7.1 – Summary of obtained results.

Metric		Scenario #1	Scenario #2	Scenario #3	Scenario #4
P. I.	Peak Load [kVA]	49.6	51.6	72.3	49.5
	Energy Losses [kWh]	2308	3821	2923	2678
	Transformer Aging [Days]	365	32377	17338	1342
E. C.	TOU 1 [EUR]	584	340	289	216
	TOU 2 [EUR]	626	360	312	217
	TOU 3 [EUR]	712	436	365	276
Key: P.I. – Performance Indicator; E.C. – Electricity Costs (annual average value per building).					

7.2. Main Findings and Contributions

Collected results show that the simple transition from regular buildings to Net-ZEBs (i.e. the transition between Scenarios #1 and #2) deteriorates the considered Performance Indicators. In fact, due to severe reverse power flows, the MV/LV transformer would have to be replaced to avoid permanent failure. Impacts on LVG Performance Indicators resulting from a gradual transformation of the 33 regular buildings into Net-ZEBs were also studied (Annex B). It was found that the PV systems impact both positive and negatively the LVG Performance Indicators during this transition. For a reduced number of buildings converted to Net-ZEB, the yearly peak load, annual energy losses due to Joule Effect occurring throughout the distribution feeder, and transformer aging are reduced by 0.2, 20.3 and 6.7 %, respectively, when compared to the original neighborhood (i.e. when no PV systems are considered). After these minimum values, when all buildings are converted to Net-ZEBs the aforementioned indicators reach values 4, 65.6 and 8770 % higher than in the first scenario, resulting on the values presented in Table 6.1 for Scenario #2.

When the BL-LMI measures were applied to mitigate the negative impacts introduced on LVG Performance Indicators due to the transition from Scenario #1 to Scenario #2, it was found that these measures can have a negative impact on LVG's yearly peak load, aggravating the problem that they should mitigate. The reason for this poor performance is related with the "greedy" approach followed by BL-LMI measures that shift controllable devices' operation to coincident periods without taking into consideration the electricity demand and on-site generation profiles of others buildings.

Regarding the results obtained for the proposed CL-LMI measure, it was found that the CNet-ZEC improves all Performance Indicators, when compared to Scenario #3, and even the yearly peak load if compared to Scenario #1. This is a consequence of the aggregated and cooperative approach followed by this measure, where the Energy Flexibility offered by all controllable devices is used to improve community's LM taking into consideration the electricity demand and on-site generation profiles of all buildings. Benefits offered to building owners are also significantly improved when compared to the remaining scenarios due to the CNet-ZEC's type of power metering; reduced amount of energy curtailed; and obtained load profiles.

Apart from the above findings, that validate both Hypotheses H #1 and #2 and, therefore, answer Research Questions RQ #1 and RQ #2, this work also contributes to the LM improvement field by providing the following:

- The CNet-ZEC concept and its components;
- A generic method to compute the aggregated Energy Flexibility offered by a set of electricity demand devices;
- A specific method to compute the Energy Flexibility offered by a set of Event-Based devices;
- A Cooperation Mechanism that uses the aggregated Energy Flexibility, offered by a set of electricity demand devices, in order to improve LM at LVG's transformer output; and
- A Genetic Algorithm for Scheduling that optimizes the operation starting-times of controllable Event-Based devices in order to achieve the referred LM improvement.

The list of publications presented in Table 6.2 also represents a contribution to the LM improvement field.

Table 7.2 – Publications summary.

Year	Authors and Title	Type	State
2017	Søren Østergaard Jensen, Henrik Madsen, Rui Lopes, et al. "Energy Flexibility as a key asset in a smart building future - Contribution of Annex 67 to the European Smart Building Initiatives". Position paper of the IEA-EBC Annex 67 "Energy Flexible Buildings".	Position Paper	Available online[13]
2017	Rui Amaral Lopes. "Literature Review on Methodologies for Quantification of Energy Flexibility". Newsletter 1 of the IEA-EBC Annex 67 "Energy Flexible Buildings".	Newsletter	Available online[14]
2016	Rui Amaral Lopes, João Martins, Daniel Aelenei, Celson Pantoja Lima. "A Cooperative Net Zero Energy Community to Improve Load Matching". Renewable Energy, Volume 93. doi: 10.1016/j.renene.2016.02.044	Journal	Published
2016	Rui Amaral Lopes, Adriana Chambel, João Neves, Daniel Aelenei, João Martins. "A Literature Review of Methodologies Used to Assess the Energy Flexibility of Buildings". Energy Procedia, Volume 91. doi: 10.1016/j.egypro.2016.06.274	Conference	Published
2015	Pedro Magalhães, Rui Amaral Lopes, Joao Martins, António Joyce. "Grid Interaction Analysis of Solar Water Heating Photovoltaic-Thermal (PV-T) Systems with Thermal Storage Tanks and Electrical Auxiliary Heaters". 9th International Conference on Compatibility and Power Electronics (CPE). doi: 10.1109/CPE.2015.7231052	Conference	Published
2015	Antonio Sá, Rui Amaral Lopes, João Martins. "Design of an Agent-Based Simulator for Real-Time Estimation of Power Consumption and Generation in Residential Buildings". Industrial Electronics Society, 41st Annual Conference of the IEEE. doi: 10.1109/IECON.2015.7392698	Conference	Published

7.3. Future Works

The work presented in this dissertation can be extended by carrying out research activities on three interrelated main directions. The first one concerns the improvement of the current version

[13] http://www.annex67.org/publications/position-paper/ (Accessed: 19/12/2017).
[14] http://www.annex67.org/newsletters/ (Accessed: 19/12/2017)

of the CNet-ZEC concept. Such improvements would comprise the development of detailed profit distribution models for building owners, to be implemented by the C-ADMIN, or the development of specific methods to compute the Energy Flexibility offered by other types of controllable devices (e.g. TC devices, ES devices, or EVs), whose Energy Flexibility could be used to improve CNet-ZEC's LM values.

The second research direction concerns the extension of the CNet-ZEC to a broader level, comprising the Low, Medium, and even the High-Voltage parts of the distribution system, still with the objective of bringing benefits to building owners and Distribution System Operators. The motivation for such extension is related with the possibility of using the Energy Flexibility offered by a higher number of controllable devices, from different types and associated with buildings from distinct natures to accomplished desired objectives, not necessary exclusively related with LM improvement.

Despite the importance of the previously referred future works, the most important research direction refers to the development of a CNet-ZEC prototype on a real LVG to: i) test the interest of both LVG operators and building owners; and ii) to improve the CNet-ZEC concept itself. For this real world application, further research would have to be carried out on the development of a computational platform that would be able to implement a C-EM version, considering, among others, user's dynamic behavior, predictive control algorithms, and actuators to enable controllable devices' operation management.

Bibliography

Athienitis, A. and O'Brien, W. (2015) *Modeling, Design, and Optimization of Net-Zero Energy Buildings*. Ernst & Sohn. doi: 10.1002/9783433604625.

Baetens, R., De Coninck, R., Van Roy, J., Verbruggen, B., Driesen, J., Helsen, L. and Saelens, D. (2012) 'Assessing electrical bottlenecks at feeder level for residential net zero-energy buildings by integrated system simulation', *Applied Energy*. Elsevier Ltd, 96, pp. 74–83. doi: 10.1016/j.apenergy.2011.12.098.

Berggren, B., Widen, J. and Wall, M. (2012) 'Evaluation and optimization of a swedish Net ZEB - using load matching and grid interaction indicators', in *First Building Simulation and Optimization Conference Loughborough, UK 10-11 September 2012*, pp. 285–292.

Bird, L., Lew, D., Milligan, M., Carlini, E. M., Estanqueiro, A., Flynn, D., Gomez-Lazaro, E., Holttinen, H., Menemenlis, N., Orths, A., Eriksen, P. B., Smith, J. C., Soder, L., Sorensen, P., Altiparmakis, A., Yasuda, Y. and Miller, J. (2016) 'Wind and solar energy curtailment: A review of international experience', *Renewable and Sustainable Energy Reviews*. Elsevier, 65, pp. 577–586. doi: 10.1016/j.rser.2016.06.082.

Bocklisch, T. (2015) 'Hybrid energy storage systems for renewable energy applications', *Energy Procedia*. Elsevier B.V., 73, pp. 103–111. doi: 10.1016/j.egypro.2015.07.582.

Bollen, M. and Hassan, F. (2011) *Integration of Distributed Generation in the Power System*. John Wiley & Sons. doi: 10.1002/9781118029039.

Bruch, M. and Müller, M. (2014) 'Calculation of the Cost-effectiveness of a PV Battery System', *Energy Procedia*, 46, pp. 262–270. doi: 10.1016/j.egypro.2014.01.181.

Cao, S. (2014) *Matching analysis for on-site building energy systems involving energy conversion, storage and hybrid grid connections.* Aalto University publication series DOCTORAL DISSERTATIONS, 18/2014.

Cao, S., Hasan, A. and Sirén, K. (2013a) 'Analysis and solution for renewable energy load matching for a single-family house', *Energy & Buildings*. Elsevier B.V., 65, pp. 398–411. doi: 10.1016/j.enbuild.2013.06.013.

Cao, S., Hasan, A. and Sirén, K. (2013b) 'On-site energy matching indices for buildings with energy conversion , storage and hybrid grid connections', *Energy & Buildings*. Elsevier B.V., 64, pp. 423–438. doi: 10.1016/j.enbuild.2013.05.030.

Cao, S., Hasan, A. and Sirén, K. (2014) 'Matching analysis for on-site hybrid renewable energy systems of office buildings with extended indices', *Applied Energy*. Elsevier Ltd, 113, pp. 230–247. doi: 10.1016/j.apenergy.2013.07.031.

Cao, S., Mohamed, A., Hasan, A. and Sirén, K. (2014) 'Energy matching analysis of on-site micro-cogeneration for a single-family house with thermal and electrical tracking strategies', *Energy & Buildings*. Elsevier B.V., 68, pp. 351–363. doi: 10.1016/j.enbuild.2013.09.037.

Cao, S. and Sirén, K. (2014) 'Impact of simulation time-resolution on the matching of PV production and household electric demand', *Applied Energy*. Elsevier Ltd, 128, pp. 192–208. doi: 10.1016/j.apenergy.2014.04.075.

Castillo-Cagigal, M., Caamaño-Martín, E., Matallanas, E., Masa-Bote, D., Gutiérrez, A., Monasterio-Huelin, F. and Jiménez-Leube, J. (2011) 'PV self-consumption optimization with storage and Active DSM for the residential sector', *Solar Energy*, 85(9), pp. 2338–2348. doi: 10.1016/j.solener.2011.06.028.

Castillo-Cagigal, M., E. Matallanas, D. Masa-Bote, E. Caamaño-Martín, A. Guiérrez, F. Monasterio and Jiménez-Leube, J. (2010) 'Self-Consumption Enhancement With Storage System and Demand - Side Management : G E Delos-Pv System', in *5th International Renewable Energy Storage Conference (IRES 2010), Berlin, Germany, November 22nd-24th, 2010.*

Chapin, D. M., Fuller, C. S. and Pearson, G. L. (1954) 'A new silicon p-n junction photocell for converting solar radiation into electrical power', *Journal of Applied Physics*, 25, pp. 676–677. doi: 10.1063/1.1721711.

Collins, L. and Ward, J. K. (2015) 'Real and reactive power control of distributed PV inverters for overvoltage prevention and increased renewable generation hosting capacity', *Renewable Energy*. Elsevier Ltd, 81, pp. 464–471. doi: 10.1016/j.renene.2015.03.012.

Crew, M. A., Fernando, C. S. and Kleindorfer, P. R. (1995) 'The theory of peak-load pricing: A survey', *Journal of Regulatory Economics*, 8(3), pp. 215–248. doi: 10.1007/BF01070807.

D'hulst, R., Labeeuw, W., Beusen, B., Claessens, S., Deconinck, G. and Vanthournout, K. (2015) 'Demand response flexibility and flexibility potential of residential smart appliances: Experiences from large pilot test in Belgium', *Applied Energy*. Elsevier Ltd, 155, pp. 79–90. doi: 10.1016/j.apenergy.2015.05.101.

Dar, U. I., Sartori, I., Georges, L. and Novakovic, V. (2014) 'Advanced control of heat pumps for improved flexibility of Net-ZEB towards the grid', *Energy and Buildings*, 69, pp. 74–84. doi: 10.1016/j.enbuild.2013.10.019.

DGGE/IP-3E (2004) Eficiência energética em equipamentos e sistemas eléctricos no sector residencial (in Portuguese). Available at: http://eficiencia-energetica.com/images/upload/Brochura_Eficiencia.pdf (Accessed 4 May 2017).

Duffie, J. a. and Beckman, W. a. (2013) *Solar Engineering of Thermal Processes*. 4th ed. Wiley. doi: 10.1115/1.2930068.

EDP Comercial (2017) *Electricity and natural gas tariff for particular entities*. Available at: https://energia.edp.pt/particulares/energia/tarifarios/ (Accessed: 12 February 2017).

EDP Distribuição (2014) Plano de Desenvolvimento e Investimento da Rede de Distribuição 2015-1019 (in Portuguese). Available at: http://www.erse.pt/pt/consultaspublicas/consultas/Documents/49_1/PDIRD%202015-2019%20-%20Plano.pdf. (Accessed 1 September 2017).

EDP Distribuição (2016) *Relatório e Contas 2016 (in Portuguese)*. Available at: https://www.edpdistribuicao.pt/pt/edpDistribuicao/indicadoresGestao/Pages/relatorioContas.aspx. (Accessed 4 September 2017).

EGGY (2017) *EGGY*. Available at: www.eggy.pt (Accessed: 4 May 2017).

Electric Imp (2017) *Electric Imp*. Available at: www.electricimp.com (Accessed: 4 May 2017).

EN 15603 (2008) *Energy performance of buildings. Overall energy use and definition of energy ratings*.

EnOB (2013) *Net zero-energy buildings – Map of international projects*. Available at: http://www.enob.info/en/net-zero-energy-buildings/nullenergie-projekte-weltweit/ (Accessed: 16 January 2017).

EPA (2017a) *Climate Change Indicators: Atmospheric Concentrations of Greenhouse Gases*, *Climate Change Indicators*. Available at: https://www.epa.gov/climate-indicators/climate-change-indicators-atmospheric-concentrations-greenhouse-gases (Accessed: 9 March 2017).

EPA (2017b) *Climate Change Indicators: Greenhouse Gases*. Available at: https://www.epa.gov/climate-indicators/greenhouse-gases#major-long-lived-greenhouse-gases-and-their-characteristics (Accessed: 9 March 2017).

European Commission (2011) 'A Roadmap for moving to a competitive low carbon economy in 2050', *Communication from the commission to the european parliament, the council, the european economic and social committee and the committee of the regions*.

European Commission (2015) 'Best practices on Renewable Energy Self-consumption', *Communication from the commission to the european parliament, the council, the european economic and social committee and the committee of the regions*.

European Commission (2016) 'EU transport in figures'*, Statistical pocketbook 2016*. doi: 10.2832/861735.

European Union (2010) 'Directive 2010/31/eu of the european parliament and of the council of 19 may 2010 on the energy performance of buildings (recast)', *Official Journal of the European Union*.

Evans, D. L. (1981) 'Simplified method for predicting photovoltaic array output', *Solar Energy*, 27(6), pp. 555–560. doi: 10.1016/0038-092X(81)90051-7.

Evans, D. L. and Florschuetz, L. W. (1977) 'Cost studies on terrestrial photovoltaic power systems with sunlight concentration', *Solar Energy*, 19(3), pp. 255–262. doi: 10.1016/0038-092X(77)90068-8.

Freris, L. and Infield, D. (2008) *Renewable Energy in Power Systems*. John Wiley & Sons, Ltd. ISBN: 978-0-470-01749-4.

Gao, C. and Redfern, M. a. (2010) 'A review of voltage control techniques of networks with distributed generations using On-Load Tap Changer transformers', *45th International Universities Power Engineering Conference UPEC2010, Cardiff, Wales, 2010, pp. 1-6*.

Garcia-Valle, R. and Lopes, J. A. P. (eds) (2013) *Electric Vehicle Integration into Modern Power Networks*. Springer. doi: 10.1007/978-1-4614-0134-6.

Garde, F., Aelenei, D., Aelenei, L., Scognamiglio, A. and Ayoub, J. (2017) *Solution Sets for Net-Zero Energy Buildings: Feedback from 30 Buildings worldwide*. Ernst & Sohn. ISBN: 978-3-433-03072-1.

González-Longatt, F. M. (2005) 'Model of photovoltaic module in Matlab', in *2do congreso Iberoamericano de Estudiantes de Ingeniería eléctrica, electrónica y computación (II Cibelec 2005)*.

Hansen, J., Sato, M., Kharecha, P., Beerling, D., Masson-delmotte, V., Pagani, M., Raymo, M., Royer, D. L. and Zachos, J. C. (2008) 'Target Atmospheric CO2: Where Should Humanity Aim?', *The Open Atmospheric Science Journal*, 2, pp. 217–231. doi: 10.2174/1874282300802010217.

Hawkes, A. and Leach, M. (2005) 'Impacts of temporal precision in optimisation modelling of micro-Combined Heat and Power', 30, pp. 1759–1779. doi: 10.1016/j.energy.2004.11.012.

Hoevenaars, E. (2012) *Temporal Resolution in Time Series and Probabilistic Models of Renewable Power Systems*. University of Victoria. Available at: http://hdl.handle.net/1828/3927. (Accessed 1 September 2017).

Hoevenaars, E. J. and Crawford, C. A. (2012) 'Implications of temporal resolution for modeling renewables-based power systems', *Renewable Energy*. Elsevier Ltd, 41, pp. 285–293. doi: 10.1016/j.renene.2011.11.013.

Hu, J., Marinelli, M., Coppo, M., Zecchino, A. and Bindner, H. W. (2016) 'Coordinated voltage control of a decoupled three-phase on-load tap changer transformer and photovoltaic inverters for managing unbalanced networks', *Electric Power Systems Research*. Elsevier B.V., 131, pp. 264–274. doi: 10.1016/j.epsr.2015.10.025.

Iberian Electricity Market (2014) *Reports on electricity spot market price*. Available at: http://www.mibel.com/index.php?mod=documentos&mem=listado&relmenu=23&relcategoria=151 (Accessed: 12 February 2017).

IEA (2014a) *Technology Roadmap: Solar Thermal Electricity - 2014*, *International Energy Agency (IEA)*.

IEA (2014b) *Technology Roadmap: Energy Storage - 2014, International Energy Agency (IEA)*.

IEA (2015a) *Technology Roadmap Hydrogen and Fuel Cells*.
doi: 10.1007/SpringerReference_7300.

IEA (2015b) *World Energy Outlook 2015, International Energy Agency (IEA)*.

IEA (2016) *World Energy Balances 2016, International Energy Agency (IEA)*.

IEA-EBC (2017) *Annex 67*. Available at: http://annex67.org/ (Accessed: 30 March 2017).

IEA-PVPS (2013) *Trends 2013 in Photovoltaic Applications: Survey Report of Selected IEA Countries between 1992 and 2012, Report IEA-PVPS T1-23:2013.*

IEA-PVPS (2016a) *Review and Analysis of PV Self-Consumption Policies, Report IEA-PVPS T1-28:2016*.

IEA-PVPS (2016b) *Trends 2016 in Photovoltaic Applications: Survey Report of Selected IEA Countries between 1992 and 2015, Report IEA PVPS T1-30:2016*.

IEA-SHC (2017) *Towards Net Zero Energy Solar Buildings, IEA SHC Task 40 and ECBCS Annex 52*. Available at: http://task40.iea-shc.org/ (Accessed: 11 March 2017).

IEC (2005) *60076-7 Loading Guide For Oil-immersed Power Transformers*.

IEEE (1981) 'Bibliography On Load Management', *IEEE Transactions on Power Apparatus and Systems*. doi: 10.1109/TPAS.1981.316729.

IEEE (2002) *IEEE Guide for Loading Mineral-Oil-Immersed Transformers. IEEE Std C57.91-1995 (R2002)*. doi: 10.1109/IEEESTD.1996.79665.

INE (2012) *Estatísticas da Construção e Habitação 2011 (in Portuguese)*. ISSN 0377-2225.

INE and DGEG (2011) *Inquerito ao consumo de energia doméstico 2010 (in Portuguese)*. ISSN 2182-0139.

IPCC (2014) *Synthesis Report Summary Chapter for Policymakers*, *Ipcc*. doi: 10.1017/CBO9781107415324.

Iqbal, M. (1983) *An introduction to solar radiation*. Academic Press.

Kabiri, R., Holmes, D. G., McGrath, B. P. and Meegahapola, L. G. (2015) 'LV Grid Voltage Regulation Using Transformer Electronic Tap Changing, with PV Inverter Reactive Power Injection', *IEEE Journal of Emerging and Selected Topics in Power Electronics*, 3(4), pp. 1182–1192. doi: 10.1109/JESTPE.2015.2443839.

Kersting, W. H. (1991) 'Radial distribution test feeders', *IEEE Transactions on Power Systems*, 6(3), pp. 975–985. doi: 10.1109/59.119237.

Lakervi, E. and Holmes, E. J. (2003) *Electricity Distribution Network Design*. 2nd Edition. The Institution of Engineering and Technology. doi: 10.1049/PBPO021E.

Lamoudi, M. Y. (2012) *Distributed model predictive control for energy management in buildings*. Dynamical Systems [math.DS]. Université de Grenoble, 2012. English. <tel-00793614v1>. (Accessed 1 September 2017).

Lang, K. R. (2006) *Sun, Earth and Sky*. Second Ed. Springer. doi: 10.1007/978-0-387-33365-6.

Letcher, T. M. (2016) *Storing Energy: with Special Reference to Renewable Energy Sources*. Elsevier. ISBN: 978-0-12-803440-8.

Liu, X., Cramer, A. M. and Liao, Y. (2015) 'Reactive power control methods for photovoltaic inverters to mitigate short-term voltage magnitude fluctuations', *Electric Power Systems Research*. Elsevier B.V., 127, pp. 213–220. doi: 10.1016/j.epsr.2015.06.003.

Livengood, D. J. (2011) *The Energy Box: Comparing Locally Automated Control Strategies of Residential Electricity Consumption under Uncertaint*, *PhD Thesis*. Massachusetts Institute of Technology. Engineering Systems Division. Available at: http://hdl.handle.net/1721.1/68190. (Accessed 1 September 2017).

Lopes, J. A. P., Madureira, A. G. and Moreira, C. C. L. M. (2013) 'A view of microgrids', *Wiley Interdisciplinary Reviews: Energy and Environment*, 2(1), pp. 86–103. doi: 10.1002/wene.34.

Lorenzi, G. and Silva, C. A. S. (2016) 'Comparing demand response and battery storage to optimize self-consumption in PV systems', *Applied Energy*. Elsevier Ltd, 180, pp. 524–535. doi: 10.1016/j.apenergy.2016.07.103.

Luque, A. and Hegedus, S. (2011) *Handbook of Photovoltaic Science and Engineering*. 2nd Editio. Wiley. doi: 10.1002/0470014008.

Luthander, R., Widén, J., Nilsson, D. and Palm, J. (2015) 'Photovoltaic self-consumption in buildings: A review', *Applied Energy*. Elsevier Ltd, 142, pp. 80–94. doi: 10.1016/j.apenergy.2014.12.028.

M. Braun, K. Büdenbender, D. Magnor, A. J. (2009) 'Photovoltaic Self-Consumption in Germany - Using Lithium-Ion Storage to Increase Self-Consumed Photovoltaic Energy', *24th European Photovoltaic Solar Energy Conference (PVSEC). Humburg (Germany)*, pp. 3121–3127. doi: 10.4229/24thEUPVSEC2009-4BO.11.2.

MAOTE (2014) 'Decreto de Lei 153/2014 (in Portuguese)'. Diário da República.

Marcelino, J. and Gavião, J. (2013) 'The Passive House in Portugal : encouraging its spread in South West Europe', in *17th International Passive House Conference in Frankfurt*.

Mastrandrea, M. D. and Schneider, S. H. (2004) 'Probabilistic Integrated Assessment of "Dangerous" Climate Change', *Science*, 304(April 2004), pp. 571–575. doi: 10.1126/science.1094147.

Matallanas, E., Castillo-Cagigal, M., Gutiérrez, A., Monasterio-Huelin, F., Caamaño-Martín, E., Masa, D. and Jiménez-Leube, J. (2012) 'Neural network controller for Active Demand-Side Management with PV energy in the residential sector', *Applied Energy*, 91(1), pp. 90–97. doi: 10.1016/j.apenergy.2011.09.004.

Meeus, J. (1998) *Astronomical Algorithms*. Second Edi. Willmann-Bell, Inc.

Merei, G., Moshövel, J., Magnor, D. and Sauer, D. U. (2016) 'Optimization of self-consumption and techno-economic analysis of PV-battery systems in commercial applications', *Applied Energy*. Elsevier Ltd, 168, pp. 171–178. doi: 10.1016/j.apenergy.2016.01.083.

Molina-Markham, A., Shenoy, P., Fu, K., Cecchet, E. and Irwin, D. (2010) 'Private memoirs of a smart meter', *Proceedings of the 2nd ACM Workshop on Embedded Sensing Systems for Energy-Efficiency in Building - BuildSys '10*, pp. 61–66. doi: 10.1145/1878431.1878446.

Munkhammar, J., Grahn, P. and Widén, J. (2013) 'Quantifying self-consumption of on-site photovoltaic power generation in households with electric vehicle home charging', *Solar Energy*. Elsevier Ltd, 97, pp. 208-216. doi: 10.1016/j.solener.2013.08.015.

NASA (2017a) *Earth's Energy Budget*, *Earth Observatory*. Available at: https://earthobservatory.nasa.gov/Features/EnergyBalance/page4.php (Accessed: 27 March 2017).

NASA (2017b) *NASA Global Climate Change and Global Warming: Vital Signs of the Planet*. Available at: http://climate.nasa.gov/vital-signs/global-temperature/ (Accessed: 9 March 2017).

NASA (2017c) *Sun Fact Sheet*. Available at: https://nssdc.gsfc.nasa.gov/planetary/factsheet/sunfact.html (Accessed: 23 March 2017).

Neufeld, J. L. (1987) 'Price Discrimination and the Adoption of the Electricity Demand Charge', *The Journal of Economic History*, 47(3), p. 693. doi: 10.1017/S0022050700049068.

Nicola, F., Toledo, D. and Zamb, W. (2013) 'Storage unit and load management in photovoltaic inverters for residential application', *IECON 2013 - 39th Annual Conference of the IEEE Industrial Electronics Society, Vienna, 2013*. doi: 10.1109/IECON.2013.6700258.

NREL (2017) *Best Research-Cell Efficiencies*. Available at: https://www.nrel.gov/pv/assets/images/efficiency_chart.jpg (Accessed: 27 March 2017).

Nykvist, B. and Nilsson, M. (2015) 'Rapidly falling costs of battery packs for electric vehicles', *Nature climate change*. doi: 10.1038/NCLIMATE2564.

Paatero, J. and Lund, P. (2010) 'Impacts of different data averaging times on statistical analysis of distributed domestic photovoltaic systems', *Solar Energy*, 84, pp. 492–500. doi: 10.1016/j.solener.2010.01.011.

PHPT (2017) *Passive House Requirements (in Portuguese)*. Available at: http://www.passivhaus.pt/requisitos.html (Accessed: 20 March 2017).

Planck, M. and Masius, M. (1914) *The theory of heat radiation*. Second Edition. P. Blakiston's Son & CO.

Reynders, G., Nuytten, T. and Saelens, D. (2013) 'Potential of structural thermal mass for demand-side management in dwellings', *Building and Environment*, 64, pp. 187–199. doi: 10.1016/j.buildenv.2013.03.010.

Richardson, I., Thomson, M. and Infield, D. (2008) 'A high-resolution domestic building occupancy model for energy demand simulations', *Energy and Buildings*, 40(8), pp. 1560–1566. doi: 10.1016/j.enbuild.2008.02.006.

Richardson, I., Thomson, M., Infield, D. and Clifford, C. (2010) 'Domestic electricity use: A high-resolution energy demand model', *Energy and Buildings*. Elsevier B.V., 42(10), pp. 1878–1887. doi: 10.1016/j.enbuild.2010.05.023.

Richardson, I., Thomson, M., Infield, D. and Delahunty, A. (2009) 'Domestic lighting: A high-resolution energy demand model', *Energy and Buildings*, 41(7), pp. 781–789. doi: 10.1016/j.enbuild.2009.02.010.

Salom, J., Marszal, A., Candanedo, J., Widén, J., Byskov Lindberg, K. and Sartori, I. (2013) *Analysis of load match and grid interaction indicators in net zero energy buildings with high-resolution data*. Report from Subtask A of IEA Task 40/Annex 52 Towards Net Zero Energy Solar Buildings.

Salom, J., Widén, J., Candanedo, J. and Lindberg, K. B. (2014) 'Analysis of grid interaction indicators in net zero-energy buildings with sub-hourly collected data', *Applied Energy*. Elsevier Ltd, 136, pp. 1–18. doi: 10.1080/17512549.2014.941006.

Salom, J., Widén, J., Candanedo, J., Sartori, I., Voss, K. and Marszal, A. (2011) 'Understanding net zero energy buildings: evaluation of load matching and grid interaction indicators', *in Proceedings of Building Simulation 2011: 12th Conference of International Building Performance Simulation Association, Sydney, 14–16 November.*

Sampaio, L. P., de Brito, M. A. G., de A. e Melo, G. and Canesin, C. A. (2016) 'Grid-tie three-phase inverter with active power injection and reactive power compensation', *Renewable Energy*. Elsevier Ltd, 85, pp. 854–864. doi: 10.1016/j.renene.2015.07.034.

Sartori, I., Napolitano, A. and Voss, K. (2012) 'Net zero energy buildings: A consistent definition framework', *Energy and Buildings*. Elsevier B.V., 48, pp. 220–232. doi: 10.1016/j.enbuild.2012.01.032.

Shroff, D. H. and Stannett, A. W. (1985) 'A review of paper aging in power transformers', *IEE Proceedings C Generation, Transmission and Distribution*, 132(6), p. 312-319. doi: 10.1049/ip-c.1985.0052.

Sioshansi, F. P. (ed.) (2013) *Evolution of Global Electricity Markets*, *Evolution of Global Electricity Markets*. Elsevier. doi: 10.1016/B978-0-12-397891-2.00002-X.

SMA (2016) *Planning Guidelines - SMA SMART HOME, The System Solution for Greater Independence*. Available at: http://files.sma.de/dl/1353/SI-HoMan-PL-en-50.pdf. (Accessed: 15 May 2017).

SMA (2017) *Solar System Smart*. Available at: https://www.sma.de/en/home-systems/solar-system-smart.html (Accessed: 15 May 2017).

SolarCity (2017) *Island in the Sun*. Available at: http://blog.solarcity.com/island-in-the-sun/ (Accessed: 6 May 2017).

Solomon, S., Qin, D., Manning, M., Chen, Z., Marquis, M., Averyt, K. B., Tignor, M., Miller, H. L. and (eds) (2007) *Contribution of Working Group I to the Fourth Assessment Report of the Intergovernmental Panel on Climate Change*. Cambridge University Press, Cambridge, United Kingdom and New York, NY, USA.

Sossan, F., Kosek, A. M., Martinenas, S., Marinelli, M. and Bindner, H. (2013) 'Scheduling of domestic water heater power demand for maximizing PV self-consumption using model predictive control', in *IEEE PES ISGT Europe 2013*. IEEE, pp. 1–5. doi: 10.1109/ISGTEurope.2013.6695317.

Staats, M. R., de Boer-Meulman, P. D. M. and van Sark, W. G. J. H. M. (2017) 'Experimental determination of demand side management potential of wet appliances in the Netherlands', *Sustainable Energy, Grids and Networks*. Elsevier Ltd, 9, pp. 80–94. doi: 10.1016/j.segan.2016.12.004.

Stamminger, R. (2008) *Synergy Potential of Smart Appliances*, *D2.3 of WP2 from the Smart-A project*. doi: 10.1109/MPE.2010.936353.

Stifter, M., Kamphuis, R., Galus, M., Renting, M., Rijneveld, A., Targosz, R., Widergren, S., Nordstrom, L., Brodén, D., Esterl, T., Galsworthy, S., Koponen, P. and Doolla, S. (2016) *Pilot Studies and Best Practices: Demand Flexibility in Households and Buildings, A report from IEA-DSM Task 17*.

The Mathworks Inc (2017) *MATLAB*. Available at: https://www.mathworks.com/products/matlab.html (Accessed: 20 April 2017).

ThingSpeak (2017) *ThingSpeak*. Available at: www.thingspeak.com (Accessed: 4 May 2017).

Thygesen, R. (2016) *Low energy buildings equipped with heat pumps for high self- consumption of photovoltaic electricity*. Mälardalen University Press Dissertations, No. 200.

Thygesen, R. and Karlsson, B. (2014) 'Simulation and analysis of a solar assisted heat pump system with two different storage types for high levels of PV electricity self-consumption', *Solar Energy*, 103, pp. 19–27. doi: 10.1016/j.solener.2014.02.013.

Tonkoski, R., Lopes, L. A. C. and El-Fouly, T. H. M. (2011) 'Coordinated active power curtailment of grid connected PV inverters for overvoltage prevention', *IEEE Transactions on Sustainable Energy*, 2(2), pp. 139–147. doi: 10.1109/TSTE.2010.2098483.

UN (1992) *Framework Convention on Climate Change*. Available at: http://newsroom.unfccc.int/ (Accessed: 27 October 2016).

Valentin Software (2017) *T*SOL*. Available at: http://www.valentin-software.com/en/products/solar-thermal/14/tsol (Accessed: 10 April 2017).

Vanhoudt, D., Geysen, D., Claessens, B., Leemans, F., Jespers, L. and Van Bael, J. (2014) 'An actively controlled residential heat pump: Potential on peak shaving and maximization of self-consumption of renewable energy', *Renewable Energy*, 63, pp. 531–543. doi: 10.1016/j.renene.2013.10.021.

Vieira, F. M., Moura, P. S. and de Almeida, A. T. (2017) 'Energy storage system for self-consumption of photovoltaic energy in residential zero energy buildings', *Renewable Energy*. Elsevier Ltd, 103, pp. 308–320. doi: 10.1016/j.renene.2016.11.048.

Voss, K. and Musall, E. (2013) *Net Zero Energy Buildings - International Projects of Carbon Neutrality in Buildings*. Detail Green Books. ISBN 978-3-920034-80-5.

Vrettos, E., Witzig, A., Kurmann, R., Koch, S. and Andersson, G. (2013) 'Maximizing Local PV Utilization Using Small-Scale Batteries and Flexible Thermal Loads', *28th European Photovoltaic Solar Energy Conference and Exhibition*, pp. 4515–4526. doi: 10.1017/CBO9781107415324.004.

Waffenschmidt, E. (2014) 'Dimensioning of decentralized photovoltaic storages with limited feed-in power and their impact on the distribution grid', *Energy Procedia*. The Authors, 46, pp. 88–97. doi: 10.1016/j.egypro.2014.01.161.

Weniger, J., Tjaden, T. and Quaschning, V. (2014) 'Sizing of Residential PV Battery Systems', *Energy Procedia*, 46, pp. 78–87. doi: 10.1016/j.egypro.2014.01.160.

Widén, J. (2014) 'Improved photovoltaic self-consumption with appliance scheduling in 200 single-family buildings', *Applied Energy*, 126, pp. 199–212.
doi: 10.1016/j.apenergy.2014.04.008.

Widén, J. and Munkhammar, J. (2013) 'Evaluating the benefits of a solar home energy management system: impacts on photovoltaic power production value and grid interaction', *Proceedings of the eceee 2013 Summer Study, Presqu'île de Giens, France, June 3-8, 2013, 2013*.

Widén, J., Wäckelgård, E. and Lund, P. D. (2009) 'Options for improving the load matching capability of distributed photovoltaics: Methodology and application to high-latitude data', *Solar Energy*, 83(11), pp. 1953–1966. doi: 10.1016/j.solener.2009.07.007.

Williams, C. J. C., Binder, J. O. and Kelm, T. (2012) 'Demand side management through heat pumps, thermal storage and battery storage to increase local self-consumption and grid compatibility of PV systems', in *3rd IEEE PES Innovative Smart Grid Technologies Europe (ISGT Europe)*. IEEE, pp. 1–6. doi: 10.1109/ISGTEurope.2012.6465874.

Wright, A. and Firth, S. (2007) 'APPLIED The nature of domestic electricity-loads and effects of time averaging on statistics and on-site generation calculations', 84, pp. 389–403. doi: 10.1016/j.apenergy.2006.09.008.

Yap, W. K., Havas, L., Overend, E. and Karri, V. (2014) 'Neural network-based active power curtailment for overvoltage prevention in low voltage feeders', *Expert Systems with Applications*. Elsevier Ltd, 41(4 PART 1), pp. 1063–1070. doi: 10.1016/j.eswa.2013.07.103.

ZEB (2017) *Living Lab*. Available at: http://www.zeb.no/index.php/en/pilot-projects/13-laboratories/158-living-lab-trondheim. (Accessed: 28 March 2017).

Zehir, M. A. and Bagriyanik, M. (2012) 'Demand Side Management by controlling refrigerators and its effects on consumers', *Energy Conversion and Management*. Elsevier Ltd, 64, pp. 238–244. doi: 10.1016/j.enconman.2012.05.012.

Annex A – Data Acquisition and Control System

A data acquisition and control system was developed to conduct the experiment whose results are depicted in Figure 3.10. The developed system acquires and saves the refrigerator's inner temperature and power consumption data, at a 1-min resolution, and interrupts the compressor's operation every 2 working cycles for 5 minutes when the inner temperature reaches its average value. Even if different types of interruption could also be configured, this type of interruption was chosen with the objective of comparing a normal operation cycle with an interrupted one. Although, higher data acquisition frequencies could also be selected, a 1-min frequency was chosen for the sake of coherence with the remaining of the dissertation. Figure A.1 presents the algorithm guiding the developed system's operation.

Regarding the implementation of the system, it was based on the Electric Imp™ solution (Electric Imp, 2017), which refers to an Internet of Things platform that securely connects physical WIFI featured microcontrollers (Imp Modules) with cloud based representations (Agents) on a one-to-one relation. The Electric Imp™ solution was chosen due to several factors: i) it is stable; ii) it is supported by a growing community; iii) it is relatively low-cost to developers; iv) and it uses the WIFI protocol. Additionally, the author has gained considerable experience using the Electric Imp™ solution in the EGGY™ project (EGGY, 2017).

During system's operation, the Agent Interacts with the Imp Module in order to measure the refrigerator's inner temperature and power consumption and to control the compressor state (ON/OFF control), according to the algorithm presented in Figure A.1. The collected data, which is transferred from the Imp Module to the Agent via a WIFI connection, is then sent to a cloud Data Base, which is provided by the ThingSpeak™ platform (ThingSpeak, 2017). This platform allows the access to the collected data through common data extensions (e.g. CSV).

To acquire the refrigerator's inner temperature and power consumption and to control the compressor state, the Imp Module uses the electronic circuit presented in Figure A.2. It comprises three main blocks, denoted as A, B and C in this figure, which are described as follows:

- Block A – Responsible for measuring the refrigerator's inner temperature. It is composed by an Analog Devices™ TMP36 sensor, which is connected to the respective Imp Module's analog input pin through dedicated cables.
- Block B – Supports the refrigerator's power consumption data acquisition using a common non-intrusive 0-30 A Hall Effect sensor. The acquired current samples are converted to power values by considering a unitary power factor and a line to neutral effective voltage of 230 V. Electronic components R_1, R_2, and C_1 are used to ensure positive voltage values at the respective Imp Module's analog input pin.
- Block C – Ensures the compressor's operation control and it is based on the D2425 solid state relay from Crydom™. Electronic components R_3, R_4, and T_1 are used to drive

enough power to operate the relay. A Light Emitter Diode (LED) shares the Imp Module's analog output pin with the relay in order to signal the compressor's operation. Figure A.3 presents the resulting experimental setup.

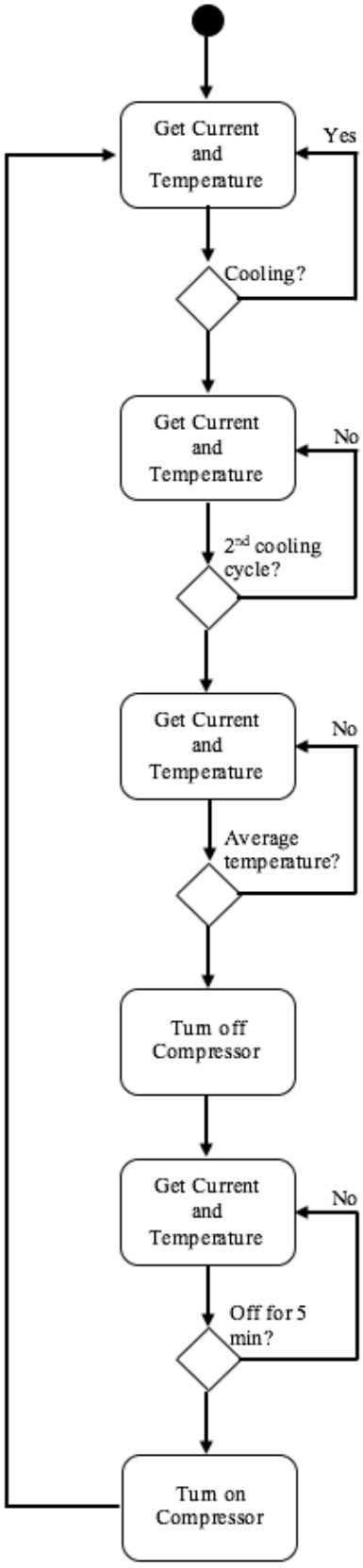

Figure A.1 – Monitoring and control Algorithm (M. and S. stand for Measure and Storage).

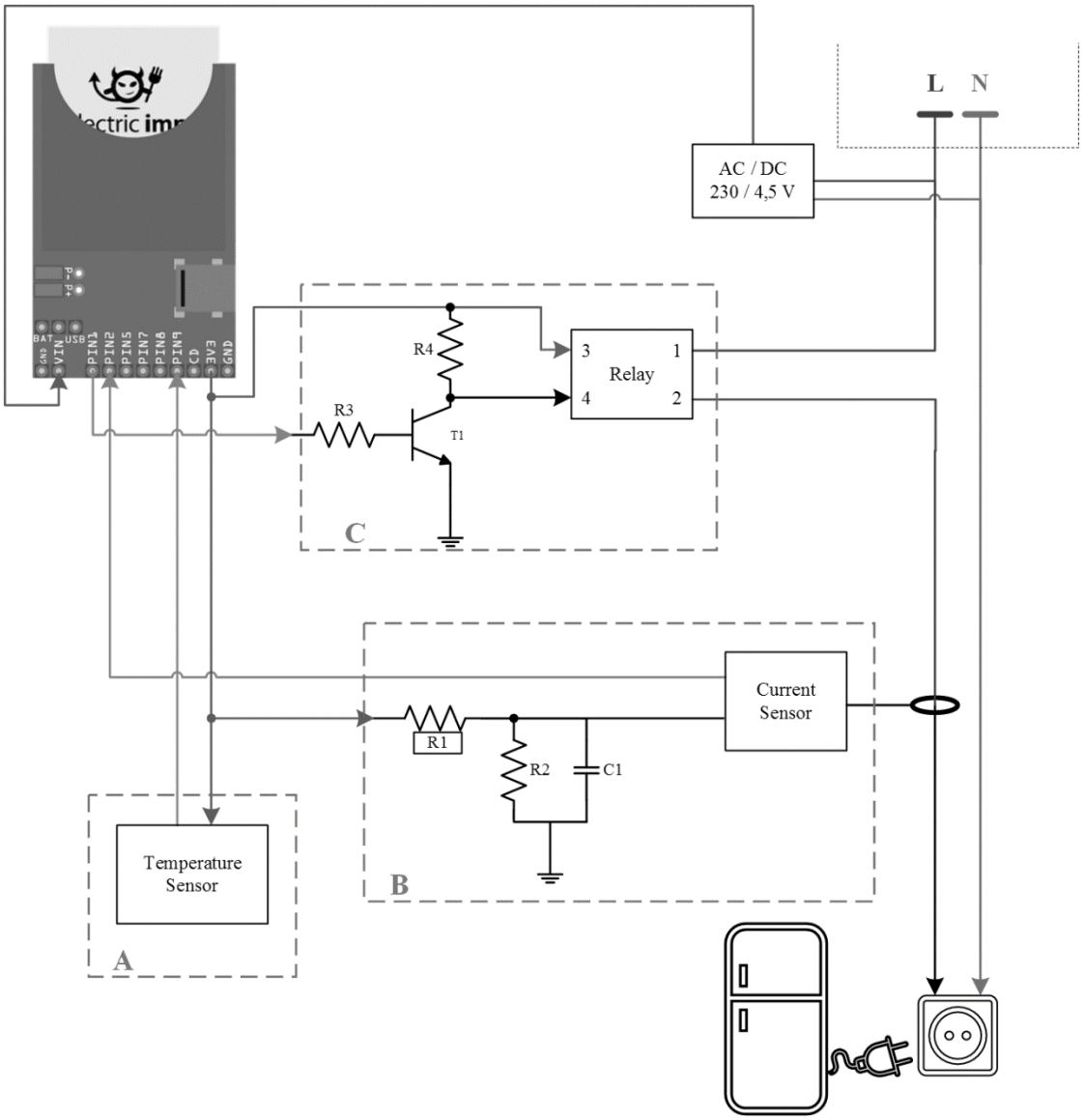

Figure A. 2 – Refrigerator's data acquisition and control system's electronic circuit.

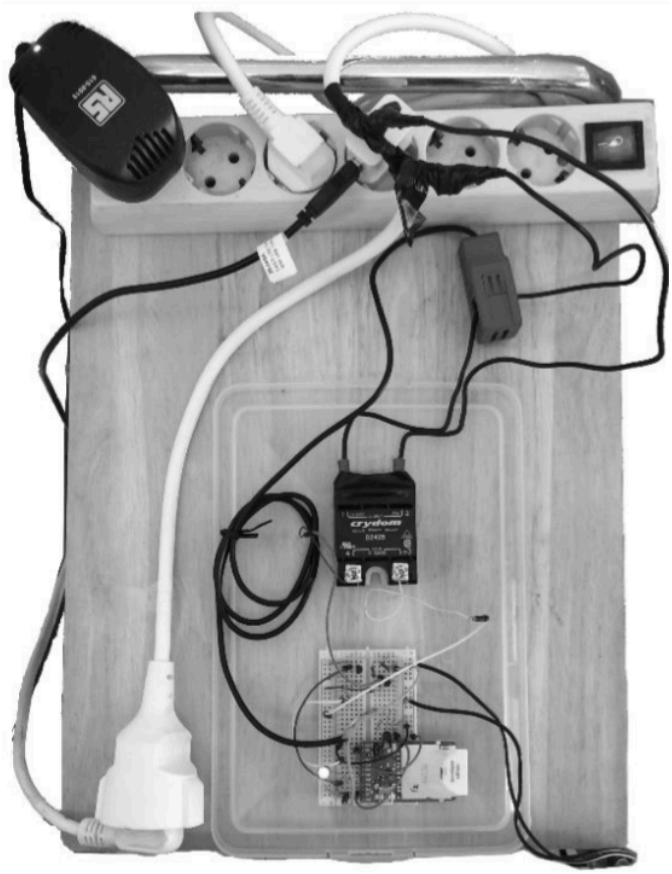

Figure A.3 – Refrigerator's data acquisition and control system's experimental setup.

Annex B – Transition from Scenario #1 to Scenario #2

This annex presents and analyses the results obtained for an extra scenario where the number of regular buildings converted to Net-ZEB evolves over time - i.e. it is focused on the transition from Scenario #1 to Scenario #2. As observed in Section 6.1, the introduction of PV systems into the studied LVG, resulting from the conversion of regular building to Net-ZEB, modifies the load cycles registered for the original neighborhood (i.e. Scenario #1). Figure B.1 shows the average net load profile at LVG's node 0 when 0, 9, 17, 25, and 33 buildings are converted to Net-ZEB. Due to the time-restricted availability of the solar resource, the original average net power profile at LVG's node 0 is only impacted during daytime. For a small amount of buildings converted to Net-ZEBs (e.g. 9), the referred net power is reduced during PV systems' operation. By increasing the number of converted buildings towards Scenario #2, reverse power flows become frequent and net power values at midday reach higher magnitudes than the original evening peak.

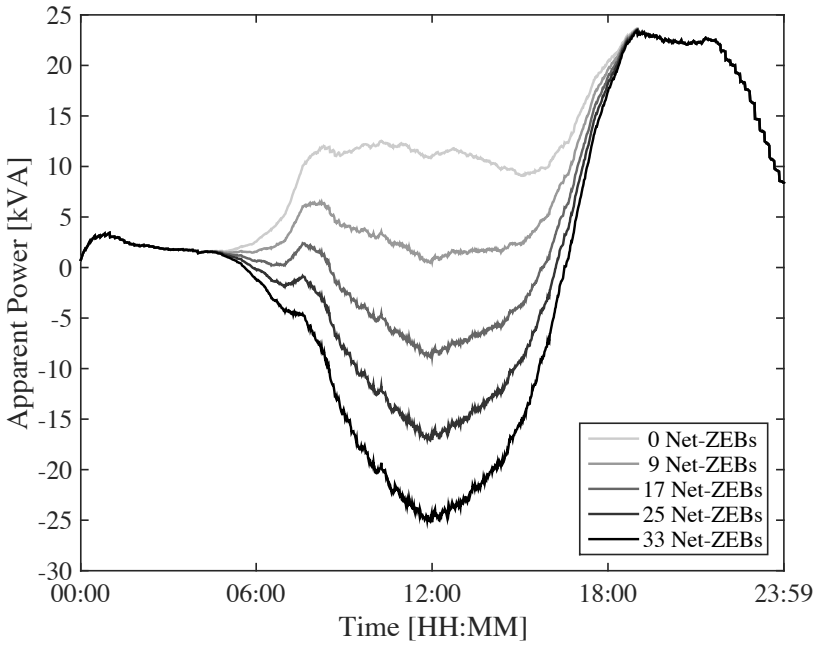

Figure B.1 – Average net power profile at LVG's node 0 for different amounts of regular buildings converted to Net-ZEB.

Figures B.2 – B.4 present the Performance Indicators variation as the number of buildings converted to Net-ZEB increases. The data used in these figures are provided in Table B.1. The obtained curves approximately follow the U-shape type curve reported by (Bollen and Hassan, 2011) – see Figure 1.2 b). The yearly peak load, annual energy losses due to Joule Effect, and annual equivalent transformer aging decrease until they reach a minimum value of 49.52 kVA, 1.84 MWh, and 340.47 days, respectively. This reduction results from the instantaneous matching between LVG's electricity demand and on-site generation, which decreases LVG's load. After

these minimum values, the considered Performance Indicators increase until they reach the values registered for Scenario #2. In the specific cases of the yearly peak load and annual equivalent transformer aging, a truncation effect can be observed when a relatively high number of buildings are converted to Net-ZEBs. This effect is introduced by the curtailment mechanism, that limits the introduction of on-site generation on LVG's sections during time-steps with voltage magnitude values close to the upper limit (110 % of the nominal value). As a result, the amount of annual energy curtailed significantly increases when an higher number of buildings are converted, as illustrated in Figure B.5.

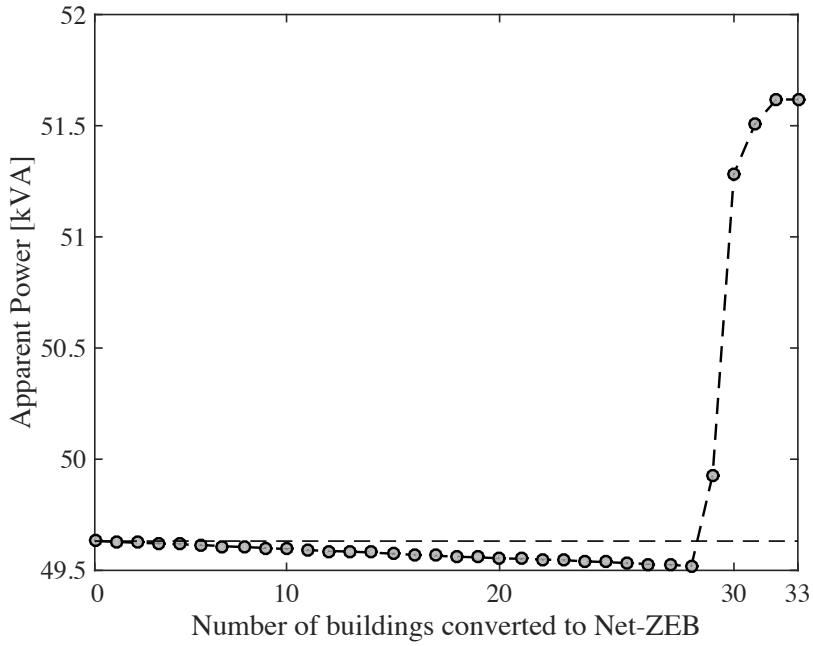

Figure B.2 – Yearly peak load for different amounts of regular buildings converted to Net-ZEB.

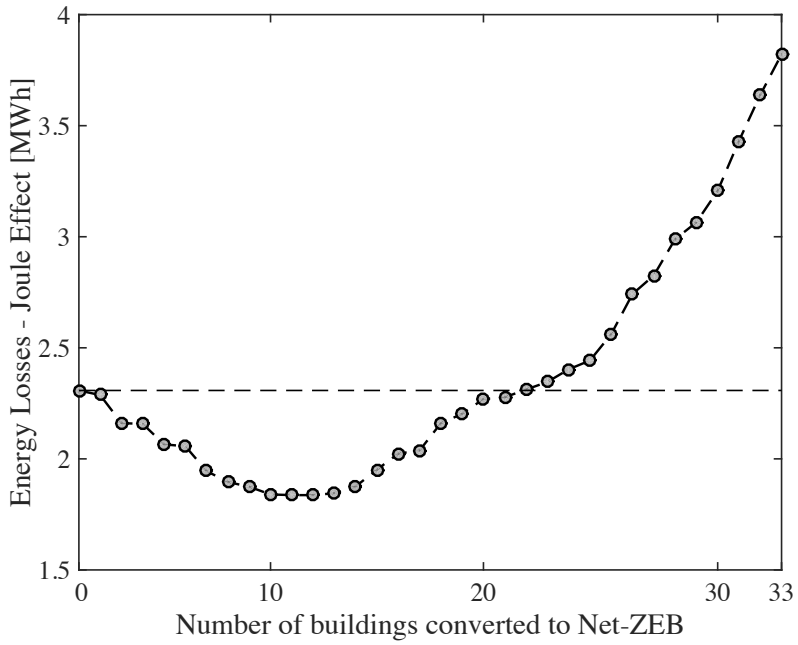

Figure B.3 – Annual total losses by Joule Effect for different amounts of regular buildings converted to Net-ZEB.

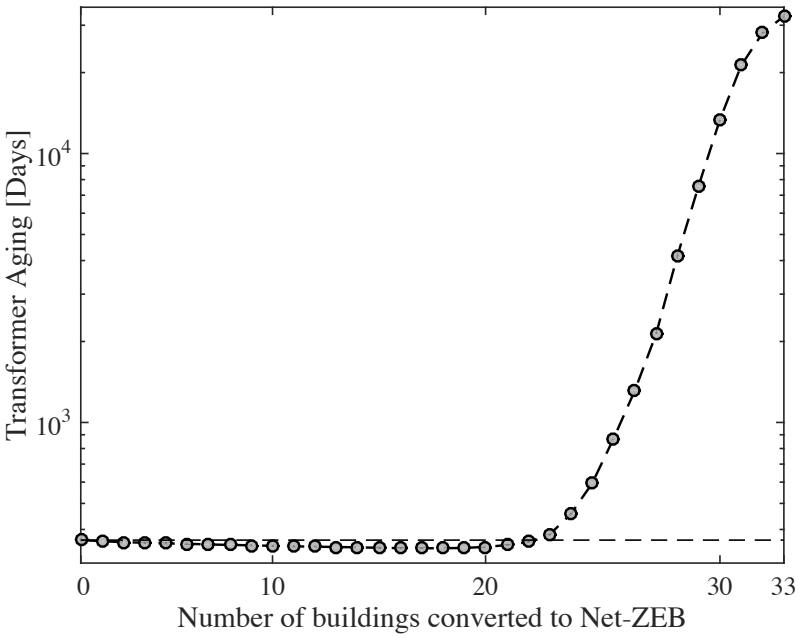

Figure B.4 – Annual equivalent transformer aging for different amounts of regular buildings converted to Net-ZEB (logarithmic scale)

Table B.1 – Performance Indicators' values associated with the transition from Scenario #1 to Scenario #2.

Nr. of Net-ZEBs	Peak Power [kVA]	Losses–Joule Effect [MWh]	Transformer Aging [Days]
0	49.63	2.31	365
1	49.63	2.29	361
2	49.62	2.16	358
3	49.62	2.16	357
4	49.62	2.07	354
5	49.61	2.06	353
6	49.61	1.94	351
7	49.60	1.90	350
8	49.60	1.87	349
9	49.60	1.84	347
10	49.59	1.84	346
11	49.59	1.84	345
12	49.58	1.85	344
13	49.58	1.88	343
14	49.57	1.95	341
15	49.57	2.02	340
16	49.57	2.04	340
17	49.56	2.16	340
18	49.56	2.20	341
19	49.55	2.27	344
20	49.55	2.28	349
21	49.55	2.31	359
22	49.55	2.35	382
23	49.54	2.40	456
24	49.54	2.44	593
25	49.53	2.56	868
26	49.53	2.74	1,312
27	49.52	2.83	2,130
28	49.52	2.99	4,159
29	49.93	3.06	7,590
30	51.28	3.21	13,376
31	51.51	3.43	21,275
32	51.62	3.64	28,066
33	51.62	3.82	32,377

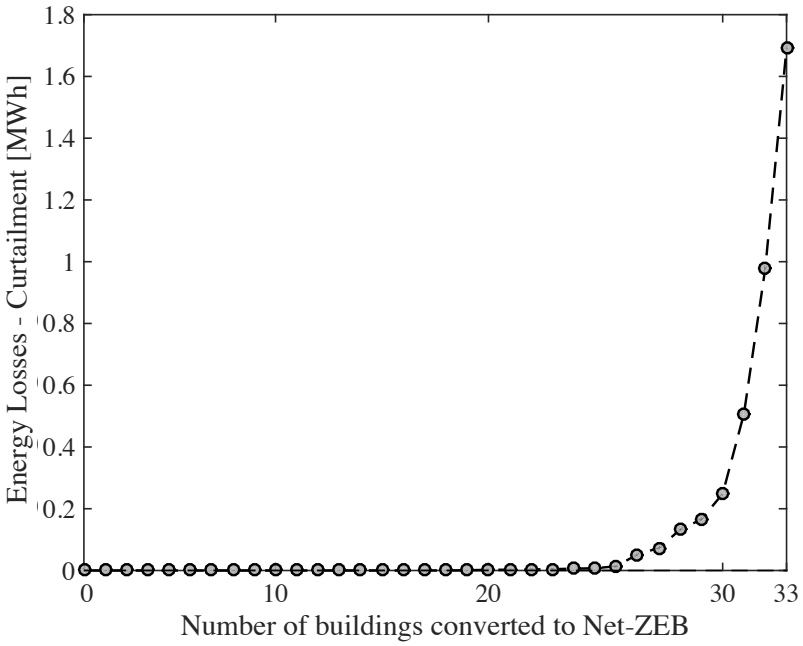

Figure B.5 – Annual total curtailment losses for different amounts of regular buildings converted to Net-ZEB.